

Design, Synthesis and Surface Modification of Lanthanide-Doped Nanoparticles for FRET- Based Biosensing Applications

Dissertation zur Erlangung des Doktorgrades der Naturwissenschaften

(Dr. rer. nat.)

an der Fakultät Chemie und Pharmazie

der Universität Regensburg

Deutschland



vorgelegt von

Verena Muhr

aus Roding

im Jahr 2017

Die vorliegende Dissertation entstand in der Zeit von November 2013 bis November 2017 am Institut für Analytische Chemie, Chemo- und Biosensorik der Universität Regensburg.

Die Arbeit wurde angeleitet von Prof. Dr. Antje J. Bäumner und Dr. Thomas Hirsch.

Promotionsgesuch eingereicht am: 06. November 2017

Kolloquiumstermin: 08. Dezember 2017

Prüfungsausschuss

Vorsitzender: Prof. Dr. Oliver Tepner

Erstgutachterin: Prof. Dr. Antje J. Bäumner

Zweitgutachter: Prof. Dr. Otto S. Wolfbeis

Drittprüfer: PD. Dr. Miriam Breunig

DANKSAGUNG

Zuallererst möchte ich mich bei **Prof. Dr. Antje Bäumner** und **Dr. Thomas Hirsch** für die Möglichkeit bedanken, meine Promotion über dieses spannende Thema anfertigen zu können. Vielen Dank für die stete Betreuung, Unterstützung und Hilfe bei Problemstellungen aller Art.

Mein herzlicher Dank geht ebenfalls an **Prof. Dr. Otto S. Wolfbeis** für das Liefern exzellenter wissenschaftlicher Fragestellungen und die Übernahme des Zweitgutachtens.

Vielen Dank an **PD Dr. Miriam Breunig** für die Übernahme der Aufgabe des Drittprüfers und **Prof. Dr. Oliver Tepner** für das Ausüben der Funktion des Prüfungsvorsitzenden.

Bei **Dr. Stefan Wilhelm**, **Dr. Christoph Fenzl** und **Sandy Himmelstoß** bedanke ich mich für ihre Geduld für die unzähligen TEM Aufnahmen.

Danke an **Joachim Rewitzer** und **Vanessa Tomanek** für ihre Unterstützung bei den ICP-OES Messungen.

Mein Dank geht auch an **Prof. Dr. Joachim Wegener**, **Barbara Goricnik** und **Lisa Sauer** für die Zusammenarbeit bei allen Zellfragen.

Den Arbeitsgruppen um **Dr. Ute Resch-Genger** an der Bundesanstalt für Materialforschung und -prüfung in Berlin und **Prof. Yves Mély** an der Universität Straßburg danke ich für die erfolgreichen Kooperationen bei der photophysikalischen Charakterisierung der Nanopartikel.

Beim **Upcon-Team**, allen voran bei **Dr. Thomas Hirsch**, bedanke ich mich für die unzähligen hilfreichen wissenschaftlichen und auch nicht-wissenschaftlichen Anregungen und Diskussionen.

Vielen, vielen Dank auch an die gesamte aktuelle und ehemalige **Arbeitsgruppe „4. Stock“** und **alle Kollegen** am Institut für die ausgezeichnete Arbeitsatmosphäre und vor allem all die geselligen Abende zur Auflockerung des Arbeitsalltags.

Zu guter Letzt möchte ich mich bei meiner **Familie** für ihre fortwährende Unterstützung in jeglicher Hinsicht herzlichst bedanken.

TABLE OF CONTENTS

1	Introduction to Lanthanide-doped Nanomaterials	1
1.1	Lanthanide Luminescence	1
1.2	Upconversion Nanoparticles	5
2	Motivation and Objectives.....	19
3	Upconversion Nanoparticles: From Hydrophobic to Hydrophilic Surfaces	21
3.1	Abstract	21
3.2	Introduction.....	23
3.3	Surface Modification of Hydrophobic UCNPs.....	25
3.3.1	Modification of the Original Ligand.....	25
3.3.2	Amphiphilic Coatings	25
3.3.3	Encapsulation with Inorganic Materials or Noble Metals Forming a Shell.....	30
3.3.4	Replacement of the Native Ligand	34
3.4	Conclusions	40
	References.....	42
4	Particle-Size Dependent Förster Resonance Energy Transfer from Upconversion Nanoparticles to Organic Dyes	51
4.1	Abstract	51
4.2	Introduction.....	53
4.3	Results and Discussion	55
4.3.1	Synthesis of Hydrophobic UCNPs with Controlled Sizes	55
4.3.2	Design of the FRET UCNP-Platform.....	56
4.3.3	Size-dependent FRET Efficiency	59
4.3.4	Influence of Luminescence Enhancement on FRET Efficiency	65
4.4	Conclusions	66
4.5	Materials and Methods	67
	Acknowledgements	70

References.....	70
5 Surface Engineering of Upconversion Nanoparticles for Time-Resolved Analysis of ATP-Responsive Energy Transfer.....	75
5.1 Abstract.....	75
5.2 Introduction.....	77
5.3 Results and Discussion.....	79
5.3.1 Design, Synthesis and Characterization of UCNPs.....	79
5.3.2 Surface Modification and Attachment of the ATP Aptamer.....	81
5.3.3 Cytotoxicity Studies and Cellular Uptake.....	83
5.3.4 Sensing Properties of Aptamer-modified UCNPs.....	85
5.3.5 Selectivity of the ATP Nanoprobe.....	88
5.4 Conclusions.....	89
5.5 Materials and Methods.....	90
Acknowledgements.....	94
References.....	95
6 Conclusions and Future Perspectives.....	99
6.1 Particle Architectures for FRET-based Applications.....	99
6.2 Future Directions.....	101
6.3 Remaining Challenges.....	104
7 Summary.....	111
8 Zusammenfassung.....	113
Curriculum Vitae.....	115
Publications.....	117
Presentations.....	119

1 INTRODUCTION TO LANTHANIDE-DOPED NANOMATERIALS

1.1 Lanthanide Luminescence

1.1.1 Luminescent Reporters in Bioanalysis

Luminescence has fascinated humans for centuries and is considered one of the most significant and powerful tools in (bio)analytical chemistry today.^{1,2} Optical biosensors consist of a combination of a bioreceptor as recognition element, e.g. enzymes, nucleic acids, or even whole cells, and an optical reporter system which generates a defined signal directly linked to the concentration of the respective analyte. Examples for the optical transducer are absorption, luminescence and reflectance.³ Fluorescence based detection is often characterized by fast responses and high resolution and sensitivities, which can even reach the single-molecule level,^{4,5} and both intensity and lifetime of the luminescence emission are available as optical reporter. The application of luminophores as tags and labels for the quantification and imaging of (bio)analytical targets that do not display intrinsic fluorescent properties at all (e.g. most small metabolites, ions) or only to an insufficient degree (e.g. DNA, proteins) is prevalent in all fields of life science. Central characteristics of ideal luminescent reporters in bioanalysis are (a) high molar absorption coefficients and (b) quantum yields for high brightness, (c) photostability, (d) chemical stability, (e) simple functionalization with receptors (f) solubility in physiological hydrophilic media, such as buffers and cell culture media, and both (g) low cytotoxicity and (h) no excitation/emission wavelengths in the ultra-violet (UV) for applications in living cells combined with minimized photo-damage and light scattering. The importance and impact of luminescence-based biosensing and -imaging in current research is reflected by the selection of Nobel Prize laureates in chemistry during the last decade. Osamu Shimomura, Martin Chalfie and Roger Y. Tsien were awarded the Nobel Prize for the discovery of the green fluorescent protein in 2008 and Eric Betzig, Stefan Hell and William E. Moerner received the Nobel Prize for their outstanding contributions to the development of super-resolution fluorescence microscopy in 2014. These accomplishments have proven that luminescence-based techniques can provide the ability to discover and understand the secrets of life, but the incredible amount of ongoing research demonstrates that there is still much left to be learned in order to cross current boundaries.

The oldest and still most common luminophores are molecular chromophores, i.e. organic dyes and metal ion complexes.⁶ The whole visible spectrum of light and the bordering ranges

are indeed covered by the huge amount of available luminophores of this type. However, common challenges of molecular luminophores are limited photostability upon prolonged photoexcitation and broad absorption and emission bands exhibiting only small Stokes shifts, which promotes reabsorption of the emitted light and impedes clear separation between excitation light, luminescence emission and background fluorescence of biological materials. Luminescent nanomaterials, such as quantum dots, carbon dots and gold nanoparticles have been established as alternatives to organic fluorophores to circumvent these issues due to their high photostability and capability of color tuning by modulation of the particle size.^{7,8}

1.1.2 Optical Properties of Lanthanide Ions

Lanthanide ions (rare earth ions) represent a class of luminescent materials with exceptional and unusual optical properties. This is represented by their diverse fields of applications, ranging from active materials in solid-state lasers (e.g. Nd³⁺- or Er³⁺-doped yttrium-aluminium-garnet),⁹ to Er³⁺-doped glass fibers used for telecommunication,¹⁰ and lanthanide complexes applied as anti-counterfeiting features,¹¹ or luminescent reporters in theranostics.¹² In contrast to many other luminophores, their luminescence shows multiple sharp emission bands and very large Stokes shifts > 100 nm. This means, emitted light can easily be distinguished from excitation radiation, which usually is ultraviolet or visible light. Their outstanding optical properties arise from the unique electronic structure that all lanthanides have in common. Lanthanides possess the ground state electronic configuration [Xe] 4fⁿ (n = 0-14). They exist almost exclusively in the trivalent state, Ln(III). The energy levels of their excited states are generally well defined and insensitive to the environment (ligand field) due to the effective shielding of the 4f orbitals by the xenon core. This leads to characteristic, almost line-like emission bands from the respective f-f transitions.¹³ The energy level diagrams of the Ln(III) aqua-ions are displayed in Figure 1.1.

Lanthanides show ladder-like energy levels with very stable excited states, leading to long luminescence decay times and efficient population of the higher energy levels. However, the small energy gaps between the single excited states facilitate non-radiative deactivation processes and suppress luminescence.¹⁴ Samarium, europium, gadolinium, terbium and dysprosium reveal the largest energy gaps between two neighboring energy levels among the lanthanide ions and thus exhibit the strongest intrinsic luminescence upon UV excitation (Stokes emission). The long-lived excited states and luminescence lifetimes of several hundred microseconds or even milliseconds make these lanthanide-based materials candidates for time-gated fluorometry in biological imaging.¹⁵ Here, background fluorescence can be almost completely excluded by exploiting the delay between excitation pulse and

acquisition of the luminescence signal, since fluorescence originating from biological matter usually decays within less than 10 ns.

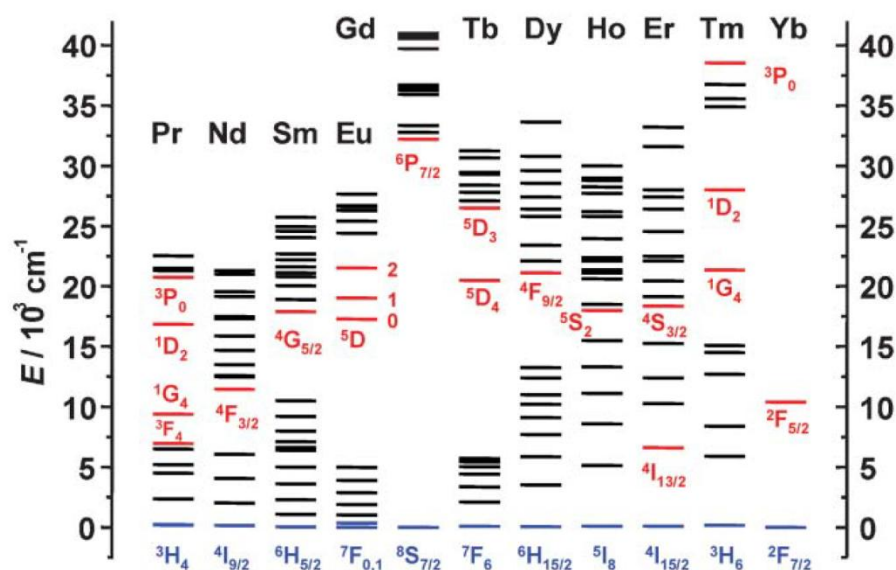


Figure 1.1 | Energy diagrams for the lanthanide aqua-ions. The luminescent levels are shown in red, while the fundamental level is indicated in blue. Adapted from reference 13 with permission of The Royal Society of Chemistry.

The molar absorption coefficient of the lanthanides is generally quite low with often less than $1 \text{ M}^{-1}\text{cm}^{-1}$, due to the f-f transitions being forbidden according to Laporte's parity rule.¹⁶ This limitation can be overcome by the use of high energy excitation sources or the introduction of strongly absorbing light harvesting ligands that collect the excitation energy and subsequently transfer it to the lanthanide ion in the center, which then emits the photon.¹⁷ These antenna ligands, however, often are susceptible to photobleaching, just like organic dyes, and limit the solubility of the lanthanide complex. Another possibility is the confinement of ions inside solid host materials that cause a distortion of the orbital symmetry and increase the probability of the f-f transitions.¹⁸ Especially during the last two decades a large variety of lanthanide doped nanomaterials has been developed. The emission color of the nanoparticles can be tuned by the amount and type of lanthanide ions doped into the host lattice.

Ln(III) doped nanoparticles display several advantages compared to other nanomaterials that are often used as alternatives to molecular fluorophores. Unlike II-IV and III-V semiconductor quantum dots¹⁹ and molecular fluorophores,²⁰ Ln(III) based materials show no fluorescence intermittence (also called blinking).²¹ Dye doped polymer particles are prone to

photobleaching and dye leakage upon swelling in aqueous environments, both of which does not apply for Ln(III) based nanoparticles.²²

Due to these exceptional features, lanthanide doped nanoparticles have found their way into bioanalytical and theranostic applications ranging from luminescence imaging and sensing based on Förster resonance energy transfer (FRET)²³ to photodynamic therapy.²⁴ We employed Eu³⁺-doped GdVO₄ nanoparticles for the detection of hydrogen peroxide and designed an enzymatic assay for glucose via measurement of the quantity of H₂O₂ formed resulting from the catalytic action of glucose oxidase in collaboration with colleagues from the University of Belgrade, Serbia (Figure 1.2).²⁵

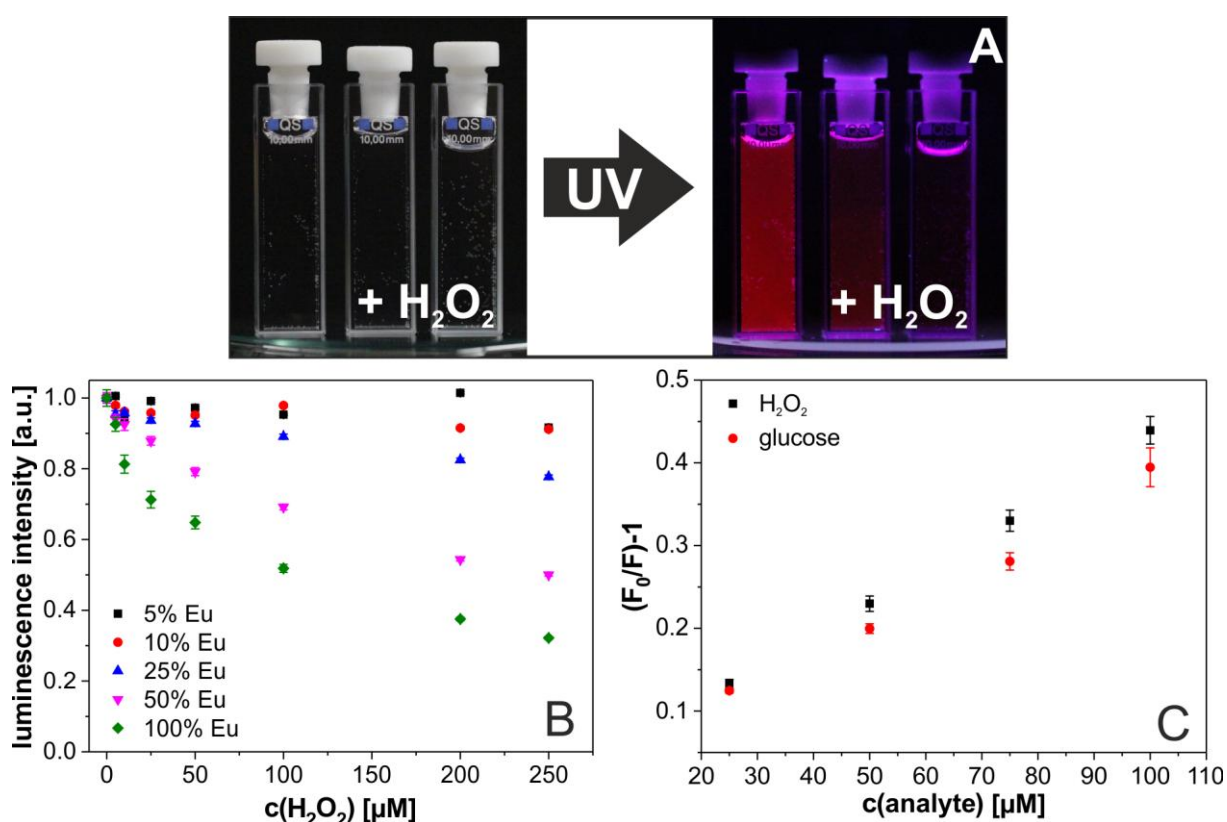


Figure 1.2 | (A) Digital photograph of a dispersion of GdVO₄(50%Eu) nanoparticles in water before and after the addition of two different concentrations of H₂O₂. The decrease of the luminescence intensity in presence of H₂O₂ is clearly visible. (B) Quenching of the (normalized) luminescence of Eu³⁺-doped GdVO₄ nanoparticles (λ_{exc} 298 nm, λ_{em} 618 nm; pH 7.4) by H₂O₂ as a function of the % fraction of Eu³⁺ dopant. The total concentration of Eu³⁺ always was adjusted to 0.4 mM. (C) Stern-Volmer plots of the emission of GdVO₄(50%Eu) nanoparticles in the presence of various concentrations of H₂O₂ and glucose.

1.2 Upconversion Nanoparticles

1.2.1 Mechanism of Upconversion Luminescence

The ladder-like and long-lived metastable excited states of the lanthanide ions enable the occurrence of another optical phenomenon that was first described for bulk materials by Auzel, Ovsyankin and Feofilov in the 1960s: photon upconversion.²⁶ This term describes a non-linear optical process generated by the sequential absorption of at least two low energy photons, which leads to the population of higher energy levels followed by the emission of one photon with higher energy and shorter wavelength than the excitation light. This unique feature makes upconversion luminescent nanoparticles (UCNPs) promising candidates for security printing,²⁷ enhancement of solar cell efficiency,²⁸ implementation as photocatalysts,²⁹ and, most importantly, application as labels, probes and reporters for theranostics, biosensing and bioimaging.³⁰ The excitation wavelength in the near-infrared region (typically at 980 nm) is within the "optical window" of biological tissue, where the absorption of the biological matrix is at a minimum. This allows for deep tissue penetration and simultaneously reduced photo-damage compared to the much higher energy of UV/visible light, which is needed to excite Stokes-emitting molecules and materials. The NIR excitation also triggers virtually no background fluorescence and enables high sensitivity during measurements with extraordinarily high signal-to-noise ratios.

Three main mechanisms for photon upconversion have been described: excited state absorption, energy transfer upconversion, and photon avalanche.³¹ Schematic representations of these mechanisms are shown in Figure 1.3. Energy transfer upconversion (ETU) is much more efficient than excited state absorption and, unlike photon avalanche, does not require a critical (high) excitation power and does not result in delayed luminescence emission caused by the reoccurring relaxation - excitation cycles.³² Therefore, most existing upconversion materials are based on ETU. The so-called sensitizer ion is responsible for the resonant photon absorption. The energy is then transferred to a neighboring activator ion. This leads to the relaxation of the sensitizer ion back to the ground state and the promotion of the activator ion to a higher energy level. This process is repeated for one (or several) more times, which leads to the population of the second (or higher) excited state of the activator. The transition of the activator back to its ground state causes the emission of a higher energy photon. In such materials upconversion emission can already be stimulated using low power (power densities starting from 10 W·cm⁻²) continuous wave (CW) diode lasers. The required excitation power is much lower than for simultaneous

two-photon absorption processes used for example in two-photon excitation microscopy, in which expensive pulsed lasers operating at power densities up to $10^9 \text{ W}\cdot\text{cm}^{-2}$ are applied.³³

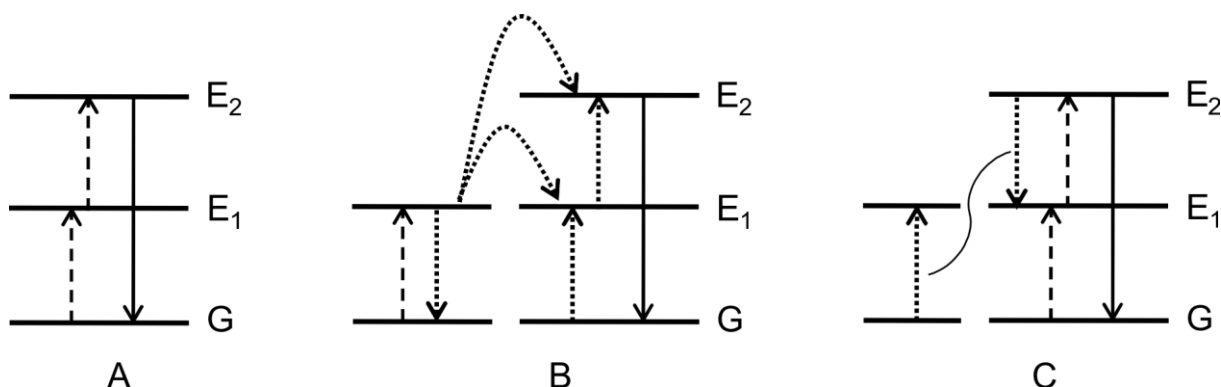


Figure 1.3 | Simplified representations of the three main upconversion processes (A) excited state absorption, (B) energy transfer upconversion, (C) photon avalanche. Dashed arrows symbolize photon absorption, full arrows show photon emission and dotted arrows refer to non-radiative processes. G, E1 and E2 represent ground state, excited level 1, and excited level 2, respectively.

1.2.2 Characteristics and Composition

Inorganic UCNPs usually are composed of an inert host crystal lattice doped with metal ions. Transition metal ions, e.g. Ti^{2+} , Re^{3+} , or Os^{4+} , have been reported as luminescent dopants,³⁴ but trivalent lanthanide ions show by far the most promising features for efficient photon upconversion. Yb^{3+} ions represent the most popular sensitizers. They possess a molar absorption coefficient of $10 \text{ M}^{-1}\text{cm}^{-1}$, which is very high considering that the absorption promotes parity forbidden f-f transitions.¹⁶ A typical absorption spectrum of Yb^{3+} is shown in Figure 1.4. The main absorbance of Yb^{3+} is in the near infrared (NIR) region at a wavelength of 978 nm. Therefore, the Yb^{3+} ions acting as sensitizers can be efficiently excited by conventional 980 nm low power (hand held) diode lasers. The energy conserved in the ${}^2\text{F}_{5/2}$ electronic state of the Yb^{3+} ions can be transferred to activator ions, which act as the luminescent centers in the nanoparticles. Most common activators are Er^{3+} and Tm^{3+} , but upconversion luminescence originating from other lanthanide ions, like Ho^{3+} , Tb^{3+} and Eu^{3+} ions has also been reported.^{35,36}

The upconversion efficiency of UCNPs is strongly dependent on the host material. The energy transfer dynamics between sensitizer-sensitizer and sensitizer-activator is influenced by the ion-ion distances within the host crystal lattice. Suitable host lattices in this regard are metal oxides and halogenides, such as Y_2O_3 , YVO_4 , LaF_3 , and NaYF_4 .³¹ The fluoride host is superior to oxide materials due to its low phonon energy around 350 cm^{-1} . This avoids energy loss caused by multiphonon relaxation between the metastable states inside the

crystal lattice and promotes upconversion efficiency. Fluoride materials with Na^+ , Ca^{2+} , and Y^{3+} as cations additionally provide chemical stability. Therefore NaYF_4 is regarded as the most efficient and most widely used upconversion host material.

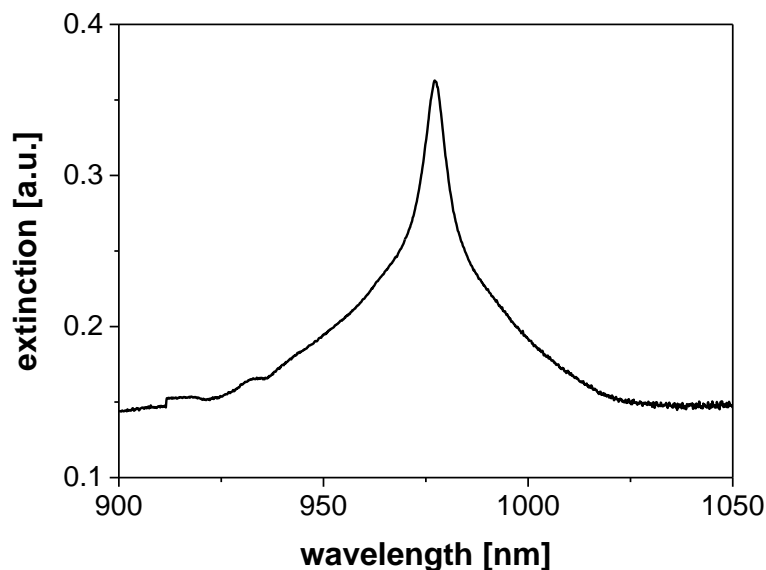


Figure 1.4 | Absorption spectrum of oleate-capped $\beta\text{-NaYF}_4$ (20% Yb, 2% Er) UCNPs dispersed in cyclohexane at a particle concentration of $22 \text{ mg}\cdot\text{mL}^{-1}$. The optical path length of the cuvette was 5 cm, the slit width was 1 nm.

The ionic radius of Y^{3+} is very similar to that of trivalent lanthanide ions and can consequently be easily exchanged by the rare earth ions without significantly disturbing the overall crystal structure.³⁷ This offers the option to design a number of various nanomaterials with diverse electromagnetic properties depending on the chosen dopants. Magnetic properties for MRT applications can be introduced, if the host material is doped with Gd^{3+} ions. Doping with Eu^{3+} or Tb^{3+} leads to “downconversion” luminescence upon UV excitation, while doping with Yb^{3+} , Tm^{3+} , Er^{3+} or Ho^{3+} produces upconversion luminescence.³⁸ The combination of such different doping possibilities enables the design of multimodal nanoparticles. Thermodynamically stable phases of NaYF_4 at room temperature are the cubic α -phase and the hexagonal β -phase. However, the upconversion efficiency is about ten times higher in $\beta\text{-NaYF}_4$ compared to $\alpha\text{-NaYF}_4$ due to a more favorable spatial arrangement of the dopants within the hexagonal β -crystal phase.³⁹ The probability of resonant energy transfer processes between Yb^{3+} and Er^{3+} is increased by optimal ion-ion distances creating efficient photoactive sites in $\beta\text{-NaYF}_4$.⁴⁰

1.2.3 Photophysical Properties

One of the highest upconversion efficiencies so far has been reported for a β -NaYF₄ host lattice doped with either 20 mol% Yb³⁺ as sensitizer and 2 mol% Er³⁺ as activator or 25 mol% Yb³⁺ as sensitizer and 0.3 mol% Tm³⁺ as activator. Upconversion quantum yields of 0.1% have been reported for these particles (diameter of 22 nm) already at low excitation power densities (around 50 W·cm⁻¹).⁴¹ While higher amounts of Yb³⁺ would increase the absorption of the material, they also induce increased sensitizer-sensitizer relaxations and activator-sensitizer back transfers that counteract the population of the higher electronic states in the activator ions. The same is true for higher doping concentrations of the activator, which can promote undesired non-radiative activator-activator relaxations.⁴²

The energy level diagrams of the lanthanide ions in NaYF₄:Yb³⁺/Er³⁺ and NaYF₄:Yb³⁺/Tm³⁺ and the mechanisms leading to the population of the excited states are shown in Figure 1.5. The pair Yb/Er generates two main upconversion emission bands upon excitation at 980 nm, one in the green region between 500 nm and 550 nm and one in the red region between 640 nm and 680 nm. The green emission originates from the transitions from ²H_{11/2} and ⁴S_{3/2} back to the ground state ⁴I_{15/2} in Er³⁺. The red emission can be ascribed to the ⁴F_{9/2} → ⁴I_{15/2} transition. The green emission is more intense than the red one as a result of different pathways leading to the population of the two distinct emissive states, which imparts a colloidal dispersion of the nanoparticles with the impression of predominantly green luminescence. All three excited electronic states in Er³⁺ are mainly populated by a two-photon ETU pathway. Higher order population pathways of energy states occur for the main upconversion emissions of the pair Yb/Tm. The ultraviolet emission around 360 nm (¹D₂ → ³H₆) and one of two blue (¹D₂ → ³F₄) emission bands at 450 nm are populated by the sequential absorption of four NIR photons. The second blue emission (¹G₄ → ³H₆) at 475 nm is generated by the absorption of three NIR photons. The most intense Tm³⁺ emission (³H₄ → ³H₆) is in the NIR around 800 nm and is populated by a two-photon ETU pathway. But since the NIR and UV emissions are not visible by the human eye, Yb/Tm doped UCNPs give the impression of blue luminescence. A photograph of colloidal dispersions of β -NaYF₄:Yb³⁺,Er³⁺ and β -NaYF₄:Yb³⁺,Tm³⁺ UCNPs in cyclohexane indicating the multicolor main upconversion emission bands is depicted in Figure 1.6.

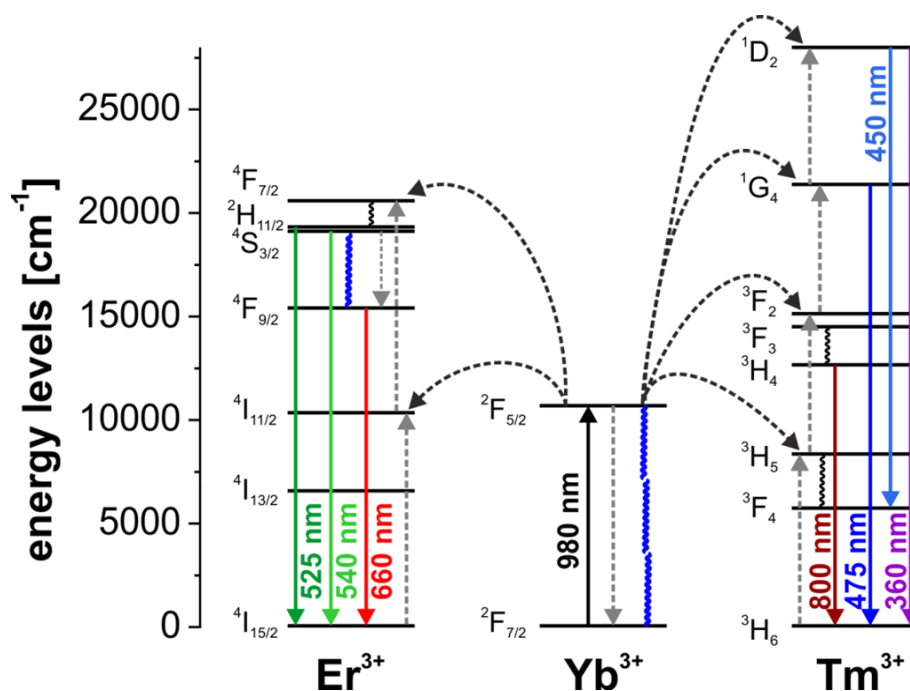


Figure 1.5 | Energy level diagrams of the lanthanide ions in $\text{NaYF}_4:\text{Yb}^{3+}/\text{Er}^{3+}$ and $\text{NaYF}_4:\text{Yb}^{3+}/\text{Tm}^{3+}$. The solid and dotted black and grey arrows represent photon absorption, the solid colored arrows photon emission, the curly black lines non-radiative relaxations, and the curly blue lines non-radiative relaxations favored by high energy O-H vibrations.

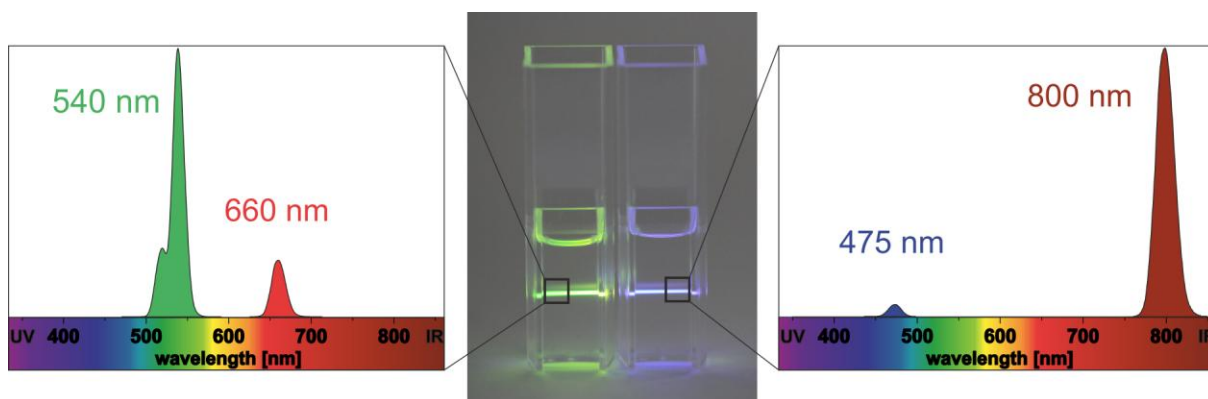


Figure 1.6 | (Middle) Dispersion of hydrophobic $\text{NaYF}_4:\text{Yb}^{3+},\text{Er}^{3+}$ and $\beta\text{-NaYF}_4:\text{Yb}^{3+},\text{Tm}^{3+}$ UCNPs in cyclohexane displaying predominantly blue or green luminescence upon 980 nm CW laser excitation. (Left and right) Corresponding upconversion luminescence spectra upon 980 nm CW laser excitation. The wavelengths of the individual peak maxima are given for each of the two distinct main peaks in either the blue and NIR or the green and red spectral region, respectively.

The small particle dimensions ($d < 50$ nm) needed for bioanalytical applications, i.e. uptake into cells and interaction with biomolecules, amplify all surface related effects. The massive increase of the surface-to-volume ratio by the reduction of the particle dimensions down to the nm regime leads to increased (non-radiative) surface deactivation caused by quenching by surface ligands, solvent molecules and crystal defects.⁴³ Consequently, the quantum yield

of UCNPs is much lower than that of the bulk material. The upconversion quantum yield in nanoparticles scarcely reaches values above 1% and heavily depends on even slight changes of the particle diameter and excitation power density.^{41,44} Surface quenching is most pronounced in aqueous solvents as a result of increased deactivation of Ln(III) excited states by O-H vibrations of water molecules.⁴¹ Core-shell particle architectures provide a possibility to minimize surface deactivation by protecting the surface of the emissive UCNP core. Inert shells, usually consisting of non-doped host material, efficiently prevent water molecules (or quenchers in general) coming close to the active particle core and lead to enhanced upconversion luminescence quantum yield, emission intensity and lifetime in all solvents.⁴⁵ A shell thickness of ≥ 10 nm almost completely suppresses surface quenching and no further luminescence enhancement is achieved with even thicker shells.⁴⁶

1.2.4 Synthesis and Surface Modification

Sophisticated and reproducible synthesis protocols are necessary to control the crystal size and composition, ensure monodisperse particle (and shell) growth, avoid crystal defects, and optimize the spatial arrangement of sensitizer and activator ions in the crystal lattice for the design of high quality upconversion nanomaterials.⁴⁷ Many synthesis methods for the fabrication of efficient UCNPs have been described during the last years. Several recent reviews give a comprehensive overview of the characteristics of different synthetic strategies, including thermal decomposition, co-precipitation, hydro-/solvothermal methods and combinations of these techniques.⁴⁸ Most prevalent is the high temperature synthesis performed in solvent mixtures of oleic acid and 1-octadecene at 300 °C first reported by Li et al. in 2008.⁴⁹ This technique enables the fabrication of oleate-capped, pure β -NaYF₄ nanocrystals doped with lanthanide ions that display outstanding quality in terms of monodispersity, shape uniformity, and upconversion luminescence efficiency for large batches of several grams of UCNPs.⁵⁰ The size and shape of the UCNPs can be tuned by altering the ratio of oleic acid and 1-octadecene,⁵¹ by varying the Na⁺ content,⁵² or by addition of Gd³⁺ as further dopant.⁵³ An example of β -NaYF₄:Yb,Er UCNPs synthesized by this high temperature procedure is depicted in Figure 1.7. The transmission electron micrograph shows the narrow size distribution structure of the resulting UCNPs.

The surface of the particles is stabilized by oleate molecules, which causes dispersibility only in hydrophobic organic solvents. Since such particles cannot be dispersed in water due to the oil-based synthesis, further surface modification is necessary before the UCNPs can be applied in biosensing and -imaging. Most common surface modification techniques that have been established for the functionalization of hydrophobic nanoparticles, such as quantum

dots, magnetic particles and UCNPs are (a) ligand exchange, (b) additional coating with amphiphilic molecules, and (c) encapsulation with silica. These three strategies greatly differ regarding time consumption and optical and physical properties of the functionalized, hydrophilic UCNPs.⁵⁴ Amphiphilic coatings and encapsulation with silica are expected to provide better protection against surface deactivation compared to ligand exchange as a result of the additional hydrophobic layer or increased distance between particle surface and solvent molecules, leading to stronger luminescence. They also tend to possess higher colloidal stability in physiological media. Colloidal stability depends on an efficient electrostatic and/or steric stabilization, which is challenging to maintain in biological environments with high ionic strengths. Ligand exchange gives the impression of the most versatile strategy resulting in overall smallest particle sizes due to direct attachment of the new ligand to the UCNP surface. Stability in buffered solutions can be improved by the use of polymers as chelating ligands or molecules containing phosphonates as strongly coordinating groups towards the UCNPs. Since all of these factors influence the performance of UCNPs in bioanalytical applications, it is of great importance to develop specific surface modification strategies precisely tailored towards the final application.

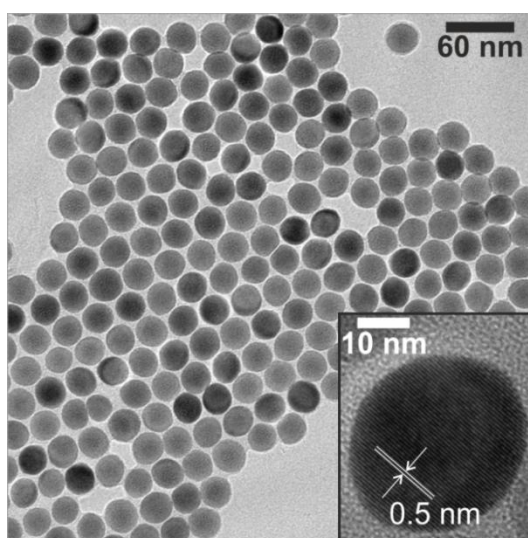


Figure 1.7 | Transmission electron micrograph (scale bar: 60 nm) of oleate-capped $\text{NaYF}_4:\text{Yb}^{3+},\text{Er}^{3+}@\text{NaYF}_4$ core-shell UCNPs with a mean diameter of 28.8 ± 1.0 nm. The core particles used for the synthesis had a diameter of 21.1 ± 1.0 nm, and the thickness of the inert shell is almost 4 nm. The inset shows a higher magnification (scale bar: 10 nm) of one core-shell particle. The difference between core and shell is not visible, since the two very similar materials display the same contrast in the images. The regular orientation of the lattice planes indicates the uniform growth of the NaYF_4 -shell in all directions. The distance between the visible lattice planes is 0.5 nm.

1.2.5 Current Applications and Challenges

The exceptional optical properties of UCNPs and advances in the field of nanoparticle synthesis leading to the controlled preparation of complex particle architectures meet many criteria that define efficient luminescent reporters in bioanalysis and for theranostic applications⁵⁵ and have led to UCNPs being the focus of intensive research in these fields over the last decade. They have been applied as luminescent reporters for the detection and quantification of a multitude of different target analytes. A vast number of recent publications report on the development of upconversion nanoproboscopes for the determination of e.g. heavy metal ions,⁵⁶ mycotoxins,⁵⁷ viruses,⁵⁸ bacteria,⁵⁹ and hemoglobin.⁶⁰ Loading of UCNPs with active ingredients enabled imaging guided drug delivery and cancer therapy.⁶¹⁻⁶³ Cellular uptake provided a nanoplatform for photodynamic therapy with UCNPs acting as *in situ* nanolamps for indirect excitation of photosensitizers with reduced damage to surrounding, healthy tissue.^{64,65} UCNPs have also been successfully used for super-resolution fluorescence microscopy to achieve nanoscopic resolutions.⁶⁶

The abundance of ongoing studies demonstrates the demand for new luminescent probes and also the perspectives offered by a complete understanding of upconversion luminescence. However, there are still some unsolved questions limiting the exploitation of the full theranostic potential of UCNPs. One major challenge is the need for efficient surface engineering providing both colloidal stabilization in physiological media and functionalization with selective receptor molecules, and simultaneously enabling (sub)cellular targeting. The combination of all these features while at the same time keeping particle crosslinking and cytotoxicity at a minimum is crucial for the creation of stable, target-responsive nanoproboscopes. Another challenge is to increase the understanding of influences on upconversion luminescence emission. The luminescence intensity is dependent on many different parameters, e.g. particle size, architecture, and concentration, solvent, excitation power density, light scattering, and surface coating. All these influences must be considered to design efficient nanoproboscopes for diverse applications.⁶⁷

Exploitation of Förster resonance energy transfer (FRET) enables the elimination of many of these dependencies. This non-radiative energy transfer process takes place between two (fluorescent) molecules very close to each other, usually within less than 10 nm, and is extremely distance dependent.⁶⁸ FRET is the most powerful analytical method for monitoring bioaffinity reactions, e.g. DNA hybridization⁶⁹ and receptor interactions,⁷⁰ due to its ability to act as a "nanoscopic ruler". The two energy transfer partners must display an overlap of the luminescence emission spectrum of one molecule (energy donor) with the absorption spectrum of the second one (energy acceptor). Characteristic for successful FRET is the

reduction of the donor luminescence intensity and lifetime, i.e. the stronger the reduction, the higher the FRET efficiency. In contrast to conventional organic dyes usually used as donors for FRET-based detection schemes, UCNPs possess long lifetimes in the range of 100 μs up to over 1 ms. Their decay times are thus ascertainable with very simple instrumentation, e.g. a conventional CW laser source and an optical chopper wheel for mechanical intermittence of the excitation light, and changes are easily detectable. Unlike the emission intensity, the lifetime of UCNPs is mostly unaffected by several critical parameters, e.g. (a) its concentration, which can be challenging to determine especially in the case of nanoparticles, (b) radiative absorption processes, i.e. inner filter effects capable of influencing the changes of the emission intensity, (c) fluctuations in the power density of the excitation source, which can cause changing intensity ratios as a result of the nonlinear nature of the absorption process preceding the UC emission, and (d) luminescence light scattering typically induced in all biological tissues. FRET also impacts the acceptor lifetime. When FRET occurs, the luminescence decay time of the acceptor molecule is equal to the donor lifetime. For organic dyes acting as acceptors in combination with UCNP donors this should lead to an elongation of their originally short lifetimes in the lower ns to ps range to $> 100 \mu\text{s}$. Such an extreme effect is also easily detectable. Despite the considerable advantages of time-resolved FRET studies, most current FRET-based detection schemes rely on changes of the upconversion intensity.⁷¹ A more detailed understanding of FRET with UCNPs may promote the development of lifetime-based upconversion nanoprobe and the expansion and improvement within their fields of application.

References

- (1) Roda, A.; Mirasoli, M.; Michelini, E.; Di Fusco, M.; Zangheri, M.; Cevenini, L.; Roda, B.; Simoni, P. Progress in Chemical Luminescence-based Biosensors: A Critical Review. *Biosens. Bioelectron.* **2016**, *76*, 164–179.
- (2) Yuan, L.; Lin, W.; Zheng, K.; He, L.; Huang, W. Far-red to Near-infrared Analyte-responsive Fluorescent Probes Based on Organic Fluorophore Platforms for Fluorescence Imaging. *Chem. Soc. Rev.* **2013**, *42*, 622–661.
- (3) Borisov, S. M.; Wolfbeis, O. S. Optical Biosensors. *Chem. Rev.* **2008**, *108*, 423–461.
- (4) Deschout, H.; Zanicchi, F. C.; Mlodzianoski, M.; Diaspro, A.; Bewersdorf, J.; Hess, S. T.; Braeckmans, K. Precisely and Accurately Localizing Single Emitters in Fluorescence Microscopy. *Nat. Methods* **2014**, *11*, 253–266.
- (5) Ma, F.; Li, Y.; Tang, B.; Zhang, C.-y. Fluorescent Biosensors Based on Single-Molecule Counting. *Acc. Chem. Res.* **2016**, *49*, 1722–1730.

- (6) Lee, M. H.; Kim, J. S.; Sessler, J. L. Small Molecule-based Ratiometric Fluorescence Probes for Cations, Anions, and Biomolecules. *Chem. Soc. Rev.* **2015**, *44*, 4185–4191.
- (7) Chen, G.; Roy, I.; Yang, C.; Prasad, P. N. Nanochemistry and Nanomedicine for Nanoparticle-based Diagnostics and Therapy. *Chem. Rev.* **2016**, *116*, 2826–2885.
- (8) Jaque, D.; Richard, C.; Viana, B.; Soga, K.; Liu, X.; García Solé, J. Inorganic Nanoparticles for Optical Bioimaging. *Adv. Opt. Photon.* **2016**, *8*, 1–103.
- (9) McCarty, R. J.; Stebbins, J. F. Investigating Lanthanide Dopant Distributions in Yttrium Aluminum Garnet (YAG) Using Solid State Paramagnetic NMR. *Solid State Nucl. Magn. Reson.* **2016**, *79*, 11–22.
- (10) Ainslie, B. J. A Review of the Fabrication and Properties of Erbium-doped Fibers for Optical Amplifiers. *J. Lightwave Technol.* **1991**, *9*, 220–227.
- (11) Andres, J.; Hersch, R. D.; Moser, J.-E.; Chauvin, A.-S. A New Anti-Counterfeiting Feature Relying on Invisible Luminescent Full Color Images Printed with Lanthanide-Based Inks. *Adv. Funct. Mater.* **2014**, *24*, 5029–5036.
- (12) Teo, R. D.; Termini, J.; Gray, H. B. Lanthanides: Applications in Cancer Diagnosis and Therapy. *J. Med. Chem.* **2016**, *59*, 6012–6024.
- (13) Bünzli, J.-C. G.; Piguet, C. Taking Advantage of Luminescent Lanthanide Ions. *Chem. Soc. Rev.* **2005**, *34*, 1048–1077.
- (14) Gai, S.; Li, C.; Yang, P.; Lin, J. Recent Progress in Rare Earth Micro/Nanocrystals: Soft Chemical Synthesis, Luminescent Properties, and Biomedical Applications. *Chem. Rev.* **2014**, *114*, 2343–2389.
- (15) Cardoso Dos Santos, M.; Hildebrandt, N. Recent Developments in Lanthanide-to-Quantum Dot FRET Using Time-gated Fluorescence Detection and Photon Upconversion. *Trends Anal. Chem.* **2016**, *84*, 60–71.
- (16) Bünzli, J.-C. G. On the Design of Highly Luminescent Lanthanide Complexes. *Coord. Chem. Rev.* **2015**, *293-294*, 19–47.
- (17) Moore, E. G.; Samuel, A. P. S.; Raymond, K. N. From Antenna to Assay: Lessons Learned in Lanthanide Luminescence. *Acc. Chem. Res.* **2009**, *42*, 542–552.
- (18) Han, S.; Deng, R.; Xie, X.; Liu, X. Enhancing Luminescence in Lanthanide-Doped Upconversion Nanoparticles. *Angew. Chem. Int. Ed.* **2014**, *53*, 11702–11715.
- (19) Galland, C.; Ghosh, Y.; Steinbruck, A.; Sykora, M.; Hollingsworth, J. A.; Klimov, V. I.; Htoon, H. Two Types of Luminescence Blinking Revealed by Spectroelectrochemistry of Single Quantum Dots. *Nature* **2011**, *479*, 203–207.
- (20) Dickson, R. M.; Cubitt, A. B.; Tsien, R. Y.; Moerner, W. E. On/Off Blinking and Switching Behaviour of Single Molecules of Green Fluorescent Protein. *Nature* **1997**, *388*, 355–358.
- (21) Zhou, J.; Xu, S.; Zhang, J.; Qiu, J. Upconversion Luminescence Behavior of Single Nanoparticles. *Nanoscale* **2015**, *7*, 15026–15036.
- (22) Reisch, A.; Klymchenko, A. S. Fluorescent Polymer Nanoparticles Based on Dyes: Seeking Brighter Tools for Bioimaging. *Small* **2016**, *12*, 1968–1992.

- (23) Sy, M.; Nonat, A.; Hildebrandt, N.; Charbonniere, L. J. Lanthanide-based Luminescence Biolabelling. *Chem. Commun.* **2016**, *52*, 5080–5095.
- (24) Bulin, A.-L.; Truillet, C.; Choukrat, R.; Lux, F.; Frochot, C.; Amans, D.; Ledoux, G.; Tillement, O.; Perriat, P.; Barberi-Heyob, M. *et al.* X-ray-Induced Singlet Oxygen Activation with Nanoscintillator-Coupled Porphyrins. *J. Phys. Chem. C* **2013**, *117*, 21583–21589.
- (25) Muhr, V.; Buchner, M.; Hirsch, T.; Jovanović, D. J.; Dolić, S. D.; Dramićanin, M. D.; Wolfbeis, O. S. Europium-doped GdVO₄ Nanocrystals as a Luminescent Probe for Hydrogen Peroxide and for Enzymatic Sensing of Glucose. *Sens. Actuators B Chem.* **2017**, *241*, 349–356.
- (26) Auzel, F. Upconversion and Anti-Stokes Processes with f and d Ions in Solids. *Chem. Rev.* **2004**, *104*, 139–174.
- (27) Meruga, J. M.; Baride, A.; Cross, W.; Kellar, J. J.; May, P. S. Red-Green-Blue Printing Using Luminescence-Upconversion Inks. *J. Mater. Chem. C* **2014**, *2*, 2221–2227.
- (28) Goldschmidt, J. C.; Fischer, S. Upconversion for Photovoltaics – a Review of Materials, Devices and Concepts for Performance Enhancement. *Adv. Opt. Mater.* **2015**, *3*, 510–535.
- (29) Xu, Z.; Quintanilla, M.; Vetrone, F.; Govorov, A. O.; Chaker, M.; Ma, D. Harvesting Lost Photons: Plasmon and Upconversion Enhanced Broadband Photocatalytic Activity in Core@Shell Microspheres Based on Lanthanide-Doped NaYF₄, TiO₂, and Au. *Adv. Funct. Mater.* **2015**, *25*, 2950–2960.
- (30) Zhou, J.; Liu, Q.; Feng, W.; Sun, Y.; Li, F. Upconversion Luminescent Materials: Advances and Applications. *Chem. Rev.* **2015**, *115*, 395–465.
- (31) Haase, M.; Schäfer, H. Upconverting Nanoparticles. *Angew. Chem. Int. Ed.* **2011**, *50*, 5808–5829.
- (32) Babu, P.; Martín, I. R.; Venkata Krishnaiah, K.; Seo, H. J.; Venkatramu, V.; Jayasankar, C. K.; Lavín, V. Photon Avalanche Upconversion in Ho³⁺-Yb³⁺ Co-doped Transparent Oxyfluoride Glass-Ceramics. *Chem. Phys. Lett.* **2014**, *600*, 34–37.
- (33) Park, Y. I.; Lee, K. T.; Suh, Y. D.; Hyeon, T. Upconverting nanoparticles: A Versatile Platform for Wide-field Two-photon Microscopy and Multi-modal in vivo Imaging. *Chem. Soc. Rev.* **2015**, *44*, 1302–1317.
- (34) Gamelin, D. R.; Güdel, H. U. Design of Luminescent Inorganic Materials: New Photophysical Processes Studied by Optical Spectroscopy. *Acc. Chem. Res.* **2000**, *33*, 235–242.
- (35) Xu, M.; Chen, D.; Huang, P.; Wan, Z.; Zhou, Y.; Ji, Z. A Dual-functional Upconversion Core@Shell Nanostructure for White-Light-Emission and Temperature Sensing. *J. Mater. Chem. C* **2016**, *4*, 6516–6524.
- (36) Dong, H.; Sun, L.-D.; Wang, Y.-F.; Xiao, J.-W.; Tu, D.; Chen, X.; Yan, C.-H. Photon Upconversion in Yb³⁺-Tb³⁺ and Yb³⁺-Eu³⁺ Activated Core/Shell Nanoparticles with Dual-band Excitation. *J. Mater. Chem. C* **2016**, *4*, 4186–4192.
- (37) Naccache, R.; Yu, Q.; Capobianco, J. A. The Fluoride Host: Nucleation, Growth, and Upconversion of Lanthanide-Doped Nanoparticles. *Adv. Opt. Mater.* **2015**, *3*, 482–509.

- (38) Chen, Q.; Wang, C.; Cheng, L.; He, W.; Cheng, Z.; Liu, Z. Protein Modified Upconversion Nanoparticles for Imaging-guided Combined Photothermal and Photodynamic Therapy. *Biomaterials* **2014**, *35*, 2915–2923.
- (39) Zeng, J.-H.; Su, J.; Li, Z.-H.; Yan, R.-X.; Li, Y.-D. Synthesis and Upconversion Luminescence of Hexagonal-Phase NaYF₄:Yb, Er³⁺ Phosphors of Controlled Size and Morphology. *Adv. Mater.* **2005**, *17*, 2119–2123.
- (40) Aebischer, A.; Hostettler, M.; Hauser, J.; Krämer, K.; Weber, T.; Güdel, H. U.; Bürgi, H.-B. Structural and Spectroscopic Characterization of Active Sites in a Family of Light-Emitting Sodium Lanthanide Tetrafluorides. *Angew. Chem. Int. Ed.* **2006**, *45*, 2802–2806.
- (41) Würth, C.; Kaiser, M.; Wilhelm, S.; Grauel, B.; Hirsch, T.; Resch-Genger, U. Excitation Power Dependent Population Pathways and Absolute Quantum Yields of Upconversion Nanoparticles in Different Solvents. *Nanoscale* **2017**, *9*, 4283–4294.
- (42) Johnson, N. J. J.; He, S.; Diao, S.; Chan, E. M.; Dai, H.; Almutairi, A. Direct Evidence for Coupled Surface and Concentration Quenching Dynamics in Lanthanide-Doped Nanocrystals. *J. Am. Chem. Soc.* **2017**, *139*, 3275–3282.
- (43) Wang, F.; Wang, J.; Liu, X. Direct Evidence of a Surface Quenching Effect on Size-Dependent Luminescence of Upconversion Nanoparticles. *Angew. Chem.* **2010**, *122*, 7618–7622.
- (44) Boyer, J.-C.; van Veggel, F. C. J. M. Absolute Quantum Yield Measurements of Colloidal NaYF₄:Er³⁺, Yb³⁺ Upconverting Nanoparticles. *Nanoscale* **2010**, *2*, 1417–1419.
- (45) Wang, F.; Deng, R.; Wang, J.; Wang, Q.; Han, Y.; Zhu, H.; Chen, X.; Liu, X. Tuning Upconversion Through Energy Migration in Core-Shell Nanoparticles. *Nat. Mater.* **2011**, *10*, 968–973.
- (46) Wang, Y.; Liu, K.; Liu, X.; Dohnalová, K.; Gregorkiewicz, T.; Kong, X.; Aalders, M. C. G.; Buma, W. J.; Zhang, H. Critical Shell Thickness of Core/Shell Upconversion Luminescence NanoplatforM for FRET Application. *J. Phys. Chem. Lett.* **2011**, *2*, 2083–2088.
- (47) Ma, C.; Xu, X.; Wang, F.; Zhou, Z.; Wen, S.; Liu, D.; Fang, J.; Lang, C. I.; Jin, D. Probing the Interior Crystal Quality in the Development of More Efficient and Smaller Upconversion Nanoparticles. *J. Phys. Chem. Lett.* **2016**, *7*, 3252–3258.
- (48) Yan, C.; Zhao, H.; Perepichka, D. F.; Rosei, F. Lanthanide Ion Doped Upconverting Nanoparticles: Synthesis, Structure and Properties. *Small* **2016**, *12*, 3888–3907.
- (49) Li, Z.; Zhang, Y.; Jiang, S. Multicolor Core/Shell-Structured Upconversion Fluorescent Nanoparticles. *Adv. Mater.* **2008**, *20*, 4765–4769.
- (50) Wilhelm, S.; Kaiser, M.; Würth, C.; Heiland, J.; Carrillo-Carrion, C.; Muhr, V.; Wolfbeis, O. S.; Parak, W. J.; Resch-Genger, U.; Hirsch, T. Water Dispersible Upconverting Nanoparticles: Effects of Surface Modification on their Luminescence and Colloidal stability. *Nanoscale* **2015**, *7*, 1403–1410.

- (51) Zhang, X.; Blasiak, B.; Marenco, A. J.; Trudel, S.; Tomanek, B.; van Veggel, F. C. J. M. Design and Regulation of NaHoF₄ and NaDyF₄ Nanoparticles for High-Field Magnetic Resonance Imaging. *Chem. Mater.* **2016**, *28*, 3060–3072.
- (52) Dühnen, S.; Rinkel, T.; Haase, M. Size Control of Nearly Monodisperse β-NaGdF₄ Particles Prepared from Small α-NaGdF₄ Nanocrystals. *Chem. Mater.* **2015**, *27*, 4033–4039.
- (53) Wang, F.; Han, Y.; Lim, C. S.; Lu, Y.; Wang, J.; Xu, J.; Chen, H.; Zhang, C.; Hong, M.; Liu, X. Simultaneous Phase and Size Control of Upconversion Nanocrystals through Lanthanide Doping. *Nature* **2010**, *463*, 1061–1065.
- (54) Wilhelm, S.; Kaiser, M.; Würth, C.; Heiland, J.; Carrillo-Carrion, C.; Muhr, V.; Wolfbeis, O. S.; Parak, W. J.; Resch-Genger, U.; Hirsch, T. Water Dispersible Upconverting Nanoparticles: Effects of Surface Modification on their Luminescence and Colloidal stability. *Nanoscale* **2015**, *7*, 1403–1410.
- (55) Chen, G.; Qiu, H.; Prasad, P. N.; Chen, X. Upconversion Nanoparticles: Design, Nanochemistry, and Applications in Theranostics. *Chem. Rev.* **2013**, *114*, 5161–5214.
- (56) Gu, B.; Zhou, Y.; Zhang, X.; Liu, X.; Zhang, Y.; Marks, R.; Zhang, H.; Liu, X.; Zhang, Q. Thiazole Derivative-modified Upconversion Nanoparticles for Hg²⁺ Detection in Living Cells. *Nanoscale* **2016**, *8*, 276–282.
- (57) Dai, S.; Wu, S.; Duan, N.; Wang, Z. A luminescence resonance energy transfer based aptasensor for the mycotoxin Ochratoxin A using upconversion nanoparticles and gold nanorods. *Microchim. Acta* **2016**, *183*, 1909–1916.
- (58) Tsang, M.-K.; Ye, W.; Wang, G.; Li, J.; Yang, M.; Hao, J. Ultrasensitive Detection of Ebola Virus Oligonucleotide Based on Upconversion Nanoprobe/Nanoporous Membrane System. *ACS Nano* **2016**, *10*, 598–605.
- (59) Wu, S.; Duan, N.; Shi, Z.; Fang, C.; Wang, Z. Simultaneous Aptasensor for Multiplex Pathogenic Bacteria Detection Based on Multicolor Upconversion Nanoparticles Labels. *Anal. Chem.* **2014**, *86*, 3100–3107.
- (60) Jo, E.-J.; Mun, H.; Kim, M.-G. Homogeneous Immunosensor Based on Luminescence Resonance Energy Transfer for Glycated Hemoglobin Detection Using Upconversion Nanoparticles. *Anal. Chem.* **2016**, *88*, 2742–2746.
- (61) Jalani, G.; Naccache, R.; Rosenzweig, D. H.; Haglund, L.; Vetrone, F.; Cerruti, M. Photocleavable Hydrogel-Coated Upconverting Nanoparticles: A Multifunctional Theranostic Platform for NIR Imaging and On-Demand Macromolecular Delivery. *J. Am. Chem. Soc.* **2016**, *138*, 1078–1083.
- (62) Lin, M.; Gao, Y.; Diefenbach, T. J.; Shen, J. K.; Hornicek, F. J.; Park, Y. I.; Xu, F.; Lu, T. J.; Amiji, M.; Duan, Z. Facial Layer-by-Layer Engineering of Upconversion Nanoparticles for Gene Delivery: Near-Infrared-Initiated Fluorescence Resonance Energy Transfer Tracking and Overcoming Drug Resistance in Ovarian Cancer. *ACS Appl. Mater. Interfaces* **2017**, *9*, 7941–7949.
- (63) Liang, L.; Care, A.; Zhang, R.; Lu, Y.; Packer, N. H.; Sunna, A.; Qian, Y.; Zvyagin, A. V. Facile Assembly of Functional Upconversion Nanoparticles for Targeted Cancer Imaging and Photodynamic Therapy. *ACS Appl. Mater. Interfaces* **2016**, *8*, 11945–11953.

- (64) Lu, F.; Yang, L.; Ding, Y.; Zhu, J.-J. Highly Emissive Nd³⁺-Sensitized Multilayered Upconversion Nanoparticles for Efficient 795 nm Operated Photodynamic Therapy. *Adv. Funct. Mater.* **2016**, *26*, 4778–4785.
- (65) Liu, B.; Li, C.; Xing, B.; Yang, P.; Lin, J. Multifunctional UCNPs@PDA-ICG Nanocomposites for Upconversion Imaging and Combined Photothermal/Photodynamic Therapy with Enhanced Antitumor Efficacy. *J. Mater. Chem. B* **2016**, *4*, 4884–4894.
- (66) Liu, Y.; Lu, Y.; Yang, X.; Zheng, X.; Wen, S.; Wang, F.; Vidal, X.; Zhao, J.; Liu, D.; Zhou, Z. *et al.* Amplified Stimulated Emission in Upconversion Nanoparticles for Super-resolution Nanoscopy. *Nature* **2017**, *543*, 229–233.
- (67) Wilhelm, S. Perspectives for Upconverting Nanoparticles. *ACS Nano* **2017**, DOI: 10.1021/acsnano.7b07120.
- (68) Hildebrandt, N.; Spillmann, C. M.; Algar, W. R.; Pons, T.; Stewart, M. H.; Oh, E.; Susumu, K.; Díaz, S. A.; Delehanty, J. B.; Medintz, I. L. Energy Transfer with Semiconductor Quantum Dot Bioconjugates: A Versatile Platform for Biosensing, Energy Harvesting, and Other Developing Applications. *Chem. Rev.* **2017**, *117*, 536–711.
- (69) Qiu, X.; Guo, J.; Jin, Z.; Petreto, A.; Medintz, I. L.; Hildebrandt, N. Multiplexed Nucleic Acid Hybridization Assays Using Single-FRET-Pair Distance-Tuning. *Small* **2017**, *13*, 1700332.
- (70) Messerer, R.; Kauk, M.; Volpato, D.; Alonso Canizal, M. C.; Klöckner, J.; Zabel, U.; Nuber, S.; Hoffmann, C.; Holzgrabe, U. FRET Studies of Quinolone-Based Bitopic Ligands and Their Structural Analogues at the Muscarinic M1 Receptor. *ACS Chem. Biol.* **2017**, *12*, 833–843.
- (71) Su, Q.; Feng, W.; Yang, D.; Li, F. Resonance Energy Transfer in Upconversion Nanoplatfoms for Selective Biodetection. *Acc. Chem. Res.* **2017**, *50*, 32–40.

2 MOTIVATION AND OBJECTIVES

The design and synthesis of efficient FRET nanoprobe using UCNP as energy donors requires detailed understanding of energy transfer cascades occurring within the particles and processes on the interface between particle surface and the solvent. The aim of this work was the complete characterization of FRET processes between UCNP and organic dyes on the particle surface in order to identify both the ideal particle architecture and surface modification technique to provide maximum FRET efficiency and colloidal stability. This comprehensive knowledge on the complex interplay between particle size and surface functionalization enables the development of enhanced FRET for an improved performance of UCNP in bioanalytical and theranostic applications.

First and most importantly, control over the surface chemistry of the innately hydrophobic UCNP needs to be established in order to create the following essential properties: (a) colloidal stability in aqueous (physiological) solvents by electrostatic stabilization, (b) preparation of UCNP exhibiting high brightness in the aqueous environment, (c) incorporation of functional groups for the subsequent attachment of FRET acceptors, selective receptors and targeting elements, (d) generation of high FRET efficiencies by controlling the donor-acceptor distance, (e) maintaining colloidal stability after further functionalization, (f) enabling fast cellular uptake, and (g) low cytotoxicity. Advantages and disadvantages of the variety of available techniques and strategies (such as ligand exchange, additional coating with amphiphilic molecules, and silica shells) with respect to the crucial requirements mentioned before need to be carefully considered and evaluated for the proper choice of surface chemistry.

Second, the particle composition and architecture must be precisely designed and controlled. One should keep in mind that UCNP are not molecular emitters, but rather a collection of single point emitters (the activator ions). Consequently, their behavior as FRET donors in combination with usually also significantly more than one molecular acceptor on the particle surface may be entirely different from conventional single donor and single acceptor systems. Aiming at the design of the ideal particle architecture the effect of UCNP size on the energy transfer efficiency to organic dyes acting as FRET acceptors needs to be investigated. "Large" dye decorated UCNP (> 20 nm) theoretically contain a great number of emitting lanthanide ions in its centers that are too far away from the surface to be able to contribute to the energy transfer. But increasing surface to volume ratios may promote surface deactivation competing with FRET. Thus, the optimum UCNP size for FRET based

application should be established by exploring FRET efficiencies determined from lifetime studies of UCNPs with varying sizes and different core-shell architectures for the manipulation of the donor-acceptor distance/ratio and brightness of the UCNPs. The FRET systems should be thoroughly characterized and the most efficient design should be reasonably identified.

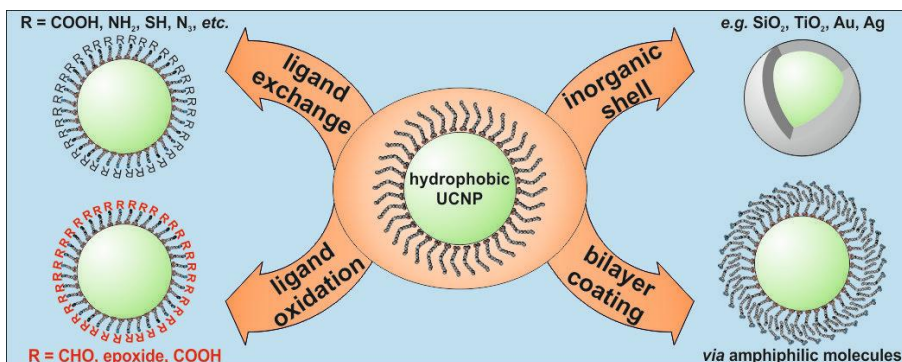
The insights gained from the systematical investigation of surface modification techniques and the impact of particle size on the FRET efficiency with UCNPs acting as donors can be exploited for the development of an efficient nanoprobe applicable for bioanalysis. Focus needs to be put on smart particle design by combining the preparation of bright UCNPs facilitating high FRET efficiencies with proper surface engineering. Protection against water quenching by inert shells and additional amphiphilic coatings is essential to attain high upconversion luminescence intensity, but is also linked to increased donor-acceptor distances compared to ligand exchange strategies. The best compromise between these two opposing effects must be identified to achieve efficient FRET. Further functionalization with bioreceptors must not impair the colloidal stability of the UCNPs and needs to facilitate defined analyte-responsive distance alterations. Structure switching receptors, such as aptamers and molecular beacons, provide a simple but reproducible way to change the donor-acceptor distance. This can be exploited to induce FRET by labeling with acceptors or by introducing specific dyes for the recognition of the structure change in presence of the analyte. Fast cellular uptake is required in order to allow for subcellular targeting and the nanoprobe should not exhibit cytotoxicity. The challenge is to combine all these features into one comprehensive probe design. Detailed characterization of the properties and performance of such detection systems will reveal insights into refined FRET-based probe designs for future theranostic applications.

3 UPCONVERSION NANOPARTICLES: FROM HYDROPHOBIC TO HYDROPHILIC SURFACES

3.1 Abstract

Photon upconversion nanoparticles (UCNPs) have emerged as a promising new class of nanomaterials due to their ability to convert near-IR light into visible luminescence. Unfortunately, most efficient methods for preparing UCNPs yield hydrophobic materials, but water-dispersibility is needed in the major fields of applications of UCNPs, that is, in bioimaging, labeling, and bioassays. Numerous methods therefore have been reported in the past years to convert the hydrophobic surface of UCNPs to a more hydrophilic one so to render them dispersible in aqueous systems. We present a classification respective for these strategies and assess the main methods. These include (A) chemical modification of the hydrophobic (typically oleate) ligand on the surface, (B) addition of an extra layer, (C) addition of a thin shell on top of the UCNP, and (D) complete replacement of the original ligand by another one. Chemical modification (A) involves oxidation of the oleate or oleylamine and leads to particles with terminal oxygen functions. This method is less often used because solutions of the resulting UCNPs in water have limited colloidal stability, protocols are time-consuming and often give low yields, and only a limited number of functional groups can be introduced. Methods B and C involve coating of UCNPs with amphiphiles or with shells made from silica oxide, titanium oxide, or metallic gold or silver. These methods are quite versatile in terms of further modifications, for example, by further cross-linking or by applying thiol–gold chemistry. Growing an extra shell is, however, often accompanied by a higher polydispersity. Method D can be divided into subgroups based on either (i) the direct (single-step) replacement of the native ligand by a new ligand or (ii) two-step protocols using nitrosyltetrafluoroborate (NOBF_4) or strong acids as reagents to produce ligand-free UCNPs prior to the attachment of a new ligand. These methods are simple and versatile, and the distance between the new ligand and the luminescent particle can be well controlled. However, the particles often have limited stability in buffer systems. The methods described also are of wider interest because they are likely to be applicable to other kinds of nanomaterials. We additionally address the need for (a) a better control of particle size and homogeneity during synthesis, (b) more reproducible methods for surface loading and modification, (c) synthetic methods giving higher yields of UCNPs, (d) materials displaying higher quantum yields in water solution without the need for tedious surface modifications, (e) improved methods for workup (including the suppression of aggregation), (f) new

methods for surface characterization, and (g) more affordable reagents for use in surface modification. It is noted that most synthetic research in the area is of the trial-and-error kind, presumably due to the lack of understanding of the mechanisms causing current limitations. Finally, all particles are discussed in terms of their biocompatibility (as far as data are available), which is quintessential in terms of imaging, the largest field of application.



Scheme 3.1 | Overview of established surface modification strategies of hydrophobic nanoparticles, including ligand exchange, ligand oxidation, encapsulation with inorganic materials and additional amphiphilic coatings.

This chapter has been published.

Verena Muhr, Stefan Wilhelm, Thomas Hirsch and Otto S. Wolfbeis. *Accounts of Chemical Research*, **2014**, 47 (12), 3481–3493

Author contributions

VM performed literature research and wrote the manuscript. SW conceived the TOC graphic. The article was revised by SW, TH and OSW. OSW is corresponding author.

3.2 Introduction

Upconverting (or upconversion) luminescent materials, first described in the 1960s, are capable of converting light of long wavelength (typically 800 – 1000 nm) into shorter-wave (mostly visible) luminescence.¹ Unlike in two-photon excitation (where two photons are absorbed at the same time), the effect is based on the sequential absorption of multiple lower energy photons, not the least because the first excited states have long lifetimes and where the probability of absorbing a second photon to form a higher excited state therefore is quite high. Relaxation from such an excited state results in the emission of light at higher energy, with typical wavelengths that lie between 350 and 800 nm. Upconverting nanoparticles (UCNPs), like the corresponding bulk phases, also display upconverted luminescence, albeit with lower brightness.² The most efficient upconverting luminescent nanomaterials known to date consist of hexagonal-phase lanthanide-doped NaYF₄ nanocrystals. The excitation wavelengths required for upconversion to occur lie in the optical window of most biological matter so that absorption of light in this range is comparably weak. This leads to a longer penetration depth of the excitation light and makes strong laser light sources (that can damage tissue) dispensable. The fact that upconverted luminescence is anti-Stokes-shifted also facilitates the separation of luminescence from Raman-bands and other scattered light. If luminescence of biomatter is induced at all, it will occur far in the NIR. In other words, the intensity of background visible fluorescence (i.e., in the region where upconverted luminescence occurs) is virtually zero. In contrast to quantum dots, the color of the emission of UCNPs does not depend on the size of the particles. UCNPs are not known to be cytotoxic, chemically stable, and neither blink nor bleach. On the other hand, their quantum yields depend on their size, on the kind of surface coating, and on the power-density of the laser used for photoexcitation.³ These features have been discussed in numerous reviews that can be easily found. Their outstanding features make UCNPs highly interesting materials for purposes including photodynamic therapy,⁴ photoinduced drug delivery,⁵ (targeted) cell imaging,⁶ sensing of fundamental parameters such as pH values,⁷ oxygen,⁸ ammonia,⁹ heavy metal ions,¹⁰ or CO₂,¹¹ in screening¹² and in immunoassays.¹³

Initially, UCNPs were produced by top-down strategies. Such methods yield stable colloidal solutions, but the particles were rather polydisperse and fairly large, this leading to slow if not lack of cellular uptake. A comparative study on upconversion luminescence and cell bioimaging based on single-step synthesized hydrophilic UCNPs capped with various functional groups has been presented by Tsang et al.¹⁴ To overcome the limitations by high polydispersity and poor flexibility in terms of surface modification (by either small molecules or thin additional layers), bottom-up strategies have been developed with the aim to

synthesize small and monodisperse nanoparticles but yet possessing bright upconversion luminescence. The most common strategies are co-precipitation, thermal decomposition, and solvothermal syntheses.¹⁵ Depending on the kind of the host lattice and the protocol used for synthesis, UCNPs can be prepared in shapes such as symmetrical spheres, rods, and even plates. The reviews by Chen *et al.*¹⁵ and DaCosta¹⁶ *et al.* provide an overview on synthetic strategies and material properties. DeCosta *et al.* also have introduced a system for the classification of methods of making apolar surfaces of UCNPs more polar (based on ligand exchange, ligand oxidation, ligand absorption, layer-by-layer assembly, ligand-free modifications and silanizations). Other reviews are available on lanthanide-doped luminescent nanoproboscopes (with a small section on UCNPs),¹⁷ and on UCNPs for use in small-animal imaging (with a short section on surface modification).¹⁸ The groups of Selvin¹⁹ and Li²⁰ have briefly reviewed methods for surface engineering of UCNPs, while other reviews are ignoring the need for converting hydrophobic to hydrophilic surfaces.²¹

Hexagonal phase NaYF₄ nanoparticles doped with trivalent lanthanides (Ln³⁺) are by far most often used. In 2008, Li and Zhang²² presented an efficient protocol for preparation of *hydrophobic* (oleate-capped) UCNPs. It involves heating of rare earth chlorides in a mixture of octadecene and oleic acid, first to generate the respective oleate salts which act as in-situ precursors. The addition of ammonium fluoride and sodium hydroxide and an increase in the reaction temperature to 300 °C leads to the formation of highly monodisperse, oleate-capped, hexagonal UCNPs that can be dispersed in nonpolar solvents. Oleylamine (OIAM) may be added to, or even used in place of oleic acid.²³ This bottom-up method in high-boiling solvents is said to be superior to others with respect to the monodispersity, shape uniformity and phase purity of the resulting UCNPs. On the other hand, it suffers from the disadvantage of giving UCNPs that are dispersible in hydrophobic solvents only, but not in aqueous solutions including buffers. If intended for use in biosciences, water dispersibility and colloidal stability in buffers is, however, mandatory. In addition, these particles are highly inert in being devoid of any useful functional group on their surface. In order to exploit the large potential of UCNPs, appropriate functional groups have to be introduced.

This review throws a critical look at the methods for surface modification and functionalization that lead to UCNPs for use in aqueous media. In terms of bioimaging (which is the most widespread application of such particles at present), features such as small size, brightness and tunable emission/excitation spectra also are paramount.²⁴ We summarize general principles, discuss advantages and disadvantages of the strategies, and give selected examples for respective applications.

3.3 Surface Modification of Hydrophobic UCNPs

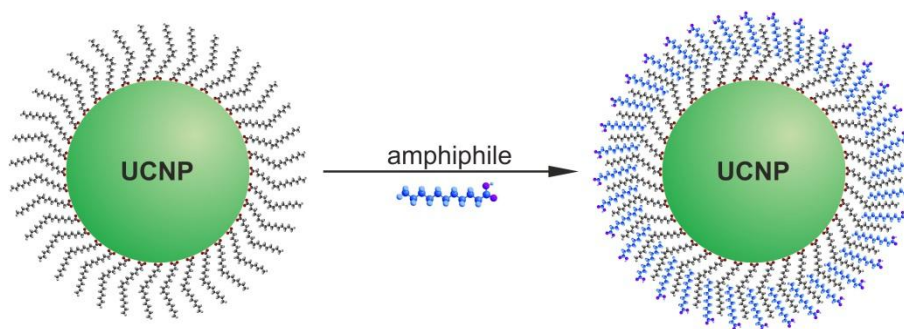
A large variety of methods for surface modification have been developed to convert hydrophobic UCNPs into more hydrophilic particles. They often are not limited to UCNPs but also may be applied to other nanoparticles.²⁵ The respective strategies can be categorized into four groups: (1) Chemical modification of the hydrophobic (usually oleate or oleylamine) ligand on the surface; (2) bilayer coating with amphiphilic molecules or polymers, (3) addition of an extra layer or shell on top of the UCNP; and (4) complete replacement of the original ligand by another one. These will be discussed in the following.

3.3.1 Modification of the Original Ligand

The direct modification of the hydrophobic ligand on a particle's surface to generate hydrophilic UCNPs is simple but not common. It is based on the oxidation of the carbon-carbon double bond of the oleate or oleylamine. Depending on the reagents employed, it can lead to the formation of carboxy groups or epoxy groups. Oxidizing agents include the Lemieux-von Rudloff reagent,²⁶ ozone,²⁷ and 3-chloroperoxybenzoic acid.²⁸ In addition to the formation of reactive groups, the dispersibility of the resulting particles in water is strongly enhanced. Such particles then may be covalently coupled to other species, for example to the cancer drug doxorubicin in order to enable controlled drug delivery,²⁹ or to poly(ethylene glycol) in order to impart biocompatibility.²⁸ Notwithstanding this, oxidative surface modification is rarely used because dispersions in water are of poor colloidal stability and only a limited number of ligands (aldehydes, epoxides, or carboxylic acids) can be introduced.

3.3.2 Amphiphilic Coatings

This technique involves coating of the UCNPs with molecules containing long alkyl chains to form a bilayer that is stabilized *via* van-der-Waals interactions between the hydrophobic oleate and the new coating. Amphiphilic molecules are preferred in this context because they (a) undergo strong van-der-Waals interaction, (b) enable the surface charge to be easily altered, and (c) may even be deposited as a so-called layer-by-layer coating, *i.e.* in the form of multiple layers of alternating charge. If oleate-capped UCNPs are treated with long-chain amphiphiles, their hydrophobic tails intercalate between the oleate chains, while their hydrophilic head groups are directed outwards. This results in the formation of a bilayer around the UCNP as shown in Scheme 3.2. The hydrophilic head groups render the particles well dispersible in water.



Scheme 3.2 | Principle of bilayer formation by coating the oleate-capped UCNP with an amphiphile with a hydrophilic or ionic end group, thus converting the hydrophobic particles to hydrophilic particles.

Phospholipids (PLs) have often been used to modify surfaces. Respective particles (not only UCNPs) are readily internalized by cells, non-immunogenic, and possess a long functional lifetime even *in vivo*. PLs have been widely used in drug delivery. Quite a variety of PLs is commercially available with various kinds of head groups such as maleimide (for binding the particle to protein thiol groups), biotin (with its high affinity for streptavidin), and several others. Phospholipids also are known with highly different chain lengths, and variation in length is often accomplished by incorporating poly(ethylene glycol) (PEG) units which has the beneficial effect of imparting biocompatibility.^{30,31} In a typical example, maleimide and folate head groups were used to conjugate UCNPs to gold nanoparticles and image HeLa cells (see Figure 3.1).¹⁹

While phospholipids with polar head groups and PEG spacers are easy to use, they are difficult to make and purify, and expensive if commercially available. The following calculation may reflect the costs to be expected in a typical experiment: The surface area of one single nanocrystal with a diameter of 20 nm is 1250 nm². If 1 μmol of such particles is to be covered with, say, a PEGylated distearoyl phospholipid (with a size of ~ 80 Å²), the total surface to be coated is as large as 760 m². This requires, roughly, 4.5 g of the phospholipid which will actually cost *more than US\$ 30,000*. This number may be even higher if phospholipids are applied in excess to warrant complete coverage of the surface. Obviously, less expensive methods are desirable to create bilayers. Zhao *et al.*³² have coated UCNPs with the detergent Tween 80 to obtain particles for use as a carrier for doxorubicin that was trapped in the hydrophobic bilayer. Other long-chain alkylammonium derived surfactants were tested by the Yang group,³³ but the colloidal stability of the particles in water was poor. Subsequent surface modification with silica was required. This will be discussed in the next section.

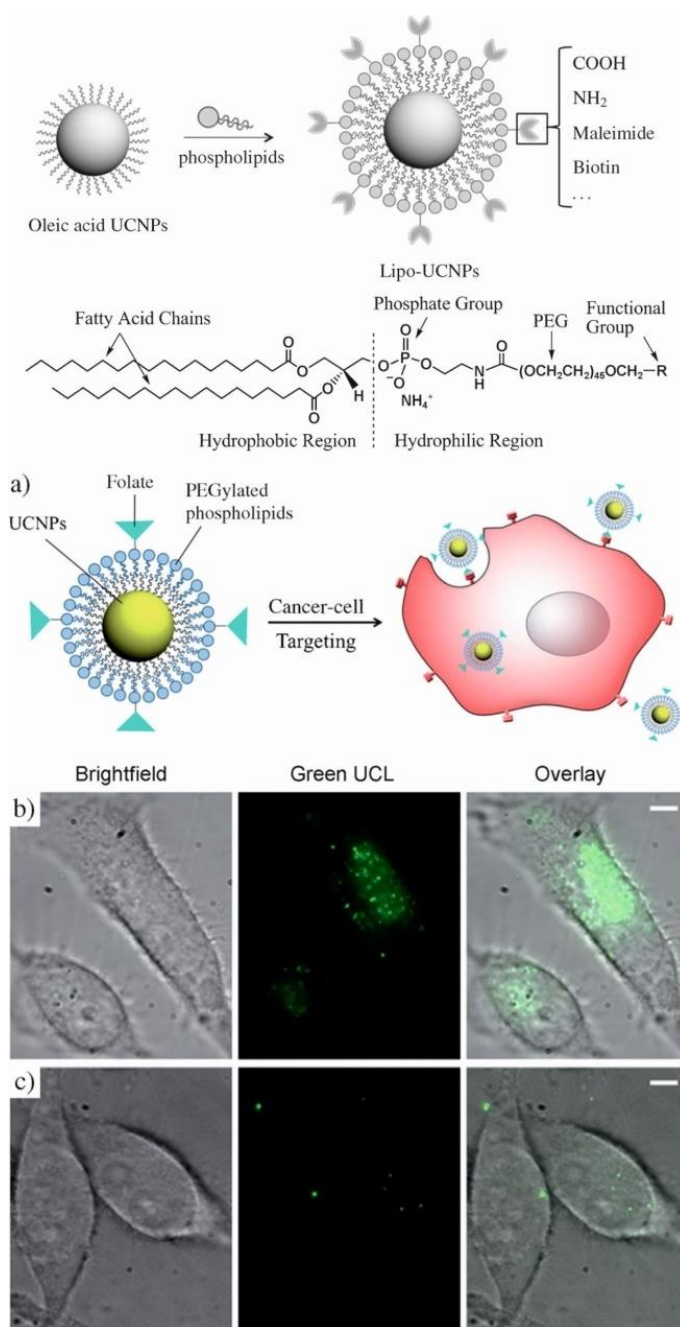


Figure 3.1 | Illustration of the assembly of the water-dispersible UCNPs by adding a monolayer of phospholipids. (a) Illustration of the targeted imaging of cancer cells with Lipo-UCNPs carrying folic acid (FA). (b, c) Transmission and luminescence microscopy images of HeLa cells treated with Lipo-UCNPs-FA (b), and with Lipo-UCNPs without folate ligand (c). Scale bar is 5 μm . UCL: upconversion luminescence. Reprinted with permission from ref.19. Copyright © 2012 by Wiley & Sons, Inc.

In another approach, amphiphilic polymers were used in place of the relatively small-molecule surfactants as shown by the Parak group³⁴ in order to modify the surface of gold nanoparticles, quantum dots, or iron oxide particles. Poly(maleic anhydride-*alt*-1-octadecene) (PMAO) is a widely used polymeric amphiphile^{35,36} as it contains multiple alkyl chains per molecule and has a weak chelating effect which stabilizes the surface coating against ligand

detachment. Particles coated with PMAO display good temporal stability in aqueous media which can be further increased by reacting the anhydride groups with bis(hexamethylene)triamine (BHMT).³⁷ This method enabled UCNPs to be stabilized over the pH 3 - 13 range and in cell cultures for even several weeks (see Figure 3.2).

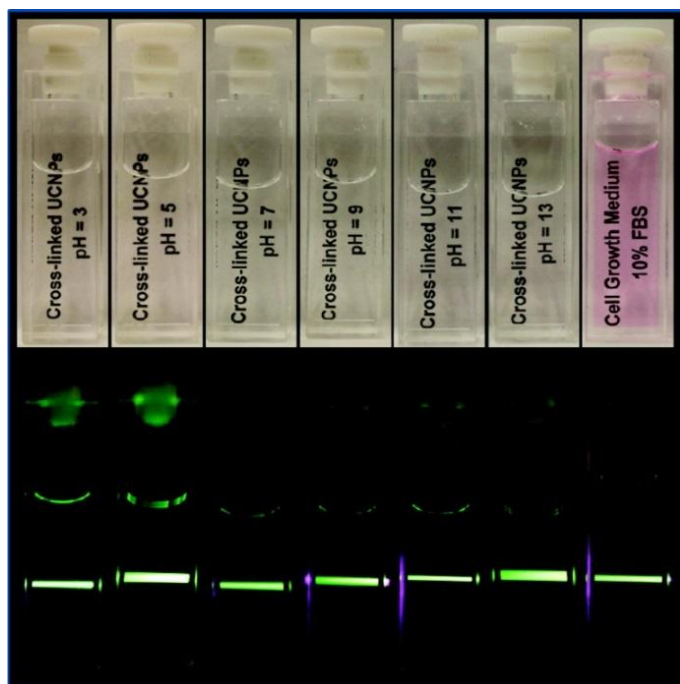


Figure 3.2 | Core/shell nanoparticles ($\text{NaYF}_4:20\% \text{ Yb}^{3+}, 2\% \text{ Er}^{3+}/\text{NaYF}_4\text{-PMAO-BHMT}$) dispersed in water at different pH from 3 to 13 and serum-supplemented cell growth medium and respective images under 980 nm excitation (bottom). Reprinted with permission from ref.37. Copyright 2012 American Chemical Society.

Poly(acrylic acid) modified with long alkyl chains also binds to the surface of oleate-capped UCNPs.³⁸ This results in the introduction of carboxy groups that are negatively charged at near-neutral pH values and will render the particles water-soluble. The carboxy groups can further serve as functional groups to couple the particles to proteins.³⁹ There have also been reports on UCNPs coated (a) with amphiphilic chitosan for use photodynamic therapy,⁴⁰ and (b) with an amphiphilic silane for use in optical probing of temperature using an Eu(III) chelate as an indicator⁴¹ as schematically shown in Figure 3.3. UCNPs that are highly stable under physiological conditions were obtained⁴² by coating them with methoxy-poly(ethylene glycol-block-caprolactone). Table 3.1 gives a selection of amphiphilic molecules applied to surface modification of UCNPs.

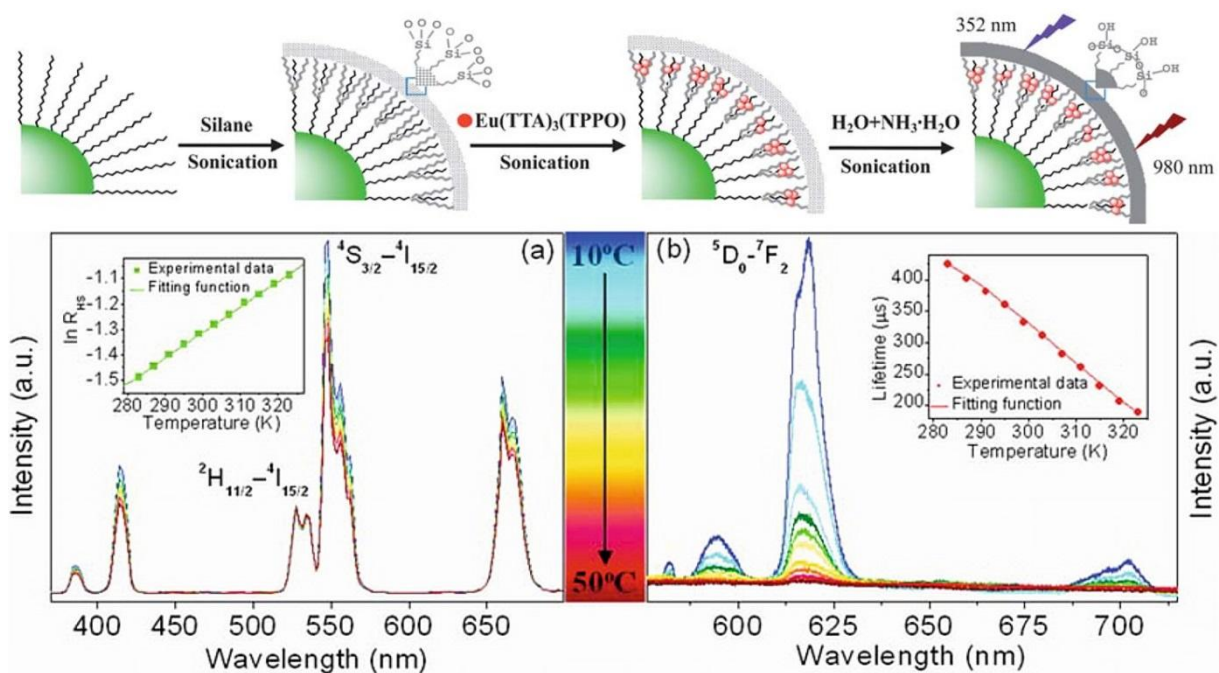


Figure 3.3 | Schematic illustration of the synthesis of silane-modified NaYF₄:Yb³⁺,Er³⁺ loaded with the probe Eu(TTA)₃(TPPO)₂ (top), and temperature-dependent spectra of C18 silane-modified NPs under 980 nm (a) and 352 nm (b) excitation (bottom). The inset in (a) shows the temperature-dependent intensity ratio value of the two upconversion luminescence emissions at 525 nm and 544 nm. The inset in (b) shows the temperature-dependent lifetime of the upconversion luminescence. Reproduced from ref. 41 with permission of The Royal Society of Chemistry.

Table 3.1 | . Examples for amphiphilic molecules used for coating of UCNPs, and selected applications of the resulting water-dispersible nanoparticles.

UCNP and native ligand	Amphiphilic molecule	Application	Reference
NaYF ₄ :Yb,Er and NaYF ₄ :Yb,Tm@oleate	phospholipids with various head groups	optical and magnetic resonance imaging	19, 30, 3132
NaYF ₄ :Yb,Er@oleate	Tween 80	bioimaging and drug delivery	32
NaYF ₄ :Yb,Er@oleate	surfactants	water dispersibility	33
NaYF ₄ :Yb,Er and NaYF ₄ :Yb,Tm@oleate	poly(maleic anhydride-alt-1-octadecene)	photodynamic therapy, detection of Hg ²⁺ ions in water	35, 36
NaYF ₄ :Yb,Er and NaYF ₄ :Yb,Tm@oleate	amphiphilic poly(acrylic acid)	bioimaging, cell tracking	38, 39
NaYF ₄ :Yb,Er@oleate	amphiphilic chitosan	photodynamic therapy	40
NaYF ₄ :Yb,Er@oleate	amphiphilic silane	temperature sensing, cell imaging	41

3.3.3 Encapsulation with Inorganic Materials or Noble Metals Forming a Shell

Water dispersibility was accomplished by deposition of an additional shell on top of hydrophobic UCNPs. Typical shell materials include oxides like SiO_2 and TiO_2 (to impart solubility and – sometimes – catalytic activity), or noble metals like gold or silver which pave the way to plasmonic modulation of upconverted luminescence (Figure 3.4). Table 3.2 gives a selection of respective materials.

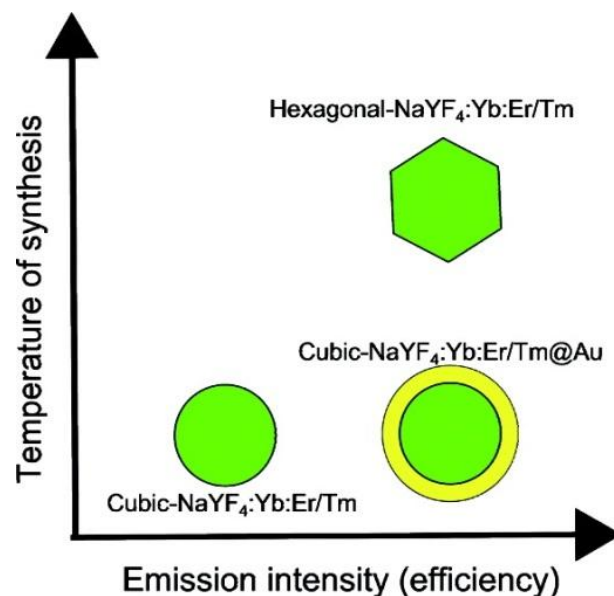


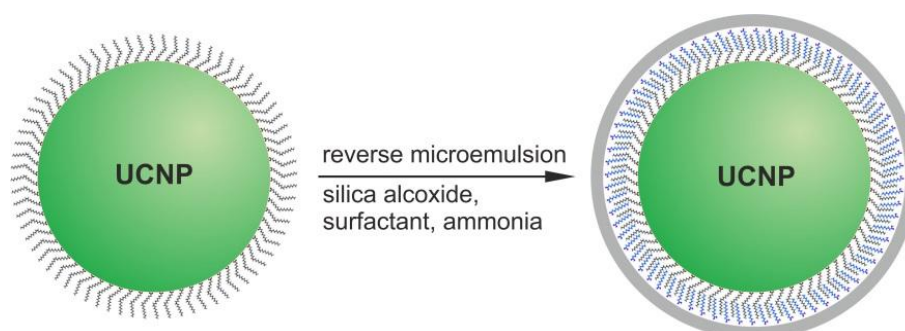
Figure 3.4 | Illustration of the luminescence enhancement of cubic $\text{NaYF}_4:\text{Yb},\text{Er}/\text{Tm}$ UCNPs achieved by the growth of a thin Au-shell compared to the luminescence intensity of conventional hexagonal $\text{NaYF}_4:\text{Yb},\text{Er}/\text{Tm}$ UCNPs. Reprinted with permission from ref 43. Copyright 2011 American Chemical Society.

Table 3.2 | Examples for lanthanide doped NaYF_4 nanoparticles encapsulated by various inorganic materials, and corresponding applications.

UCNP and its native ligand	Shell	Application	Reference
$\text{NaYF}_4:\text{Yb},\text{Tm}$, $\text{NaYF}_4:\text{Yb},\text{Er}@$ oleate	SiO_2	imaging, drug delivery	44, 45
$\text{NaYF}_4:\text{Yb},\text{Tm}@$ oleate $\text{NaYF}_4:\text{Yb},\text{Er}@$ SiO_2	TiO_2	dye sensitized solar cells, photocatalysis	46, 47
$\text{NaYF}_4:\text{Yb},\text{Tm}@$ oleate	Au	plasmonic modulation of upconversion emission	43, 48
$\text{NaYF}_4:\text{Yb},\text{Er}@$ oleylamine	Ag	imaging, photothermal therapy	49

The deposition of a silica shell on a UCNP is a useful technique to generate functionalized and water dispersible NPs. Both hydrophilic and hydrophobic UCNPs can be coated by using

either the Stöber method or the reverse microemulsion method. The latter is better suited for oleate or oleylamine-capped UCNPs and gives core-shell particles coated with a uniform layer of silica (SiO_2).⁵⁰ A product having the tradename Igepal CO-520 is widely used as it forms adequately stable reverse microemulsions for polymerization of precursors such as tetraethyl orthosilicate. Ammonia is added as a catalyst. It causes the formation of silicic acid at a concentration above the nucleation concentration, thus warranting a steady growth of the silica shell as schematically shown in Scheme 3.3. The resulting silica-coated particles (usually referred to as UCNPs@ SiO_2) readily disperse in water. They have a negative zeta potential that depends on solvent, salinity, and surface charges, and display low cytotoxicity.⁵⁰ The silica coating strategy suffers from the classical drawback of almost all coating methods of that kind in that polydispersity increases when compared to the untreated particles. In case of thin silica shells, it is difficult to prove whether the formation of the shell is complete. In addition, UCNPs@ SiO_2 possess poor temporal stability in aqueous solution in that they tend to aggregate and precipitate within a couple of hours.^{51, 52} On the positive side, coatings with comparably thick layers of silica do not strongly compromise the "brightness" of particles which is in contrast to coatings with small molecules or thin films (see below). If UCNPs@ SiO_2 are separated by centrifugation, they often cannot be redispersed in water and do no longer form a clear dispersion. This problem may be overcome by introducing a high density of surface charges which will reduce the tendency towards aggregation.⁵³ It was shown that agarose gel electrophoresis (AGE) is well suited for the purification of silica-coated UCNPs.⁵⁴ The silica shell of a fraction of the particles was doped with a fluorescent dye for direct detection. The silica shell was prepared by reverse microemulsion and resulted in individual nanoparticles but also in aggregates that were separated and isolated. The preparation of an ultrathin carboxylated silica shell, in contrast, yielded non-aggregated UCNPs that can be directly used for protein conjugation.



Scheme 3.3 | Schematic representation of the silica shell formed on oleate-capped UCNPs. The initially hydrophobic particles are converted to hydrophilic particles. This process is accompanied by large changes in the zeta-potential.

Functional groups can be created on the surface of the UCNPs in two ways. In one, the preformed UCNPs@SiO₂ particles are modified with organically modified silanizing agents. In the other, functional organosilanes are added during the polymerization process that leads to the formation of the shell so that post-synthetic modification is not needed. Organosilanes that have been used in either method are summarized in Table 3.3.

Table 3.3 | Examples of silane reagents used for coating or modification of UCNPs to render them water-dispersible (and sometimes also reactive), and corresponding applications of the hydrophilic particles.

UCNP and native ligand	Silane reagent	Application	Ref.
NaYF ₄ :Yb,Er@oleate	aminopropyltrimethoxysilane	targeting and imaging of tumor cells	55
NaYF ₄ :Yb,Er@oleate	aminopropyltriethoxysilane	targeting and imaging of tumor cells	44
NaYF ₄ :Yb,Er@oleate	carboxyethylsilanetriol	biolabeling, energy transfer	56
NaYF ₄ :Yb,Er and NaYF ₄ :Yb,Tm@oleate	mesoporous silica loaded with doxorubicin	imaging and drug delivery	5,57
NaYF ₄ :Yb,Er and NaYF ₄ :Yb,Tm@oleate	silane-modified PEG-NHS	protein conjugation	58
NaYF ₄ :Yb,Er@oleate	silane modified IR-783	NIR imaging and photothermal therapy	59
NaYF ₄ :Yb,Er@oleate	mesoporous silica loaded with zinc(II) phthalocyanine	photodynamic therapy	4
NaYF ₄ :Yb,Er@oleate	silica@mesoporous silica loaded with ibuprofen	imaging and drug delivery	45

Amino-functionalized UCNPs@SiO₂ may be prepared by adding aminopropyltriethoxysilane to the microemulsion.⁴⁴ The water-dispersible UCNPs can then be conjugated to folic acid to enable targeting of tumor cells. Similarly, silica-coated NaYF₄:Yb,Er UCNPs were coated with folic acid and anti-Her2 antibody to label the folate receptors and Her2 receptors of certain cells. Our group has reported the preparation of protein-reactive hydrophilic particles (Figure 3.5) by modifying the surface of UCNPs@SiO₂ with a silane-modified poly(ethylene glycol) with a terminal N-hydroxysuccinimide group.⁵⁸ The nanoparticles were then conjugated to proteins as verified by surface plasmon resonance spectroscopy.

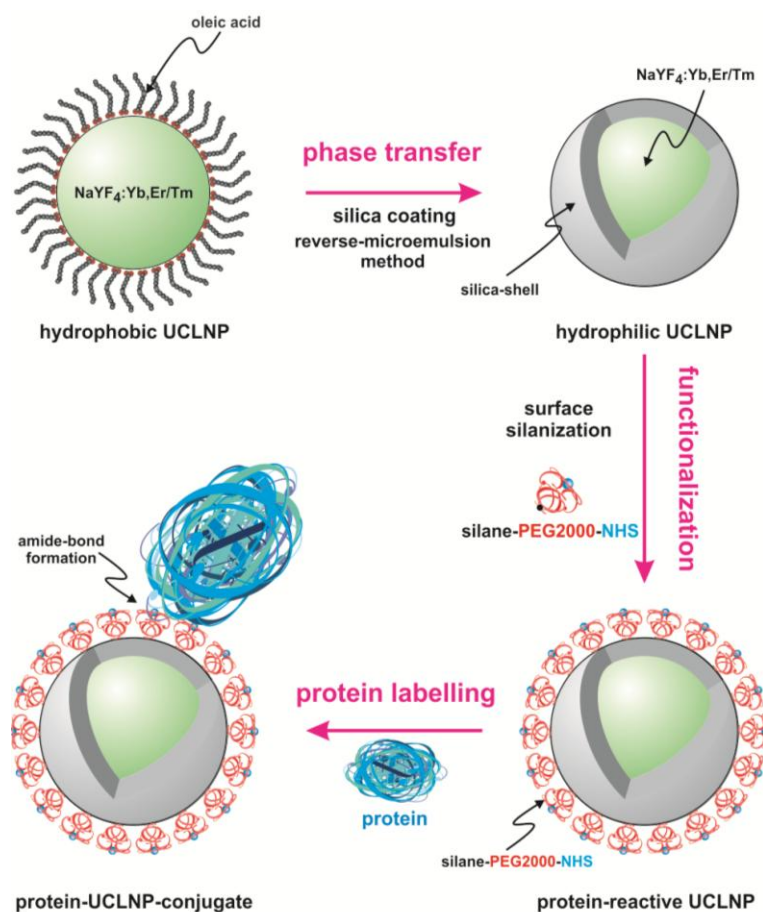


Figure 3.5 | Surface engineering of UCNPs towards protein-reactive, multicolor upconverting labels by coating them with a reagent of the type silane-PEG-NHS .58

UCNPs coated with mesoporous silica were modified with azo groups *via* silanization and then loaded with the cancer drug doxorubicin.⁵ The azo groups acted as motors to trigger the controlled release of the drug under photoexcitation at 980 nm. Mesoporous silica shells are characterized by a large specific surface area and a pore size that can be fine-tuned (Figure 3.6).

Other UCNPs were coated with mesoporous silica and loaded with photosensitizers such as zinc(II) phthalocyanine that causes the formation of singlet oxygen upon NIR excitation.⁴ Li *et al.*⁶⁰ have incorporated doxorubicin into particles coated with mesoporous silica which then were studied with respect to cellular uptake and cytotoxicity. Their potential for imaging of nasopharyngeal epidermal carcinoma cells was demonstrated.⁶¹ More recently, core-shell particles of the type $\beta\text{-NaYF}_4:\text{Yb,Er}@SiO_2@mSiO_2$ have been reported,⁴⁵ again for use in imaging and drug storage and delivery. So-called yolk-shell UCNPs were obtained by forming a hollow mesoporous silica shell around $\text{NaLuF}_4:\text{Yb,Er,Tm}$ nanoparticles.⁶² Their large cavities were loaded with a chromophore to construct nanoprobes for cysteine, homocysteine, and cyanide.

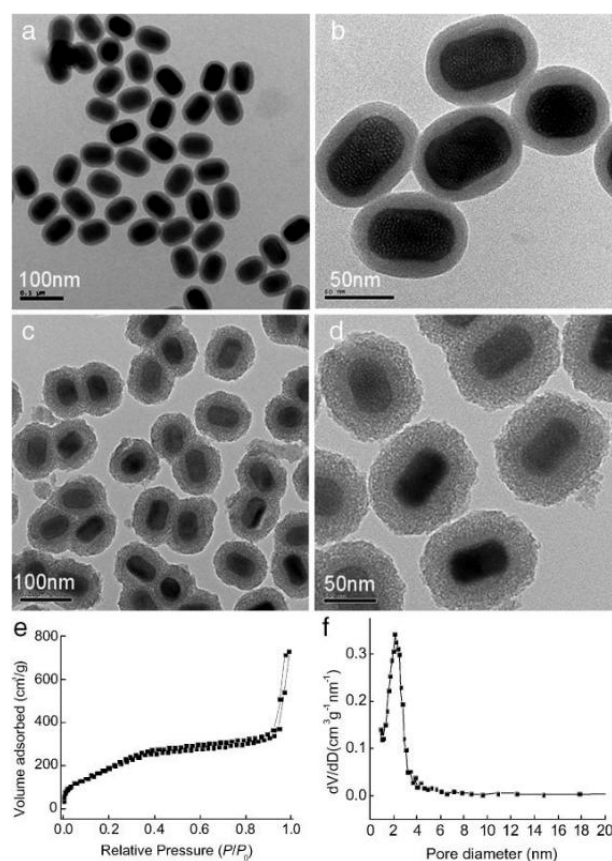


Figure 3.6 | Transmission electron microscopy images of NaYF₄:Yb,Er@silica nanoparticles (a,b) and mesoporous-silica-coated NaYF₄:Yb,Er@silica nanoparticles (c, d). N₂ adsorption/desorption isotherm (e) and pore-size distribution (f) of mesoporous-silica-coated NaYF₄:Yb,Er@silica nanoparticles. Reprinted with permission from ref.4. Copyright © 2009 by John Wiley Sons, Inc.

3.3.4 Replacement of the Native Ligand

Ligand exchange is a versatile strategy to modify the surface of UCNPs. Two major methods are known. One is based on direct exchange of the first ligand by the new one; the other is based on two-step strategies using NOBF₄ or acid treatment with HCl to strip off the oleate or oleylamine and subsequent attachment of a new coating. Unfortunately, practically all coatings with small molecules (for example via oleate replacement or the NOBF₄ technique) for phase transfer to aqueous solvents drastically reduce the “brightness” of UCNPs. Coating the particles with NaYF₄, in contrast, does not cause such an effect. However, a systematic study on the effect of small-molecule coatings on quantum yields and luminescence decay times has not been presented so far.

3.3.4.1 Direct (Single Step) Replacement of the Native Ligand by a New Ligand

In this case, the native ligand on the UCNP is (almost) completely displaced by another ligand that is supposed to be more polar so to confer water solubility. Ideally, it contains a

functional group that coordinates to the surface of the UCNP so that it can easily replace the native ligand. The strength of interaction is likely to increase in the order $-\text{SH}$, $-\text{NH}_2$, $-\text{COOH}$, $-\text{PO}_3\text{H}$, but no comparative study covering the different binding strengths is available. Respective methods are fairly simple, at least in principle, but work up is tedious and more challenging than the chemical reaction itself. In a typical procedure, oleate-capped UCNPs and the new ligand are stirred for 4 h up to several days, usually at elevated temperature.^{63,49} The protocols have to be optimized for each single ligand because its single ligand requires specific reaction conditions in terms of concentrations, stirring time, temperature, and need for an inert atmosphere. Furthermore, the particles tend to aggregate during ligand exchange.⁶⁴ The group of Pérez-Prieto used hetero-bifunctional PEG with a thiol group at one end and an amine or carboxylic group at the other.⁶⁵ In this protocol, the PEG ligands are used as both the capping ligand and the water-stabilizing agent. PEG moieties can function as polydentate ligands and bind to lanthanide ions. Representative reagents/cappings, and the properties and application of the resulting hydrophilic UCNPs are summarized in Table 3.4. Ligands usually have to be added in excess in order to displace the former ligand. Even organic polymers may be used in this replacement strategy as can be seen in Table 3.4.

The introduction of PEG chains not only imparts hydrophilicity but also results in improved biocompatibility when used in imaging or cell targeting. Ultrasmall core-shell UCNPs of the type $\text{NaYF}_4:\text{Yb},\text{Tm}@\text{SiO}_2$ were further modified with PEG and found to be bound by MCF-7 tumors,⁶⁶ while others were coated with similarly hydrophilic multihydroxy dendritic molecules to warrant water-dispersibility and hydrophilicity.⁶⁷ The introduction of carboxy groups, in turn, allows UCNPs to be conjugated to biomolecules containing amino groups (see Figure 3.7),⁶⁸ and maleimides can be conjugated to thiols.⁶⁹

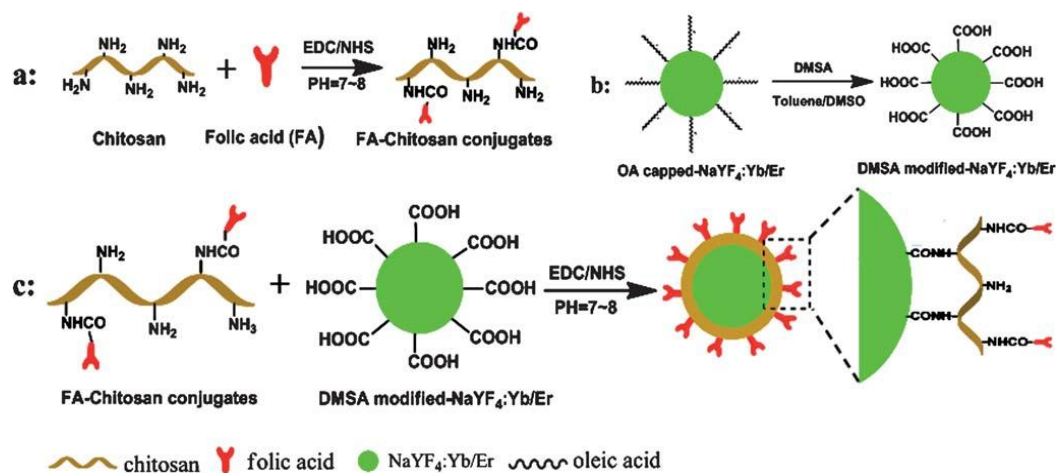


Figure 3.7 | Illustration of the formation of $\text{NaYF}_4:\text{Yb},\text{Er}$ nanoparticles coated with folic acid (FA) and chitosan. From ref. 68 with permission of The Royal Society of Chemistry.

Table 3.4 | Examples for direct replacement of hydrophobic surface ligands by hydrophilic ligands, and properties and uses of the resulting water-dispersible products.

UCNP and native ligand	Reagent or new ligand	Application	Reference
NaYF ₄ :Yb,Er@oleate	citrate	bioimaging, conjugation	70
NaYF ₄ :Yb,Er and NaYF ₄ :Yb,Tm@oleylamine	hexanedioic acid	making particles water soluble, conjugation	71
NaYF ₄ :Yb,Er and NaYF ₄ :Yb,Tm@oleylamine	PEGylated carboxylate	making particles water soluble, biocompatibility	72
NaYF ₄ :Yb,Er and NaYF ₄ :Yb,Tm@oleate	PEGylated phosphate	making particles water soluble, biocompatibility	73
NaGdF ₄ :Yb,Er@oleate	poly(amido amine) (PAMAM)	conjugation to carbohydrates and recognition of lectins	74
NaYF ₄ :Yb,Er@oleate	poly(allyl amine)	conjugation to zinc(II)-phthalocyanine as photosensitizer for photodynamic therapy	64
NaYF ₄ :Yb,Tm@oleate	mercaptopropionic acid	imaging and photothermal therapy	75
NaYF ₄ :Yb,Er@oleylamine	thioglycolic acid	growth of Ag-shell for photothermal therapy	49
NaYF ₄ :Yb,Tm and NaGdF ₄ :Yb,Ho@oleate	poly(acrylic acid)	studies on the distribution and toxicity of polyacrylate-coated UCNPs	76,77
NaYF ₄ :Yb, Er@oleate	poly(vinyl pyrrolidone)	making particles water-soluble	78
NaYF ₄ :Yb,Er@oleate	mono-thiolated hetero- bifunctional PEGs	bioimaging, conjugation	65, 79, 80

If the oleate ligand is exchanged by 2-bromo-2-methylpropionic acid and polymerized with the hydrophilic polymer oligo(ethylene glycol) methacrylate, a dispersion is obtained that is stable in phosphate buffer.⁸¹ The UCNPs obtained were conjugated to lectins and applied to imaging of cancer cells. Strong interaction of UCNPs with the phosphate groups of DNA also has been claimed,⁸² but questions remain such as the lack of cross-linking between particles (via DNA chains) and how hybridization can occur such that one end of the oligomer remains bound to the UCNP.

Modification of oleylamine-capped magnetic UCNPs via ligand exchange with a mixture of aminocaproic acid, oleic acid, and folic acid and simultaneous cation exchange with Gd³⁺ ions gives mixed hydrophobic surfaces.⁸³ Positively or negatively charged layers consisting of small molecules or even of polymers may be deposited alternatively, a technique known

as layer-by-layer coating. This strategy allows for a precise control of surface charge and thickness of the particles. Various kinds of molecules may be placed between (or in) the layers to result in materials for e.g. controlled drug delivery and photodynamic therapy⁸⁴ as shown in Figure 3.8. Dispersions of polymer-modified UCNPs generally display better colloidal stability in aqueous media than their small molecule-modified counterparts. Nonetheless, their tendency to aggregate if placed in buffers or cell culture media remains to be a problem.^{73,85}

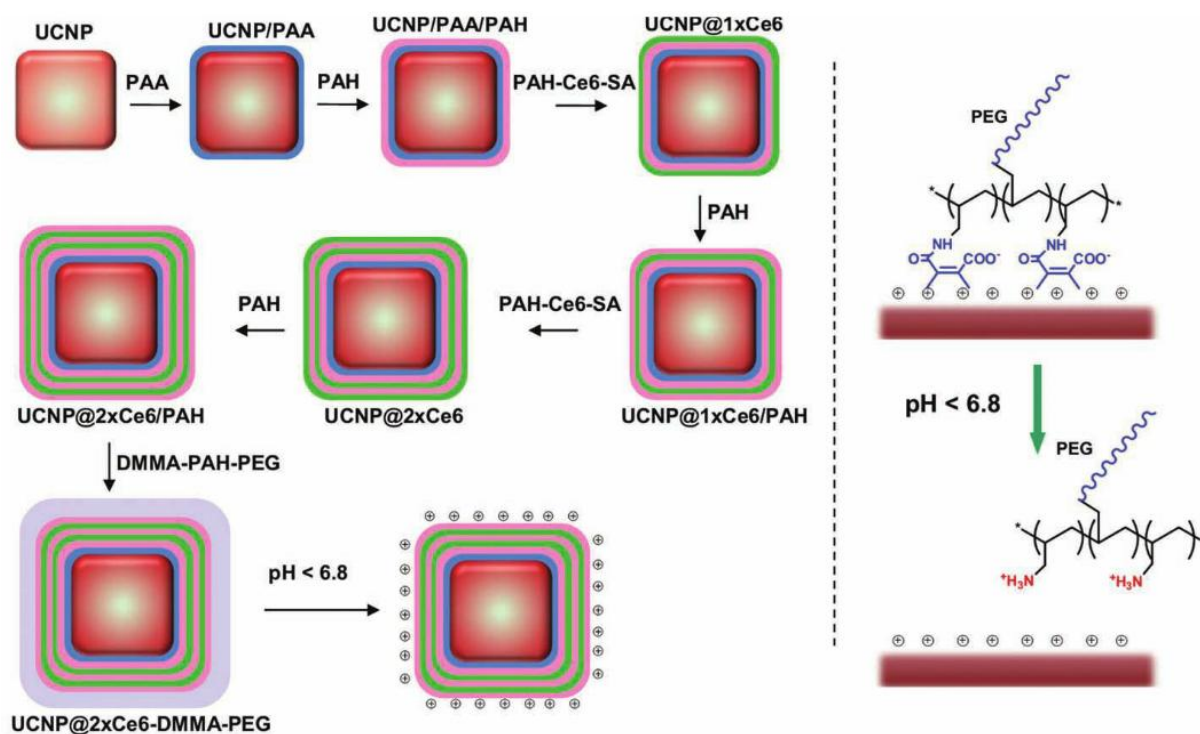


Figure 3.8 | Illustration of pH-responsive smart theranostic UCNPs. Left: A schematic showing the fabrication process of pH-sensitive charge-reversible UCNPs with multi-layers of Ce6 loading. Right: Detachment of the PEGylated polymer layer from the surface of a positively charged nanoparticle surface by adjusting the pH value to below 6.8. Reprinted with permission from ref. 84. Copyright © 2013 by John Wiley Sons, Inc.

3.3.4.2 Two-step Replacement of the Native Ligand Using the NOBF_4 Reagent.

The group of Murray⁸⁶ have introduced a widely applicable strategy for modification of surfaces of nanoparticles by using the reagent nitrosyl tetrafluoroborate (NOBF_4). If added to dispersions of nanoparticles capped with oleate or oleylamine, the ligand is stripped off and the BF_4^- ions are said to take their place. Other tetrafluoroborates work much less well – or even not at all – so that the involvement of the NO^+ cation in the process also should be taken into consideration. Aggregation during the exchange process is strongly reduced compared to other protocols, and dispersions of the resulting and quasi ligand-free particles

in DMF are stable for months. New ligands (such as oleylamine, tetradecylphosphonic acid, or poly(vinyl pyrrolidone)) can then be attached to the surface in a second step as schematically shown in Figure 3.9. This method is quite important because it is independent of the core of the particles and thus has a wide scope. It also works with iron oxide nanoparticles, titanium oxide nanorods, or NaYF_4 nanoplates. Additional advantages include the direct attachment of the new ligand to the surface of the UCNPs. Linkers – like those needed in surface modifications with amphiphilic molecules or silica shells – are not required. Examples are given in Table 3.5. The so-called Meerwein salt (Et_3OBF_4) was also applied to ligand stripping of oleate-passivated nanocrystals.⁸⁷

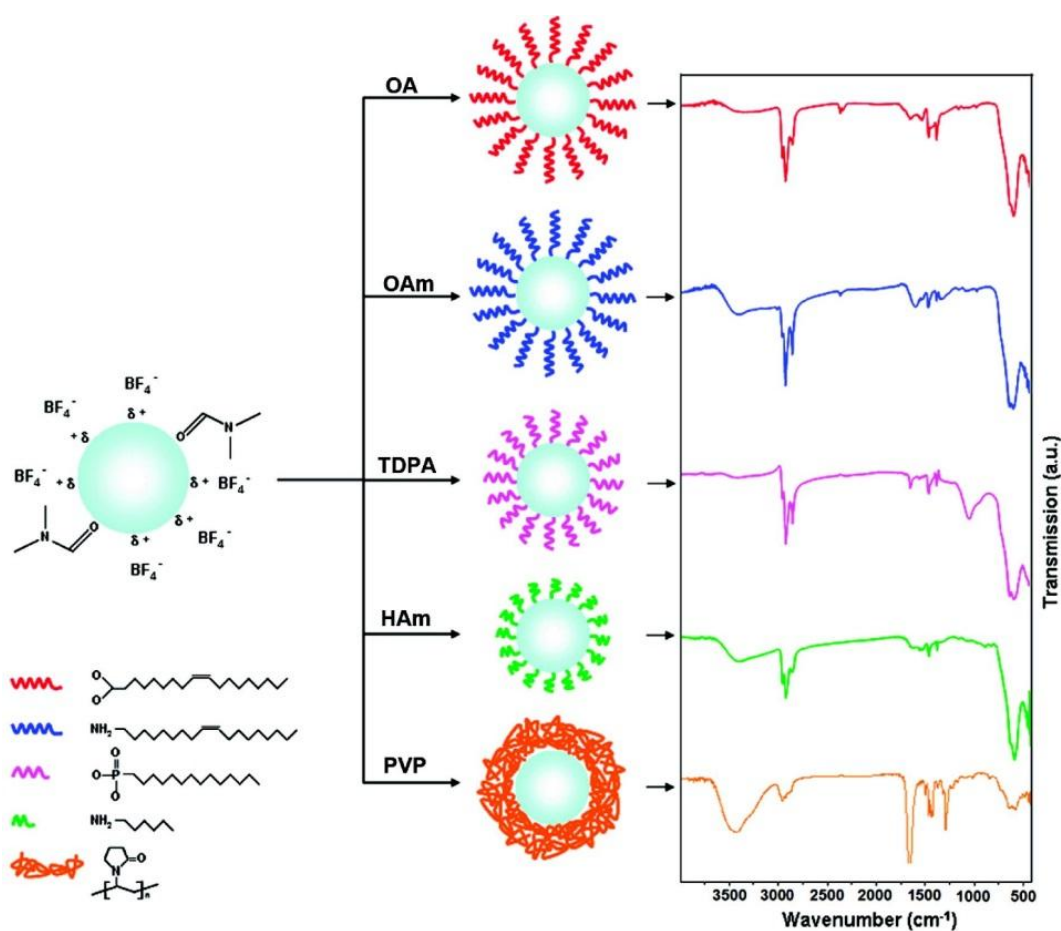


Figure 3.9 | Illustration of the ligand exchange process at the surface of Fe_3O_4 nanocrystals modified with the BF_4^- by various capping molecules. The right column shows the corresponding FTIR spectra. Reprinted with permission from ref. 86. Copyright 2011 American Chemical Society.

Table 3.5 | Typical examples for indirect replacement of oleate ligands by using the NOBF_4 reagent, new ligands, and properties and uses of the resulting water-dispersible nanoparticles (NPs).

UCNP and native ligand	New surface capping	Properties and applications	Reference
$\text{NaYF}_4:\text{Nd},\text{Yb},\text{Er}$ and $\text{NaYF}_4:\text{Nd},\text{Yb},\text{Tm}@$ oleate	poly(acrylic acid)	results in water-soluble NPs; method for tuning the excitation wavelength	88
$\text{NaYF}_4:\text{Yb},\text{Er}@$ oleate	poly(acrylic acid)	multiphoton microscopy with low-power continuous wave light sources	89
$\text{NaGdF}_4:\text{Nd},\text{Yb},\text{Er}@$ oleate	poly(acrylic acid)	<i>in vivo</i> bioimaging with minimized heating effect	90
$\text{NaYF}_4:\text{Yb},\text{Tm}@$ oleate	poly(vinyl pyrrolidone)	photo-induced release of biomacromolecules from hydrogels loaded with upconversion NPs	91

3.3.4.3 Two-step Replacement of Native Ligands via Strong Acids

A strategy developed by Capobianco *et al.*⁹² involves treatment of hydrophobic UCNPs with hydrochloric acid that can strip the native ligands off the surface to generate ligand-free and water-dispersible particles. These can then be coated with new ligands as demonstrated by the attachment of heparin⁹³ as schematically shown in Figure 3.10. The strategy was transferred to other ligands (see Table 3.6) and represents a quick and easy way to make UCNPs water dispersible. However, further studies on the stability and aggregation tendency of the uncoated particles may be needed.

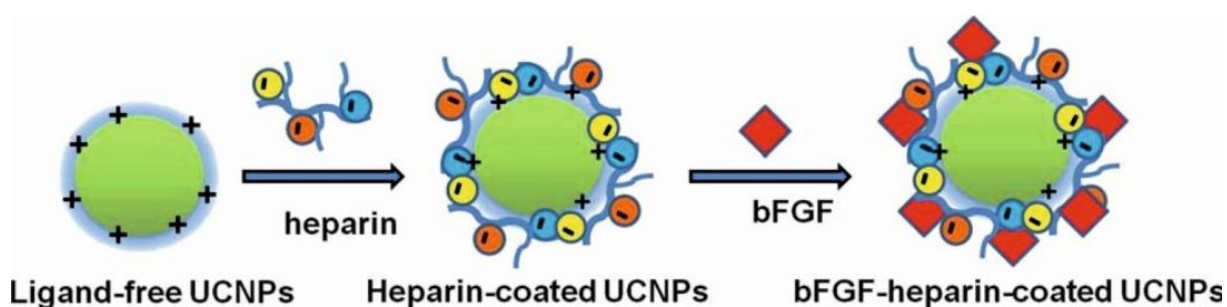


Figure 3.10 | Illustration of the procedure for preparing UCNPs coated with heparin and basic fibroblast growth factor (bFGF). Reproduced from ref. 93 with permission of The Royal Society of Chemistry.

Table 3.6 | Examples for indirect replacement of native ligands by first stripping off the ligand with hydrochloric acid and then adding the new capping ligand, and properties and applications of the resulting water-dispersible particles.

UCNP and native ligand	New surface capping	Properties and applications	Reference
NaYF ₄ :Yb,Tm@oleate	azobenzene-modified mesoporous silica	drug delivery	5
NaYF ₄ :Yb,Er,Tm@oleate	polyallylamine	conjugation to PEGylated graphene oxide for combined imaging and photothermal and photodynamic cancer therapy	94
NaYF ₄ :Yb,Er@oleate	lysine	conjugation to AuNPs for fluorescence resonance energy transfer assay to detect Cr(III) ions	95
NaYF ₄ :Yb,Tm,Gd@oleate	HS-PEG-NH ₂	bimodal magnetic resonance and fluorescence imaging of intracranial glioblastoma	96
NaYF ₄ :Yb,Er@oleate	citrate	conjugation to streptavidin for fluorescence hybridization assay on paper	97

3.4 Conclusions

In short and somewhat simplified terms one can make the following statements: Ligand modification (mainly by oxidation) gives low yields, is time consuming, and the particles tend to aggregate. It is the least often applied method. The formation of an additional layer on the surface of an UCNP using amphiphilic reagents gives particles of good stability in water solution, enables a large variety of head groups to be deposited, but requires expensive reagents and increases the thickness of the outer layer and thus the distance of the functional group to the particle core. Coatings with SiO₂, TiO₂, silver or gold result in water-stable particles that have low cytotoxicity but those coated with SiO₂ or TiO₂ tend to aggregate during work-up, and the size of the particle is enlarged. Two-step methods based on complete ligand exchange (using HCl or NOBF₄) are simple, affordable, and the new ligands are directly attached to the surface without substantially enlarging the particle size. While aggregation can occur after stripping off the oleate, the method results in particles of superior quality and homogeneity but of limited stability in buffer solution.

In terms of biocompatibility, there is no systematic study available so far that would allow comparisons to be made. We note that the term biocompatibility is often used in a wrong way. It shall be reminded that biocompatibility is defined by IUPAC as the *"ability to be in*

contact with a living(!) system without producing an adverse effect." This definition applies to adverse effects on both the NP and the living system. Biocompatibility and potential toxicity of NPs usually are being tested via (commercial) test kit using normal rat kidney cells. Biocompatibility is not an issue when studying blood or urine samples. UCNPs coated with PEG or phospholipids generally are likely to possess excellent biocompatibility, while chemical coatings such as silica are adequate but not excellent in this respect. Even surfaces are preferred over uneven surfaces, and surface defects (that may cause the release of lanthanide ions compromise biocompatibility and/or cause an immunoresponse) are disadvantageous even though the trivalent ions released by conventional UCNPs are less toxic than those released by Cd-based quantum dots. No studies are available on the biocompatibility of the less often used UCNPs based on heavy metal ions, though.

In terms of cytotoxicity, it appears that UCNPs are less toxic than other particles, but, as was stated by Gu et al.,⁹⁸ data from in-vivo cytotoxicity studies may not reflect chronic toxicity. Few data are available on dose-effect relationships, and less data on quantitative correlations between their toxicological properties and their nano-characteristics including size, surface chemistry, surface charge, shape and morphology. While not a compromising current uses in imaging of cells and tissue, the lack of systematic fundamental research on the toxicity of UCNPs may obstruct medical applications at present.

In terms of applications, the following comments may be useful. If UCNPs are intended for use in (cellular) imaging, coatings with SiO₂ and the like result in particles of good stability in culture media. UCNPs for use in bioconjugation may be better coated with amphiphilic molecules where a variety of functional head groups is available, or with gold that can be further modified, for example via gold-thiol interactions. FRET studies are best performed with UCNPs modified by ligand exchange (using NOBF₄ as a reagent, for example) because this results in a small, constant and well controllable distance between the core and any fluorophore on the surface. UCNPs for use in electrophoresis, in turn, can be well modified by using amphiphilic polymers which warrant long-term stability because ligand detachment hardly occurs.

Current challenges include a better control of particle size and homogeneity, more reproducible methods for surface loading and/or modification, the search for synthetic methods yielding higher yields of UCNPs, the need for materials displaying higher quantum yields in water solution (ideally without tedious surface modification), improved methods for work-up (including the suppression of aggregation), new methods for surface characterization, and the design of more affordable reagents for surface modifications. Unfortunately, much synthetic research in the area is of the trial-and-error kind due to the

lack of understanding of the mechanisms causing the above limitations. Better control of the reproducibility of particle size and composition requires experimental skill, chemicals of high purity, non-leaching labware (glass!), and the careful exclusion of oxygen. Surface loading can be tested best *via* thermogravimetric analysis (TGA) which presently is the method of choice, but requires 10 to 15 mg of particles. Interestingly, inductively coupled plasma mass spectrometry – which is a powerful technique – is not often applied, possibly because of costs. The fight against aggregation is never-ending. No single good method can be recommended as its tendency strongly depends on the kind of surface and its charge. A simple rule of thumb tells that particles with negatively charged surfaces tend to aggregate in presence of divalent ions, while positively charged do (less) so in presence of bivalent anions. One also notes the lack of a fast method for the determination of the degree of aggregation and sedimentation. Despite these challenges, UCNPs are considered to represent very promising new materials as evidenced by the almost exponential increase in the number of articles covering the subject.

References

- (1) Auzel, F. Upconversion and Anti-Stokes Processes with f and d Ions in Solids. *Chem. Rev.* **2004**, *104*, 139–173.
- (2) Boyer, J.-C.; van Veggel, F. C. J. M. Absolute Quantum Yield Measurements of Colloidal NaYF₄:Er³⁺, Yb³⁺ Upconverting Nanoparticles. *Nanoscale* **2010**, *2*, 1417–1419.
- (3) van Veggel, F. C. J. M.; Dong, C.; Johnson, N. J. J.; Pichaandi, J. Ln³⁺-Doped Nanoparticles for Upconversion and Magnetic Resonance Imaging: Some Critical Notes on Recent Progress and Some Aspects to Be Considered. *Nanoscale* **2012**, *4*, 7309–7321.
- (4) Qian, H. S.; Guo, H. C.; Ho, P. C.-L.; Mahendran, R.; Zhang, Y. Mesoporous-Silica-Coated Up-Conversion Fluorescent Nanoparticles for Photodynamic Therapy. *Small* **2009**, *5*, 2285–2290.
- (5) Liu, J.; Bu, W.; Pan, L.; Shi, J. NIR-Triggered Anticancer Drug Delivery by Upconverting Nanoparticles with Integrated Azobenzene-Modified Mesoporous Silica. *Angew. Chem. Int. Ed.* **2013**, *52*, 4375–4379.
- (6) Mader, H. S.; Kele, P.; Saleh, S. M.; Wolfbeis, O. S. Upconverting Luminescent Nanoparticles for Use in Bioconjugation and Bioimaging. *Curr. Opin. Chem. Biol.* **2010**, *14*, 582–596.
- (7) Arppe, R.; Nareoja, T.; Nylund, S.; Mattsson, L.; Koho, S.; Rosenholm, J. M.; Soukka, T.; Schäferling, M. Photon Upconversion Sensitized Nanoprobes for Sensing and Imaging of pH. *Nanoscale* **2014**, *6*, 6837–6843.

- (8) Achatz, D. E.; Meier, R. J.; Fischer, L. H.; Wolfbeis, O. S. Luminescent Sensing of Oxygen Using a Quenchable Probe and Upconverting Nanoparticles. *Angew. Chem. Int. Ed.* **2011**, *50*, 260–263.
- (9) Mader, H. S.; Wolfbeis, O. S. Optical Ammonia Sensor Based on Upconverting Luminescent Nanoparticles. *Anal. Chem.* **2010**, *82*, 5002–5004.
- (10) Saleh, S. M.; Ali, R.; Wolfbeis, O. S. Quenching of the Luminescence of Upconverting Luminescent Nanoparticles by Heavy Metal Ions. *Chem. Eur. J.* **2011**, *17*, 14611–14617.
- (11) Ali, R.; Saleh, S. M.; Meier, R. J.; Azab, H. A.; Abdelgawad, I. I.; Wolfbeis, O. S. Upconverting Nanoparticle Based Optical Sensor for Carbon Dioxide. *Sens. Actuators, B* **2010**, *150*, 126–131.
- (12) Achatz, D. E.; Ali, R.; Wolfbeis, O. S. Fluorescent Sensing, Biosensing, and Screening Using Upconverting Nanoparticles. *Topics Curr. Chem.* **2011**, *300*, 29–50.
- (13) Wang, M.; Hou, W.; Mi, C.-C.; Wang, W.-X.; Xu, Z.-R.; Teng, H.-H.; Mao, C.-B.; Xu, S.-K. Immunoassay of Goat Antihuman Immunoglobulin G Antibody Based on Luminescence Resonance Energy Transfer between Near-Infrared Responsive NaYF₄:Yb, Er Upconversion Fluorescent Nanoparticles and Gold Nanoparticles. *Anal. Chem.* **2009**, *81*, 8783–8789.
- (14) Tsang, M.-K., Chan, C.-F., Wong, K.-L., Hao, J. Comparative Studies of Upconversion Luminescence Characteristics and Cell Bioimaging Based on One-step Synthesized Upconversion Nanoparticles Capped with Different Functional Groups. *J. Lumin.* **2015**, *157*, 172–178.
- (15) Chen, G.; Qiu, H.; Prasad, P. N.; Chen, X. Upconversion Nanoparticles: Design, Nanochemistry, and Applications in Theranostics. *Chem. Rev.* **2014**, *114*, 5161–5214.
- (16) DaCosta, M. V.; Doughan, S.; Han, Y.; Krull, U. J. Lanthanide Upconversion Nanoparticles and Applications in Bioassays and Bioimaging: A Review. *Anal. Chim. Acta* **2014**, *832*, 1–33.
- (17) Liu, Y., Tu, D., Zhu, H., Chen, X. Lanthanide-doped Luminescent Nanoprobes: Controlled Synthesis, Optical Spectroscopy, and Bioapplications. *Chem. Soc. Rev.* **2013**, *42*, 6924–6958.
- (18) Zhou, J., Liu, Z., Li, F. Upconversion Nanophosphors for Small-Animal Imaging. *Chem. Soc. Rev.* **2012**, *41*, 1323–1349.
- (19) Li, L.-L.; Zhang, R.; Yin, L.; Zheng, K.; Qin, W.; Selvin, P. R.; Lu, Y. Biomimetic Surface Engineering of Lanthanide-Doped Upconversion Nanoparticles as Versatile Bioprobes. *Angew. Chem.* **2012**, *124*, 6225–6229.
- (20) Feng, W., Zhu, X., Li, F. Recent Advances in the Optimization and Functionalization of Upconversion Nanomaterials for in vivo Bioapplications. *NPG Asia Mater.* **2013**, *5*, e75.
- (21) Rao, L., Lu, W., Ren, G., Wang, H., Yi, Z., Liu, H., Zeng, S. Monodispersed LaF₃ Nanocrystals: Shape-Controllable Synthesis, Excitation-Power-Dependent Multi-Color Tuning and Intense Near-Infrared Upconversion Emission. *Nanotechnology* **2014**, *25*, 065703.

- (22) Li, Z.; Zhang, Y.; Jiang, S. Multicolor Core/Shell-Structured Upconversion Fluorescent Nanoparticles. *Adv. Mater.* **2008**, *20*, 4765–4769.
- (23) Chan, E. M.; Han, G.; Goldberg, J. D.; Gargas, D. J.; Ostrowski, A. D.; Schuck, P. J.; Cohen, B. C.; Milliron, D. J. Combinatorial Discovery of Lanthanide-Doped Nanocrystals with Spectrally Pure Upconverted Emission. *Nano Lett.* **2012**, *12*, 3839–3845.
- (24) Sun, L.-D.; Wang, Y.-F.; Yan, C.-H. Paradigms and Challenges for Bioapplication of Rare Earth Upconversion Luminescent Nanoparticles: Small Size and Tunable Emission/Excitation Spectra. *Acc. Chem. Res.* **2014**, *47*, 1001–1009.
- (25) Erathodiyil, N.; Ying, J. Y. Functionalization of Inorganic Nanoparticles for Bioimaging Applications. *Acc. Chem. Res.* **2011**, *44*, 925–935.
- (26) Chen, Z.; Chen, H.; Hu, H.; Yu, M.; Li, F.; Zhang, Q.; Zhou, Z.; Yi, T.; Huang, C. Versatile Synthesis Strategy for Carboxylic Acid-functionalized Upconverting Nanophosphors as Biological Labels. *J. Am. Chem. Soc.* **2008**, *130*, 3023–3029.
- (27) Zhou, H.-P.; Xu, C.-H.; Sun, W.; Yan, C.-H. Clean and Flexible Modification Strategy for Carboxyl/Aldehyde-Functionalized Upconversion Nanoparticles and their Optical Applications. *Adv. Funct. Mater.* **2009**, *19*, 3892–3900.
- (28) Hu, H.; Yu, M.; Li, F.; Chen, Z.; Gao, X.; Xiong, L.; Huang, C. Facile Epoxidation Strategy for Producing Amphiphilic Up-Converting Rare-Earth Nanophosphors as Biological Labels. *Chem. Mater.* **2008**, *20*, 7003–7009.
- (29) Dai, Y.; Yang, D.; Ma, P.; Kang, X.; Zhang, X.; Li, C.; Hou, Z.; Cheng, Z.; Lin, J. Doxorubicin Conjugated NaYF₄:Yb³⁺/Tm³⁺ Nanoparticles for Therapy and Sensing of Drug Delivery by Luminescence Resonance Energy Transfer. *Biomaterials* **2012**, *33*, 8704–8713.
- (30) Park, Y. I.; Kim, J. H.; Lee, K. T.; Jeon, K.-S.; Na, H. B.; Yu, J. H.; Kim, H. M.; Lee, N.; Choi, S. H.; Baik, S.-I.; Kim, H.; Park, S. P.; Park, B.-J.; Kim, Y. W.; Lee, S. H.; Yoon, S.-Y.; Song, I. C.; Moon, W. K.; Suh, Y., D.; Hyeon, T. Nonblinking and Nonbleaching Upconverting Nanoparticles as an Optical Imaging Nanoprobe and T1 Magnetic Resonance Imaging Contrast Agent. *Adv. Mater.* **2009**, *21*, 4467–4471.
- (31) Nam, S. H.; Bae, Y. M.; Park, Y. I.; Kim, J. H.; Kim, H. M.; Choi, J. S.; Lee, K. T.; Hyeon, T.; Suh, Y. D. Long-Term Real-Time Tracking of Lanthanide Ion Doped Upconverting Nanoparticles in Living Cells. *Angew. Chem.* **2011**, *123*, 6217–6221.
- (32) Ren, W.; Tian, G.; Jian, S.; Gu, Z.; Zhou, L.; Yan, L.; Jin, S.; Yin, W.; Zhao, Y. Tween-Coated NaYF₄:Yb,Er/NaYF₄ Core/Shell Upconversion Nanoparticles for Bioimaging and Drug Delivery. *RSC Adv.* **2012**, *2*, 7037–7041.
- (33) Liang, S.; Zhang, X.; Wu, Z.; Liu, Y.; Zhang, H.; Sun, H.; Sun, H.; Yang, B. Decoration of Up-Converting NaYF₄:Yb,Er(Tm) Nanoparticles with Surfactant Bilayer. A Versatile Strategy to Perform Oil-to-Water Phase Transfer and Subsequently Surface Silication. *CrystEngComm* **2012**, *14*, 3484–3489.
- (34) Pellegrino, T.; Manna, L.; Kudera, S.; Liedl, T.; Koktysh, D.; Rogach, A. L.; Keller, S.; Rädler, J.; Natile, G.; Parak, W. J. Hydrophobic Nanocrystals Coated with an Amphiphilic Polymer Shell: A General Route to Water Soluble Nanocrystals. *Nano Lett.* **2004**, *4*, 703–707.

- (35) Wang, C.; Tao, H.; Cheng, L.; Liu, Z. Near-Infrared Light Induced *in vivo* Photodynamic Therapy of Cancer Based on Upconversion Nanoparticles. *Biomaterials* **2011**, *32*, 6145–6154.
- (36) Li, X.; Wu, Y.; Liu, Y.; Zou, X.; Yao, L.; Li, F.; Feng, W. Cyclometallated Ruthenium Complex-Modified Upconversion Nanophosphors for Selective Detection of Hg²⁺ Ions in Water. *Nanoscale* **2014**, *6*, 1020–1028.
- (37) Jiang, G.; Pichaandi, J.; Johnson, N. J. J.; Burke, R. D., van Veggel, F. C. J. M. An Effective Polymer Cross-Linking Strategy to Obtain Stable Dispersions of Upconverting NaYF₄ Nanoparticles in Buffers and Biological Growth Media for Biolabeling Applications. *Langmuir* **2012**, *28*, 3239–3247.
- (38) Yi, G.-S.; Chow, G.-M. Water-Soluble NaYF₄:Yb,Er(Tm)/NaYF₄/Polymer Core/Shell/Shell Nanoparticles with Significant Enhancement of Upconversion Fluorescence. *Chem. Mater.* **2007**, *19*, 341–343.
- (39) Cheng, L.; Yang, K.; Zhang, S.; Shao, M.; Lee, S.; Liu, Z. Highly-Sensitive Multiplexed *in vivo* Imaging Using PEG-ylated Upconversion Nanoparticles. *Nano Res.* **2010**, *3*, 722–732.
- (40) Cui, S.; Chen, H.; Zhu, H.; Tian, J.; Chi, X.; Qian, Z.; Achilefu, S.; Gu, Y. Amphiphilic Chitosan Modified Upconversion Nanoparticles for *in vivo* Photodynamic Therapy Induced by Near-Infrared Light. *J. Mater. Chem.* **2012**, *22*, 4861–4873.
- (41) Chen, B.; Dong, B.; Wang, J.; Zhang, S.; Xu, L.; Yu, W.; Song, H. Amphiphilic Silane Modified NaYF₄:Yb,Er Loaded with Eu(TTA)₃(TPPO)₂ Nanoparticles and their Multi-Functions: Dual Mode Temperature Sensing and Cell Imaging. *Nanoscale* **2013**, *5*, 8541–8549.
- (42) Budijono, S. J.; Shan, J.; Yao, N.; Miura, Y.; Hoye, T.; Austin, R. H.; Ju, Y., Prud'homme, R. K. Synthesis of Stable Block-Copolymer-Protected NaYF₄:Yb³⁺, Er³⁺ Up-Converting Phosphor Nanoparticles. *Chem. Mater.* **2010**, *22*, 311–318.
- (43) Sudheendra, L.; Ortalan, V.; Dey, S.; Browning, N. D.; Kennedy, I. M. Plasmonic Enhanced Emissions from Cubic NaYF₄:Yb:Er/Tm Nanophosphors. *Chem. Mater.* **2011**, *23*, 2987–2993.
- (44) Hu, H.; Xiong, L.; Zhou, J.; Li, F.; Cao, T.; Huang, C. Multimodal-Luminescence Core–Shell Nanocomposites for Targeted Imaging of Tumor Cells. *Chem. Eur. J.* **2009**, *15*, 3577–3584.
- (45) Liu, B.; Li, C.; Yang, D.; Hou, Z.; Ma, P.; Cheng, Z.; Lian, H.; Huang, S.; Lin, J. Upconversion-Luminescent Core/Mesoporous-Silica-Shell-Structured β-NaYF₄:Yb³⁺,Er³⁺@SiO₂@mSiO₂ Composite Nanospheres: Fabrication and Drug-Storage/Release Properties. *Eur. J. Inorg. Chem.* **2014**, *2014*, 1906–1913.
- (46) Liang, L.; Liu, Y.; Zhao, X.-Z. Double-Shell β-NaYF₄:Yb³⁺, Er³⁺/SiO₂/TiO₂ Submicroplates as a Scattering and Upconverting Layer for Efficient Dye-Sensitized Solar Cells. *Chem. Commun.* **2013**, *49*, 3958–3960.
- (47) Zhang, Y.; Hong, Z. Synthesis of Lanthanide-Doped NaYF₄@TiO₂ Core-Shell Composites with Highly Crystalline and Tunable TiO₂ Shells Under Mild Conditions and Their Upconversion-Based Photocatalysis. *Nanoscale* **2013**, *5*, 8930–8933.

- (48) Zhang, H.; Li, Y.; Ivanov, I. A.; Qu, Y.; Huang, Y.; Duan, X. Plasmonic Modulation of the Upconversion Fluorescence in NaYF₄:Yb/Tm Hexaplate Nanocrystals Using Gold Nanoparticles or Nanoshells. *Angew. Chem. Int. Ed.* **2010**, *49*, 2865–2868.
- (49) Dong, B.; Xu, S.; Sun, J.; Bi, S.; Li, D.; Bai, X.; Wang, Y.; Wang, L.; Song, H. Multifunctional NaYF₄:Yb³⁺,Er³⁺@Ag Core/Shell Nanocomposites: Integration of Upconversion Imaging and Photothermal Therapy. *J. Mater. Chem.* **2011**, *21*, 6193–6200.
- (50) Jalil, R. A.; Zhang, Y. Biocompatibility of Silica Coated NaYF₄ Upconversion Fluorescent Nanocrystals. *Biomaterials* **2008**, *29*, 4122–4128.
- (51) Wang, M.; Mi, C.; Zhang, Y.; Liu, J.; Li, F.; Mao, C.; Xu, S. NIR-Responsive Silica-Coated NaYbF₄:Er/Tm/Ho Upconversion Fluorescent Nanoparticles with Tunable Emission Colors and Their Applications in Immunolabeling and Fluorescent Imaging of Cancer Cells. *J. Phys. Chem. C* **2009**, *113*, 19021–19027.
- (52) Idris, N. M.; Gnanasammandhan, M. K.; Zhang, J.; Ho, P. C.; Mahendran, R.; Zhang, Y. In Vivo Photodynamic Therapy Using Upconversion Nanoparticles as Remote-Controlled Nanotransducers. *Nat. Med.* **2012**, *18*, 1580–1585.
- (53) Bagwe, R. P.; Hilliard, L. R.; Tan, W. Surface Modification of Silica Nanoparticles to Reduce Aggregation and Nonspecific Binding. *Langmuir* **2006**, *22*, 4357–4362.
- (54) Hlavacek, A.; Sedlmeier, A.; Skladal, P.; Gorriss, H. H. Electrophoretic Characterization and Purification of Silica-Coated Photon-Upconverting Nanoparticles and Their Bioconjugates. *ACS Appl. Mater. Interf.* **2014**, *6*, 6930–6935.
- (55) Wang, M.; Mi, C.-C.; Wang, W.-X.; Liu, C.-H.; Wu, Y.-F.; Xu, Z.-R.; Mao, C.-B.; Xu, S.-K. Immunolabeling and NIR-Excited Fluorescent Imaging of HeLa Cells by Using NaYF₄:Yb,Er Upconversion Nanoparticles. *ACS Nano* **2009**, *3*, 1580–1586.
- (56) Liu, F.; Zhao, Q.; You, H.; Wang, Z. Synthesis of Stable Carboxy-terminated NaYF₄:Yb³⁺, Er³⁺@SiO₂ Nanoparticles with Ultrathin Shell for Biolabeling Applications. *J. Phys. Chem. C* **2013**, *5*, 1047–1053.
- (57) Li, C.; Hou, Z.; Dai, Y.; Yang, D.; Cheng, Z.; Ma, P.; Lin, J. A. Facile Fabrication of Upconversion Luminescent and Mesoporous Core-Shell Structured β-NaYF₄:Yb³⁺, Er³⁺@mSiO₂ Nanocomposite Spheres for Anti-Cancer Drug Delivery and Cell Imaging. *Biomater. Sci.* **2013**, *1*, 213–223.
- (58) Wilhelm, S.; Hirsch, T.; Patterson, W. M.; Scheucher, E.; Mayr, T.; Wolfbeis, O. S. Multicolor Upconversion Nanoparticles for Protein Conjugation. *Theranostics* **2013**, *3*, 239–248.
- (59) Shan, G.; Weissleder, R.; Hilderbrand, S. A. Upconverting Organic Dye Doped Core-Shell Nano-Composites for Dual-Modality NIR Imaging and Photo-Thermal Therapy. *Theranostics* **2013**, *3*, 267–274.
- (60) Li, C.; Hou, Z.; Dai, Y.; Yang, D.; Cheng, Z.; Ma, P.; Lin, J. A Facile Fabrication of Upconversion Luminescent and Mesoporous Core-Shell Structured β-NaYF₄:Yb³⁺, Er³⁺@mSiO₂ Nanocomposite Spheres for Anti-Cancer Drug Delivery and Cell Imaging. *Biomater. Sci.* **2013**, *1*, 213–223.

- (61) Sun, L.; Liu, T.; Qiu, Y.; Liu, J.; Shi, L.; Wolfbeis, O. Direct Formation of Mesoporous Upconverting Core-Shell Nanoparticles for Bioimaging of Living Cells. *Microchim. Acta* **2013**, *180*, 1-7.
- (62) Zhao, L.; Peng, J.; Chen, M.; Liu, Y.; Yao, L.; Feng, W.; Li, F. Yolk-Shell Upconversion Nanocomposites for LRET Sensing of Cysteine/Homocysteine. *ACS Appl. Mater. Interf.* **2014**. ASAP article. DOI: 10.1021/am501249p.
- (63) Schäfer, H.; Ptacek, P.; Kömpe, K.; Haase, M. Lanthanide-Doped NaYF₄ Nanocrystals in Aqueous Solution Displaying Strong Up-Conversion Emission. *Chem. Mater.* **2007**, *19*, 1396–1400.
- (64) Xia, L.; Kong, X.; Liu, X.; Tu, L.; Zhang, Y.; Chang, Y.; Liu, K.; Shen, D.; Zhao, H.; Zhang, H. An Upconversion Nanoparticle - Zinc Phthalocyanine Based Nanophotosensitizer for Photodynamic Therapy. *Biomaterials* **2014**, *35*, 4146–4156.
- (65) Voliani, V.; González-Béjar, M.; Herranz-Pérez, V.; Duran-Moreno, M.; Signore, G.; Garcia-Verdugo, J. M.; Pérez-Prieto, J. Orthogonal Functionalization of Upconverting NaYF₄ Nanocrystals. *Chem. Eur. J.* **2013**, *19*, 13538–13546.
- (66) Zhu, X., Da Silva, B., Zou, X., Shen, B., Sun, Y., Feng, W., Li, F. Intra-Arterial Infusion of PEGylated Upconversion Nanophosphors to Improve the Initial Uptake by Tumors in vivo. *RSC Adv.* **2014**, *4*, 23580–23584.
- (67) Zhou, L., He, B., Huang, J., Cheng, Z., Xu, X., Wei, C. Multihydroxy Dendritic Upconversion Nanoparticles with Enhanced Water Dispersibility and Surface Functionality for Bioimaging. *ACS Appl. Mater. Interfaces* **2014**, *6*, 7719–7727.
- (68) Chen, Q.; Wang, X.; Chen, F.; Zhang, Q.; Dong, B.; Yang, H.; Liu, G.; Zhu, Y. Functionalization of Upconverted Luminescent NaYF₄:Yb/Er Nanocrystals by Folic Acid-Chitosan Conjugates for Targeted Lung Cancer Cell Imaging. *J. Mater. Chem.* **2011**, *21*, 7661–7667.
- (69) Liebherr, R. B.; Soukka, T.; Wolfbeis, O. S.; Gorris, H. H. Maleimide Activation of Photon Upconverting Nanoparticles for Bioconjugation. *Nanotechnology* **2012**, *23*, 485103.
- (70) Cao, T.; Yang, T.; Gao, Y.; Yang, Y.; Hu, H.; Li, F. Water-Soluble NaYF₄:Yb/Er Upconversion Nanophosphors: Synthesis, Characteristics and Application in Bioimaging. *Inorg. Chem. Comm.* **2010**, *13*, 392–394.
- (71) Zhang, Q.; Song, K.; Zhao, J.; Kong, X.; Sun, Y.; Liu, X.; Zhang, Y.; Zeng, Q.; Zhang, H. Hexanedioic Acid Mediated Surface-Ligand-Exchange Process for Transferring NaYF₄:Yb/Er (or Yb/Tm) Up-Converting Nanoparticles from Hydrophobic to Hydrophilic. *J. Colloid Interface Sci.* **2009**, *336*, 171–175.
- (72) Yi, G. S.; Chow, G. M. Synthesis of Hexagonal-Phase NaYF₄:Yb,Er and NaYF₄:Yb,Tm Nanocrystals with Efficient Up-Conversion Fluorescence. *Adv. Funct. Mater.* **2006**, *16*, 2324–2329.
- (73) Boyer, J.-C.; Manseau, M.-P.; Murray, J. I.; van Veggel, F. C. J. M. Surface Modification of Upconverting NaYF₄ Nanoparticles with PEG-Phosphate Ligands for NIR (800 nm) Biolabeling within the Biological Window. *Langmuir* **2010**, *26*, 1157–1164.

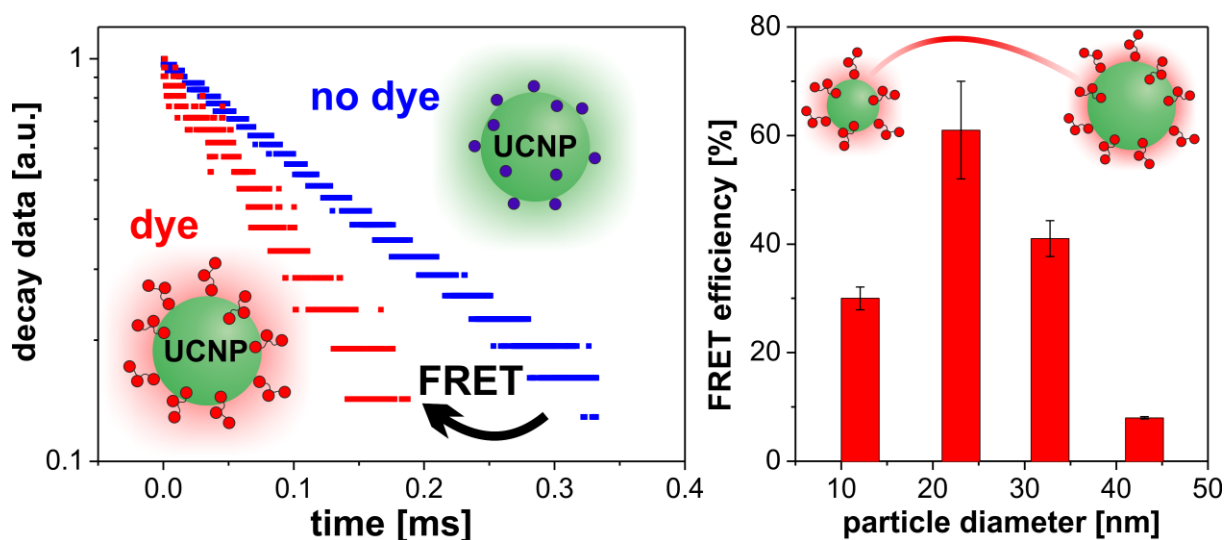
- (74) Bogdan, N.; Vetrone, F.; Roy, R.; Capobianco, J. A. Carbohydrate-Coated Lanthanide-Doped Upconverting Nanoparticles for Lectin Recognition. *J. Mater. Chem.* **2010**, *20*, 7543–7550.
- (75) Nyk, M.; Kumar, R.; Ohulchanskyy, T. Y.; Bergey, E. J.; Prasad, P. N. High Contrast *in vitro* and *in vivo* Photoluminescence Bioimaging Using Near Infrared to Near Infrared Up-Conversion in Tm^{3+} and Yb^{3+} Doped Fluoride Nanophosphors. *Nano Lett.* **2008**, *8*, 3834–3838.
- (76) Xiong, L.; Yang, T.; Yang, Y.; Xu, C.; Li, F. Long-Term *in vivo* Biodistribution Imaging and Toxicity of Polyacrylic Acid-Coated Upconversion Nanophosphors. *Biomaterials* **2010**, *31*, 7078–7085.
- (77) Naccache, R.; Vetrone, F.; Mahalingam, V.; Cuccia, L. A.; Capobianco, J. A. Controlled Synthesis and Water Dispersibility of Hexagonal Phase $\text{NaGdF}_4:\text{Ho}^{3+}/\text{Yb}^{3+}$ Nanoparticles. *Chem. Mater.* **2009**, *21*, 717–723.
- (78) Johnson, N. J. J.; Sangeetha, N. M.; Boyer, J.-C.; van Veggel, F. C. J. M. Facile Ligand-Exchange with Polyvinylpyrrolidone and Subsequent Silica Coating of Hydrophobic Upconverting $\beta\text{-NaYF}_4:\text{Yb}^{3+}/\text{Er}^{3+}$ Nanoparticles. *Nanoscale* **2010**, *2*, 771–777.
- (79) González-Béjar, M.; Liras, M.; Francés-Soriano, L.; Voliani, V.; Herranz-Pérez, V.; Duran-Morena, M.; Garcia-Verdugo, J. M.; Alarcon, E. I.; Scaiano, J. C.; Pérez-Prieto, J. NIR excitation of upconversion nanohybrids containing a surface grafted Bodipy induces oxygen-mediated cancer cell death. *J. Mater. Chem. B* **2014**, *2*, 4554–4563.
- (80) Liras, M.; González-Béjar, M.; Peinado, E.; Francés-Soriano, L.; Pérez-Prieto, J.; Quijada-Garrido, I.; García, O. Thin Amphiphilic Polymer-Capped Upconversion Nanoparticles: Enhanced Emission and Thermoresponsive Properties. *Chem. Mater.* **2014**, *26*, 4014–4022.
- (81) Zhang, W.; Peng, B.; Tian, F.; Qin, W.; Qian, X. Facile Preparation of Well-Defined Hydrophilic Core-Shell Upconversion Nanoparticles for Selective Cell Membrane Glycan Labeling and Cancer Cell Imaging. *Anal. Chem.* **2014**, *86*, 482–489.
- (82) Li, L.-L.; Wu, P.; Hwang, K.; Lu, Y. An Exceptionally Simple Strategy for DNA-Functionalized Up-Conversion Nanoparticles as Biocompatible Agents for Nanoassembly, DNA Delivery, and Imaging. *J. Am. Chem. Soc.* **2013**, *135*, 2411–2414.
- (83) Liu, Q.; Sun, Y.; Li, C.; Zhou, J.; Li, C.; Yang, T.; Zhang, X.; Yi, T.; Wu, D.; Li, F. ^{18}F -Labeled Magnetic-Upconversion Nanophosphors via Rare-Earth Cation-Assisted Ligand Assembly. *ACS Nano* **2011**, *5*, 3146–3157.
- (84) Wang, C.; Cheng, L.; Liu, Y.; Wang, X.; Ma, X.; Deng, Z.; Li, Y.; Liu, Z. Imaging-Guided pH-Sensitive Photodynamic Therapy Using Charge Reversible Upconversion Nanoparticles under Near-Infrared Light. *Adv. Funct. Mater.* **2013**, *23*, 3077–3086.
- (85) Budijono, S. J.; Shan, J.; Yao, N.; Miura, Y.; Hoyer, T.; Austin, R. H.; Ju, Y.; Prud'homme, R. K. Synthesis of Stable Block-Copolymer-Protected $\text{NaYF}_4:\text{Yb}^{3+}, \text{Er}^{3+}$ Up-Converting Phosphor Nanoparticles. *Chem. Mater.* **2010**, *22*, 311–318.

- (86) Dong, A.; Ye, X.; Chen, J.; Kang, Y.; Gordon, T.; Kikkawa, J. M.; Murray, C. B. A Generalized Ligand-Exchange Strategy Enabling Sequential Surface Functionalization of Colloidal Nanocrystals. *J. Am. Chem. Soc.* **2011**, *133*, 998–1006.
- (87) Rosen, E. L.; Buonsanti, R.; Llordes, A.; Sawvel, A. M.; Milliron, D. J.; Helm, B. A. Exceptionally Mild Reactive Stripping of Native Ligands from Nanocrystal Surfaces by Using Meerwein's Salt. *Angew. Chemie* **2012**, *51*, 684–689.
- (88) Shen, J.; Chen, G.; Vu, A.-M.; Fan, W.; Bilsel, O. S.; Chang, C.-C.; Han, G. Engineering the Upconversion Nanoparticle Excitation Wavelength: Cascade Sensitization of Tri-Doped Upconversion Colloidal Nanoparticles at 800 nm. *Adv. Opt. Mater.* **2013**, *1*, 644–650.
- (89) Esipova, T. V.; Ye, X.; Collins, J. E.; Sakadžić, S.; Mandeville, E. T.; Murray, C. B.; Vinogradov, S. A. Dendritic Upconverting Nanoparticles Enable *in vivo* Multiphoton Microscopy with Low-Power Continuous Wave Sources. *Proc. Natl. Acad. Sci. U.S.A.* **2012**, *109*, 20826–20831.
- (90) Wang, Y.-F.; Liu, G.-Y.; Sun, L.-D.; Xiao, J.-W.; Zhou, J.-C.; Yan, C.-H. Nd³⁺-Sensitized Upconversion Nanophosphors: Efficient *in vivo* Bioimaging Probes with Minimized Heating Effect. *ACS Nano* **2013**, *7*, 7200–7206.
- (91) Yan, B.; Boyer, J.-C.; Habault, D.; Branda, N. R.; Zhao, Y. Near Infrared Light Triggered Release of Biomacromolecules from Hydrogels Loaded with Upconversion Nanoparticles. *J. Am. Chem. Soc.* **2012**, *134*, 16558–16561.
- (92) Bogdan, N.; Vetrone, F.; Ozin, G. A.; Capobianco, J. A. Synthesis of Ligand-Free Colloidally Stable Water Dispersible Brightly Luminescent Lanthanide-Doped Upconverting Nanoparticles. *Nano Lett.* **2011**, *11*, 835–840.
- (93) Bogdan, N.; Rodríguez, E. M.; Sanz-Rodríguez, F.; de la Cruz, M. C. I.; Juarranz, Á.; Jaque, D.; Solé, J. G.; Capobianco, J. A. Bio-Functionalization of Ligand-Free Upconverting Lanthanide Doped Nanoparticles for Bio-Imaging and Cell Targeting. *Nanoscale* **2012**, *4*, 3647–3650.
- (94) Wang, Y.; Wang, H.; Liu, D.; Song, S.; Wang, X.; Zhang, H. Graphene Oxide Covalently Grafted Upconversion Nanoparticles for Combined NIR Mediated Imaging and Photothermal/Photodynamic Cancer Therapy. *Biomaterials* **2013**, *34*, 7715–7724.
- (95) Liu, B.; Tan, H.; Chen, Y. Upconversion Nanoparticle-Based Fluorescence Resonance Energy Transfer Assay for Cr(III) Ions in Urine. *Anal. Chim. Acta* **2013**, *761*, 178–185.
- (96) Ni, D.; Zhang, J.; Bu, W.; Xing, H.; Han, F.; Xiao, Q.; Yao, Z.; Chen, F.; He, Q.; Liu, J.; Zhang, S.; Fan, W.; Zhou, L.; Peng, W.; Shi, J. Dual-Targeting Upconversion Nanoprobes across the Blood-Brain Barrier for Magnetic Resonance/Fluorescence Imaging of Intracranial Glioblastoma. *ACS Nano* **2014**, *8*, 1231–1242.
- (97) Zhou, F.; Noor, M. O.; Krull, U. J. Luminescence Resonance Energy Transfer-Based Nucleic Acid Hybridization Assay on Cellulose Paper with Upconverting Phosphor as Donors. *Anal. Chem.* **2014**, *86*, 2719–2726.
- (98) Gu, Z.; Yan, L.; Tian, G.; Li, S.; Chai, Z.; Zhao, Y. Recent Advances in Design and Fabrication of Upconversion Nanoparticles and Their Safe Theranostic Applications. *Adv. Mater.* **2013**, *25*, 3758–3779.

4 PARTICLE-SIZE DEPENDENT FÖRSTER RESONANCE ENERGY TRANSFER FROM UPCONVERSION NANOPARTICLES TO ORGANIC DYES

4.1 Abstract

The potential of upconversion nanoparticles (UCNPs) as donors in Förster resonance energy transfer (FRET) applications has been vividly debated, ranging from directly bound acceptor dyes to core-shell designs and steady-state and time-resolved detection schemes. In order to identify the ideal particle architecture for FRET-based applications, we performed a systematic spectroscopic study of the influence of UCNP size on FRET efficiencies with the fluorescent dyes rose bengal and sulforhodamine B acting as acceptors for the green upconversion emission. Eight high-quality Yb,Er-doped UCNPs with precisely controlled sizes between 10 nm and 43 nm were prepared using a high temperature synthesis. All particles were functionalized with the organic dyes by a two-step ligand exchange procedure, thereby minimizing donor-acceptor distances. Time-resolved studies on the donor luminescence allowed for the elimination of dependencies on excitation power and particle concentration and for the discrimination between FRET and inner filter effects. The FRET efficiency increased from almost 0% to a maximum of 60% when reducing the particle diameter from 43 nm to 21 nm, which was attributed to an increasing fraction of the total amount of Er^{3+} donors inside the UCNPs being within Förster distance of the respective FRET pair. Further reduction of the particle diameter did not benefit the energy transfer, demonstrating the contribution of opposing effects, e.g. an increasing competition of non-radiative surface deactivation at larger surface-to-volume ratios. Thus, for small UCNPs with diameters below 17 nm, the growth of a thin inactive, protective shell led to a substantial increase in the FRET efficiency of up to 60%, contrary to the behavior of larger UCNPs. Such dye-UCNP architectures can also provide an elegant way to shift the UCNP emission color, since the fluorescence intensity of the organic dyes excited by FRET was comparable to that of the upconversion emission of smaller particles ($d \leq 21$ nm).



Scheme 4.1 | Schematic representation of upconversion luminescence lifetime changes induced by FRET between UCNPs and organic dyes. The reduction of the lifetime and the resulting FRET efficiencies are dependent on the nanoparticle size with an optimum at diameters around 20 – 25 nm.

This chapter has been published.

Verena Muhr, Christian Würth, Marco Kraft, Markus Buchner, Antje J. Baeumner, Ute Resch-Genger and Thomas Hirsch. *Analytical Chemistry*, **2017**, 89 (9), 4868–4874

Author contributions

The experimental work was carried out by VM. CW and MK performed control lifetime measurements on a different device. MB discussed surface modification and characterization. All authors discussed the results. VM wrote the manuscript. The article was revised by AJB, URG, and TH. URG and TH are corresponding authors.

4.2 Introduction

Luminescence-based techniques are powerful tools in biological sensing and imaging due to their versatility and high sensitivity.^{1–3} Methods based on Förster resonance energy transfer (FRET), that is also referred to as luminescence resonance energy transfer (LRET) in lanthanide-based systems, have been thoroughly investigated especially for bioanalytical applications.^{4,5} This energy transfer process involves the non-radiative energy transfer between two chromophores, with the electronically excited emissive donor chromophore transferring its energy to an absorbing emissive or non-emissive acceptor chromophore through non-radiative dipole–dipole coupling. As the efficiency of FRET is inversely proportional to the sixth power of the distance (r) between donor and acceptor, making this process extremely sensitive to small changes in distance, it has become known as a "nanoscopic ruler"(Equation 1):⁶

$$k_T(r) = \frac{1}{\tau_D} \left(\frac{R_0}{r} \right)^6 \quad (1)$$

with τ_D representing the donor lifetime and R_0 denoting the Förster distance of the donor-acceptor pair. Typically, FRET occurs only at distances below 10 nm. Consequently, it has been established for the observation of bioaffinity reactions such as DNA hybridization and receptor interactions^{7,8} and the design of certain types of optical probes like molecular beacons or cleavable probes.⁹ Common FRET systems consisting of two fluorescent organic dyes often suffer from photobleaching, high background fluorescence in biological matrices, spectral crosstalk, and short fluorescence lifetimes in the lower ns range. In order to circumvent at least some of these drawbacks, luminescent nanomaterials have been increasingly used.^{10–12} Particularly the potential of lanthanide-doped upconversion nanoparticles (UCNPs),¹³ a promising class of emitters as donors in FRET applications, has been vividly debated.¹⁴ Near infrared (NIR) excitation of UCNPs by sequential absorption of two or more photons leads to multiple emission bands in the ultraviolet, visible, and NIR characterized by large anti-Stokes shifts.¹⁵ Together with long luminescence lifetimes in the μ s range, outstanding photostability and chemical inertness these class of luminophores enable high penetration depth in biological tissue while generating basically zero background fluorescence and thus high signal-to-noise ratios.¹⁶ Moreover, in contrast to quantum dots they do not blink.¹⁷ One of the most efficient materials for photon upconversion is NaYF₄ doped with the rare earth ion Yb³⁺ as sensitizer in combination with either Er³⁺ or Tm³⁺ as emissive activators.¹⁸ Substantial progress has been made regarding an improved synthesis of monodisperse, size controlled and colloidally stable UCNPs with optimized upconversion characteristics.^{19–21} Within the last years, an increasing number of sensing schemes for

DNA,^{22,23} small biomolecules,²⁴ temperature,²⁵ and metal ions,²⁶ or applications for photodynamic therapy with simultaneous imaging²⁷ have been described using UCNP-based FRET systems. The majority of these applications rely on the ratiometric readout of the emission intensity of the donor UCNPs, utilizing the intensity of the UCNP emission band that is not involved in FRET, as reference signal.^{28,29} Time-resolved detection schemes have been rarely used for UCNPs even though FRET is accompanied by a reduction of the donor luminescence lifetime and, additionally, by a prolongation of the acceptor emission in the case of donors with long lifetimes, such as lanthanide emitters.³¹⁻³³ Time-resolved measurements are, however, particularly attractive as unlike the emission intensity, the lifetime is mostly unaffected by several critical parameters, *i.e.* the luminophore concentration, which can be challenging to determine especially in the case of nanoparticles. Moreover, in the case of UCNPs with their nonlinear excitation properties, lifetime measurements are much less sensitive to fluctuations in the excitation power density as intensity measurements.³⁴ Despite its obvious (bio)analytical potential, FRET in UCNP systems is still poorly explored³⁵⁻³⁷ and can differ significantly from FRET in pairs of molecular emitters or in quantum dot-dye pairs. It has to be kept in mind that a UCNP consists of a large number of individual emitters like Er³⁺ ions in different environments. The surface of the UCNPs is capable of binding multiple FRET acceptors at varying distances to the different donor lanthanide ions. This yields a situation substantially different from the 1:1 stoichiometry in pairs of organic emitters.³⁸ It also differs from the situation found in semiconductor nanocrystal-dye FRET systems, as here, each nanoscale donor presents a single emitter.³⁹ The fact that the upconversion process relies on intra-particle energy transfer cascades between the different emitting lanthanide ions, competing with non-radiative deactivation pathways, distinguishes UCNP-based FRET systems from many other multichromophoric donor-acceptor systems, *e.g.* conventional dye-doped polymer particles.⁴⁰ Assuming that the lanthanide donor ions are equally distributed within the volume of the UCNP, this implies that particles with diameters > 15 nm contain a large fraction of donor ions in the UCNP center beyond the effective Förster distance of roughly 5 nm that cannot take part in an efficient FRET process. As a consequence, the particle size is expected to significantly influence the FRET efficiency,^{41,42} yet such effects have not been explored systematically until now. Aiming at the rational design of efficient FRET sensors based on UCNPs, this encouraged us to assess the efficiency of FRET from Yb,Er-doped UCNPs with sizes between 10 and 43 nm to the organic dyes rose bengal and sulforhodamine B, acting as model FRET acceptors for the green emission of Er³⁺. Energy transfer efficiencies were studied by steady state and time resolved fluorometry.

4.3 Results and Discussion

4.3.1 Synthesis of Hydrophobic UCNPs with Controlled Sizes

In order to study the influence of the particle diameter on the FRET efficiency, Yb,Er-doped NaYF₄ UCNPs with eight different mean diameters ranging from 10 nm to 43 nm were prepared. A molar doping ratio of 20% Yb and 2% Er, for sensitizer and activator ions, respectively, was chosen according to the reported composition of the most common upconversion (UC) system so far. Higher amounts of both sensitizer and activator can facilitate the concentration quenching, leading to a decrease of the UC emission.¹³ All UCNPs were characterized by transmission electron microscopy (TEM), inductively coupled plasma optical emission spectrometry, and X-ray diffraction (XRD). As shown in Figure 4.1, all UCNPs were monodisperse with a coefficient of variation < 5% and of hexagonal crystal structure. Smaller diameters led to a broadening and a slight shift of the reflexes observed by XRD. While the broadening is the result of the decreasing particle size, the shift can be explained by a change in crystal lattice. The increasing amounts of Gd³⁺ in the smaller UCNPs induced the transition of the hexagonal NaYF₄ crystal lattice to a hexagonal NaGdF₄ crystal lattice (e.g., particles with a diameter of 10 nm contain 48% Y³⁺- and 30% Gd³⁺-ions).⁴³ Colloidal stability was proven by DLS measurements in cyclohexane. In all cases the UCNPs did not show signs of aggregation, even when dispersed at concentrations of up to 35 mg·mL⁻¹.

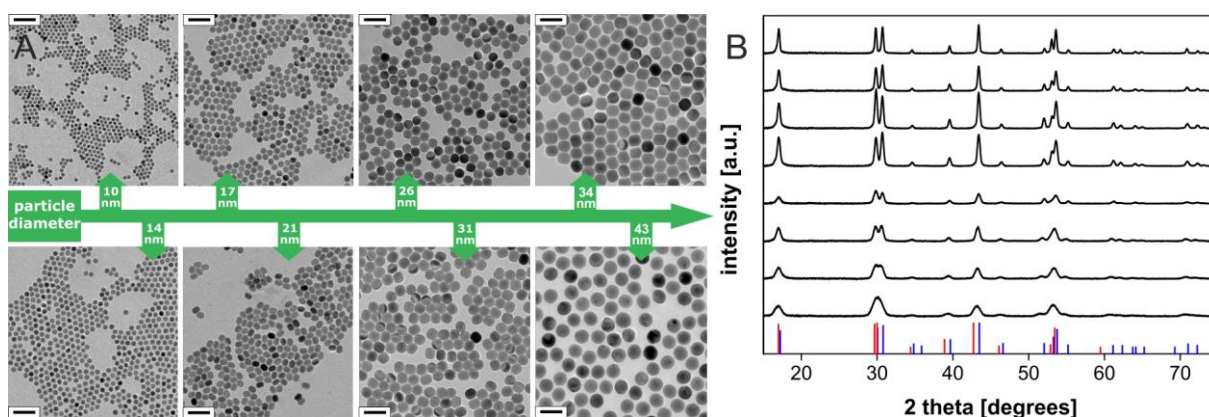


Figure 4.1 | (A) Transmission electron micrographs of monodisperse, hexagonal-phase, oleate-capped NaYF₄ (20% Yb, 2% Er) nanocrystals of eight different sizes with increasing additional concentrations of Gd³⁺ ions with decreasing size. The scale bars are 60 nm. (B) XRD patterns of NaYF₄ (20% Yb, 2% Er, 0-30% Gd) nanoparticles with decreasing size from 43 nm to 10 nm (top to bottom) and the corresponding standard patterns of hexagonal phase NaYF₄ (blue, ICDD PDF #16-0334) and NaGdF₄ (red, ICDD PDF #27-0699).

Table 4.1 | Overview of mean particle diameters obtained by transmission electron microscopy, real lanthanide contents determined by inductively coupled plasma optical emission spectroscopy, and qualitative comparison of the dye loading of NaYF₄:Yb,Er,(Gd)@dye UCNPs. The real lanthanide contents are very close, but not exactly identical, to the theoretical contents, i.e. the stoichiometric amount of the lanthanide chlorides applied in the synthesis. The resulting dye loading was much higher in the case of sulforhodamine B compared to the amount of rose bengal present on the particle surface.

diameter [nm]	lanthanide content [%]			dye molecules per particle	
	Yb	Er	Gd	rose bengal	sulforhodamine B
10.1 ± 0.4	19.34 ± 0.09	1.64 ± 0.08	30.5 ± 0.6	10	64
13.6 ± 0.5	19.4 ± 0.1	1.76 ± 0.07	19.9 ± 0.2	27	57
17.4 ± 0.4	19.1 ± 0.1	1.86 ± 0.03	15.3 ± 0.1	39	173
21.1 ± 1.0	20.13 ± 0.06	1.90 ± 0.02	-	70	497
26.4 ± 0.7	19.58 ± 0.05	1.88 ± 0.03	-	5	118
30.6 ± 1.1	20.0 ± 0.2	1.85 ± 0.02	-	24	261
34.1 ± 1.2	18.85 ± 0.05	1.92 ± 0.03	-	471	615
42.8 ± 1.7	17.14 ± 0.09	1.77 ± 0.02	-	267	3888

4.3.2 Design of the FRET UCNP-Platform

Ligand replacement represents the most versatile approach for the surface modification of nanomaterials. Here, a two-step ligand exchange protocol assisted by NOBF₄ was used in order to prevent nanoparticle aggregation during the exchange process. The overall process is depicted in Figure 4.2. The BF₄⁻-stabilized UCNPs were easily dispersible in polar organic solvents such as DMF and DMSO, without any noticeable agglomeration for at least one month. The absorption bands of the two model organic dyes RB and SRB show a strong spectral overlap with the green emission of the Yb,Er-doped UCNPs (for chemical structures of the dyes see insets in Figure 4.3). These dyes were attached to the surface of the UCNPs, utilizing their carboxyl or sulfonyl groups, thereby replacing BF₄⁻.⁴⁴ The resulting dye-coated UCNPs were readily dispersible in DMF, forming clear, colored dispersions. The colloidal stability including the absence of particle aggregates was confirmed by DLS measurements (Figure 4.4 D). Additional to versatility, simplicity, and reproducibility (Figure 4.4 A-C) of the ligand exchange, this modification procedure enabled direct attachment of the dyes to the UCNP surface.⁴⁵ The minimized distance between donors and acceptors is expected to enhance the rate of the energy transfer according to Equation 1.

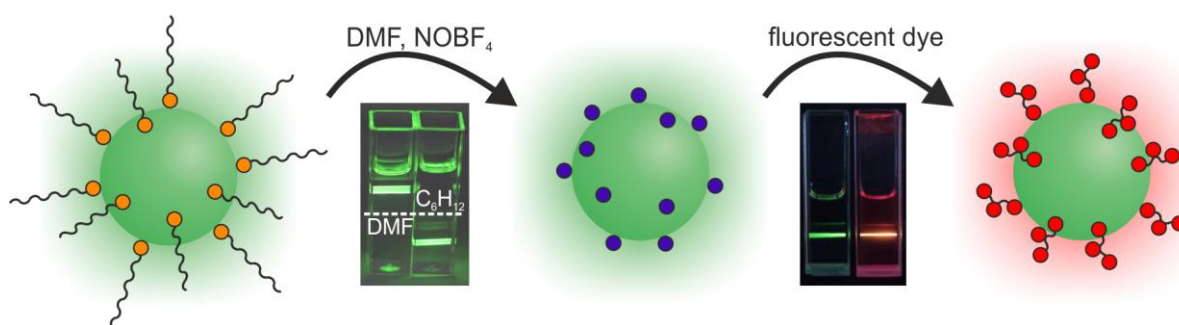


Figure 4.2 | Schematic representation of the two-step ligand exchange process assisted by NOBF_4 . First, the oleate was removed from the particle surface upon the addition of NOBF_4 and the particles were electrostatically stabilized by weakly coordinating BF_4^- ions, leading to the transfer of the particles from the hydrophobic solvent cyclohexane (C_6H_{12}) into more hydrophilic DMF. In the second step the particles were coated with the fluorescent dyes. The attachment of the dyes caused the formation of strongly pink colored particle dispersions in DMF and the impression of red emitting UCNPs. The photographs display the phase transfer process from cyclohexane (top phase) into DMF (bottom phase) and the change in the optical properties of the particle dispersion after subsequent attachment of the dyes. The UCNPs were excited with a handheld 980 nm CW laser module.

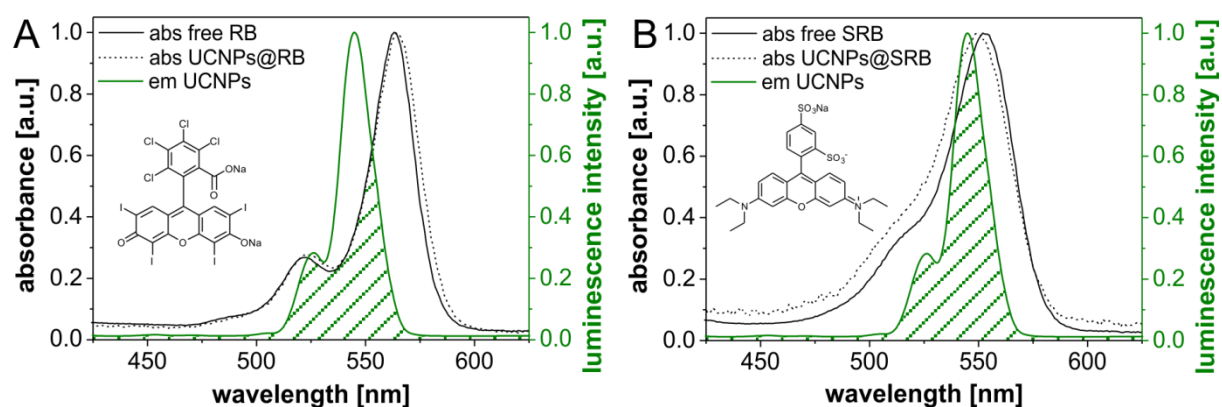


Figure 4.3 | Normalized emission spectrum (green) of NaYF_4 (20% Yb, 2% Er) UCNPs ($\lambda_{\text{ex}} = 980 \text{ nm}$) and normalized absorption spectra (black) of the free dyes (solid black line) (A) rose bengal and (B) sulforhodamine B and of the same two dyes after attachment to UCNPs (dotted line). The hatched sections represent the spectral overlap necessary for the occurrence of FRET in the two respective donor-acceptor systems. Almost no change in shape was observed for the absorption band of both dyes before and after binding to the particle surface. All spectra were recorded in DMF.

The absorption behavior of the organic dyes did not change when attached to the nanoparticles, as revealed by the close match of the absorption spectra of the free dyes and the UCNP-bound fluorophores even at very high optical densities (Figure 4.3). Accordingly, dimerization of the dyes known to induce fluorescence self-quenching can be excluded.⁴⁶

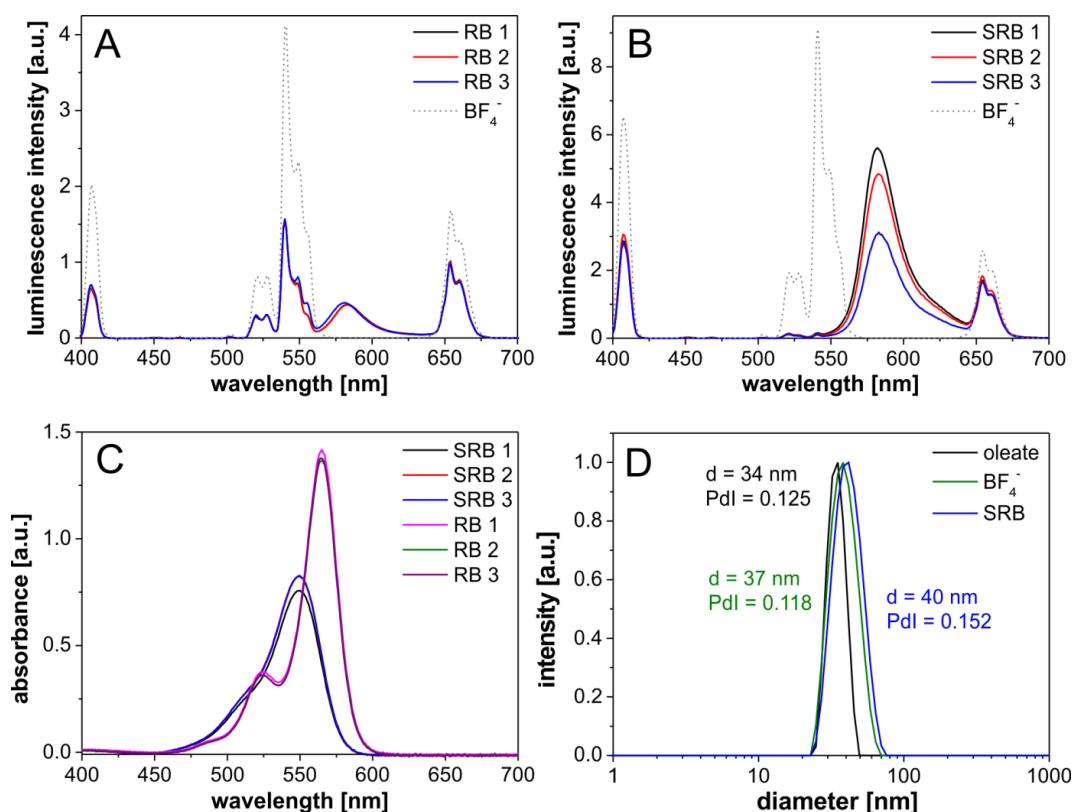


Figure 4.4 | Luminescence spectra of NaYF₄ (20%Yb, 2%Er) ($d = 31$ nm) UCNPs capped with (A) rose bengal and (B) sulforhodamine B upon 980 nm CW laser excitation and (C) respective absorption measurements in DMF. The spectra show the results of three independent modification procedures of dye-capped UCNPs performed under the same conditions during both modification and measurement. The particle concentrations as well as the amount of dye on the particle surface were highly reproducible as shown by the similar emission intensities of the UCNPs of the three different batches and absorption behavior of the immobilized dyes. (D) Intensity weighted dynamic light scattering measurements in backscatter mode of NaYF₄ (20%Yb, 2%Er) UCNPs capped with oleate (black) dispersed in cyclohexane and capped with BF₄⁻ (green) and sulforhodamine B (SRB, blue) dispersed in DMF. The diameter of the particles determined by transmission electron microscopy was 31 nm. The solvodynamic diameter did not change significantly during the surface modification process. The single peaks revealed that the dispersions were colloidally stable and no aggregation occurred.

The emission properties of the UCNPs changed significantly due to an efficient transfer of the green luminescence to the dyes RB and SRB, exemplarily displayed in the photograph in Figure 4.2. The now red colored emission upon excitation at 980 nm, originates from a combination of the red UC emission of Er³⁺ and the red dye fluorescence. Interestingly, for particles with diameters up to 21 nm, the fluorescence of the dyes triggered by NIR excitation of the UCNPs equaled the original green emission of the BF₄⁻-stabilized particles (Figure 4.5). This underlines that FRET can be also utilized to tune the emission color of UCNPs, here shifted to longer wavelengths.^{18,47,48} The reduction of the green UC emission band and the intensity of the dye emission, however, did not allow for a quantitative evaluation of the corresponding FRET efficiencies. These two parameters are strongly

dependent on the total amount of dye molecules bound to the UCNPs present in the dispersion. For example, even for the largest particles, where only a low FRET efficiency was observed, the green emission of the UCNPs completely disappeared. Consequently, we used lifetime measurements of the luminescence of the UCNPs instead for the determination of FRET efficiencies.

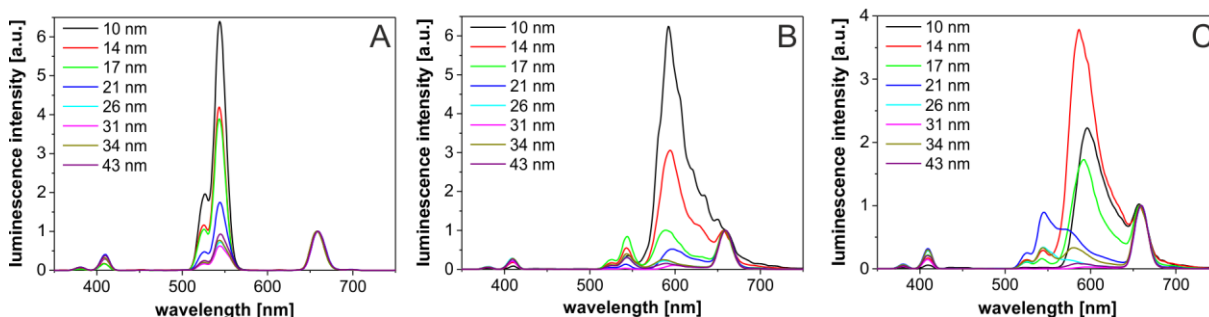


Figure 4.5 | Luminescence spectra of BF_4^- stabilized NaYF_4 (20%Yb, 2%Er, x%Gd) UCNPs and the same particles capped with (B) rose bengal and (C) sulforhodamine B upon 980 nm CW laser excitation. The particles with mean diameters of 17 nm, 14 nm, and 10 nm contained 15%, 20%, and 30% Gd^{3+} , respectively. The spectra were normalized on the red emission band at 660 nm. All measurements were performed, in DMF. The emission of the two dyes triggered by the energy transfer is clearly visible when exciting the UCNPs.

4.3.3 Size-dependent FRET Efficiency

For the determination of the FRET efficiencies of the various dye-capped UCNPs, the changes in the lifetime of the green emission band at 540 nm were measured before and after dye attachment. From these lifetime measurements, the resulting FRET efficiencies E were calculated according to Equation 2.

$$E = 1 - \frac{\tau_{\text{DA}}}{\tau_{\text{D}}} \quad (2)$$

Here, τ_{DA} and τ_{D} represent the lifetime of the donor in the presence and absence of the acceptor, respectively. As shown in Figure 4.6, the lifetime of the green emission of BF_4^- -modified particles is dependent on the surface area of the UCNPs due to the strong influence of surface deactivation on overall luminescence lifetimes. A linear dependence on the surface area of the nanoparticles was observed in the absence of the acceptor dyes. Smaller sizes led to an increase of the surface-to-volume ratio of the UCNPs by a factor of $r_1 \cdot r_2^{-1}$ ($r_1 > r_2$) and hence, to a more pronounced surface quenching as revealed by the respective reduction in the overall luminescence lifetime of the UC emission. This is illustrated best by plotting the lifetime data against the UCNP surface area. A similar relationship was observed for the two different dye-capped systems. Exemplary decay curves of the green

upconversion emission of the nanoparticles before and after the attachment of the dyes are shown in Figure 4.7. This underlines that we clearly observe FRET and not inner filter-related effects.

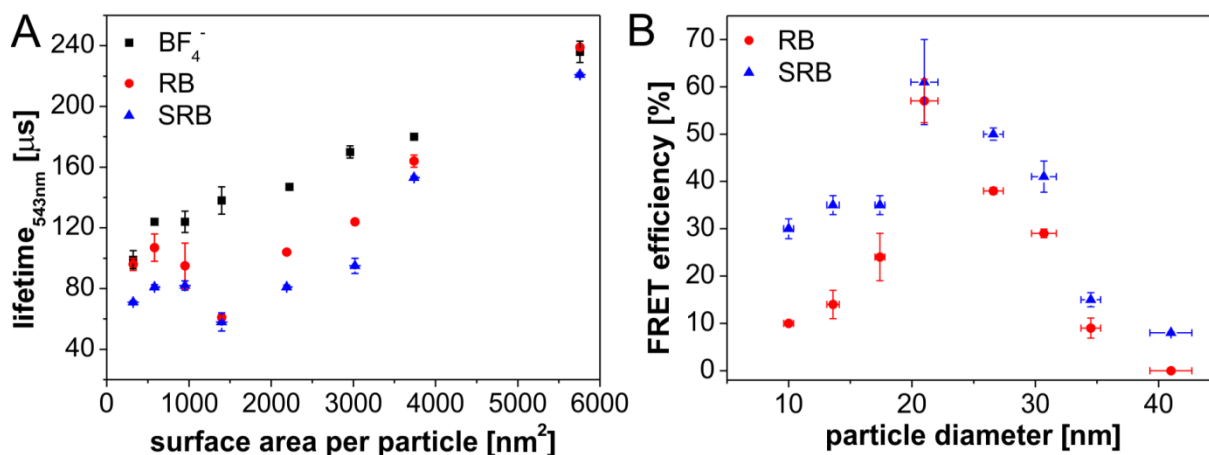


Figure 4.6 | Comparison of (A) the lifetimes of differently sized NaYF_4 (20% Yb, 2% Er, 0-30% Gd) nanoparticles ($\lambda_{\text{ex}} = 980 \text{ nm}$, $\lambda_{\text{em}} = 540 \text{ nm}$) capped with BF_4^- , RB and SRB dispersed in DMF and (B) the resulting FRET efficiencies calculated according to equation 2. The maximum lifetime change in presence of the FRET acceptors and thus the highest FRET efficiency was observed in UCNPs with a mean diameter around 21 nm ($n = 3$, monoexponential fit of the decay curve).

Interestingly, the dye-induced reduction of the lifetime of the green UC emission was always more pronounced in the case of SRB than RB. This is attributed to the better spectral overlap between the UCNP emission and absorption of SRB. The overlap integral J for the pair UCNP-SRB ($2.7 \cdot 10^{15} \text{ nm}^4 \text{ M}^{-1} \text{ cm}^{-1}$) is 35% higher than for that UCNP-RB ($2.0 \cdot 10^{15} \text{ nm}^4 \text{ M}^{-1} \text{ cm}^{-1}$). According to absorption measurements of the dye-coated particle dispersions, a higher surface loading was achieved in the case of SRB for all particle diameters. This is tentatively ascribed to a stronger binding affinity to the UCNP surface of SRB bearing a sulfonate group compared to RB equipped with a single carboxylate group (Figure 4.3 and). A similar trend was found for ligands with phosphonate functionalities compared to carboxylated ones.⁴⁹ For the 21 nm sized particles, the lifetimes of both particle-dye systems match closely. The maximum FRET efficiencies of both dyes do not necessarily need to occur at the same particle size, but rather fall within a certain size range around 21 nm due to a difference in dye loading of RB and SRB.

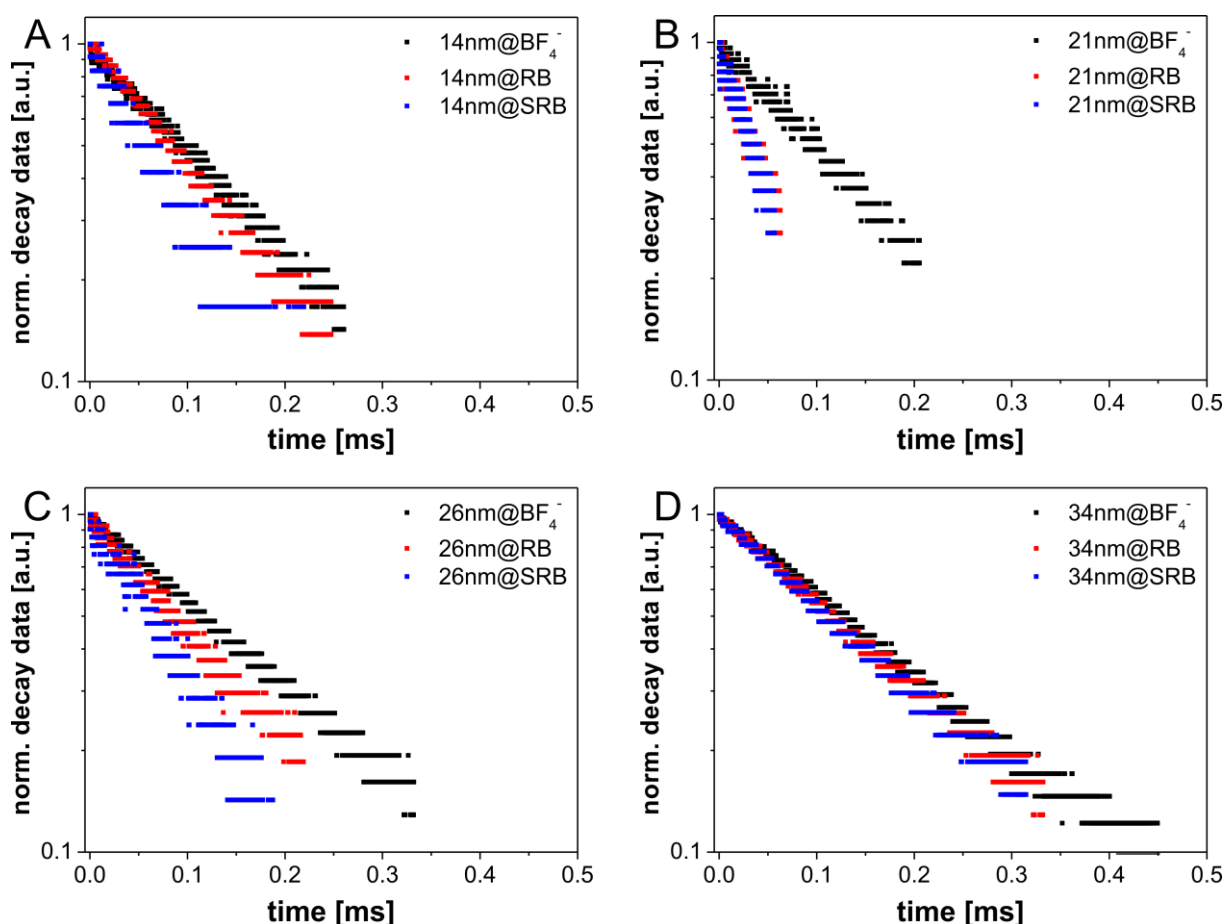


Figure 4.7 | Cut and normalized decay data of UCNPs before and after attachment of the dyes rose bengal (RB) and sulforhodamine B (SRB). The mean diameters of the particles shown were (A) 14 nm, (B) 21 nm, (C) 26 nm, and (D) 34 nm. Particles dispersed in DMF were excited at 980 nm and the luminescence decay of the green upconversion emission around 540 nm was recorded. Depending on the particle diameter, a reduction of the upconversion luminescence lifetime was observed upon binding of the FRET acceptor dyes.

According to Equation 2, the same trend was determined for the corresponding FRET efficiencies. The higher the difference between the lifetime in the absence and presence of the acceptor, the higher is the FRET efficiency. Maximum FRET efficiencies of about 60% were obtained at a particle diameter of 21 nm for both UCNP@dye systems. Assuming close dye packing on the particle surface, the donor lanthanide ions are always present in excess. At a size of 21 nm the donor/acceptor ratio for approximately spherical UCNPs is 23. The smallest particles with a diameter of 10 nm still contain eleven times the amount of donors compared to the number of surface bound dye acceptor molecules. Consequently, a 1:1 ratio between donor and acceptor for a higher FRET efficiency cannot be achieved in the case of approximately spherical particles. Here, the surface-to-volume ratio is always > 1 . Small diameters below 20 nm led to FRET efficiencies in the range of only 10 - 30%. This is ascribed to the stronger influence of surface deactivation and quenching caused by solvent molecules and crystal defects, counterbalancing FRET to the organic dyes.

As the increasing surface quenching leads to a decreasing quantum yield (QY)⁵⁰ of the donor, the Förster distance R_0 is accordingly shortened, consequently lowering the number of lanthanide donor ions within the radius for effective FRET (Equation 3).

$$R_0^6 = \frac{9 \cdot (\ln 10) \cdot \kappa^2 \cdot Q_D \cdot J}{128 \pi^5 \cdot N_A \cdot n^4} \quad (3)$$

In Equation 3, κ^2 represents the dipole orientation factor, n is the refractive index of the medium, N_A is Avogadro's number, Q_D is the quantum yield of the donor, and J is the spectral overlap integral of the FRET pair. Typical mean R_0 values for the FRET pair combinations UCNP/RB and UCNP/SRB were estimated to around 3 - 5 nm (Figure 4.8).

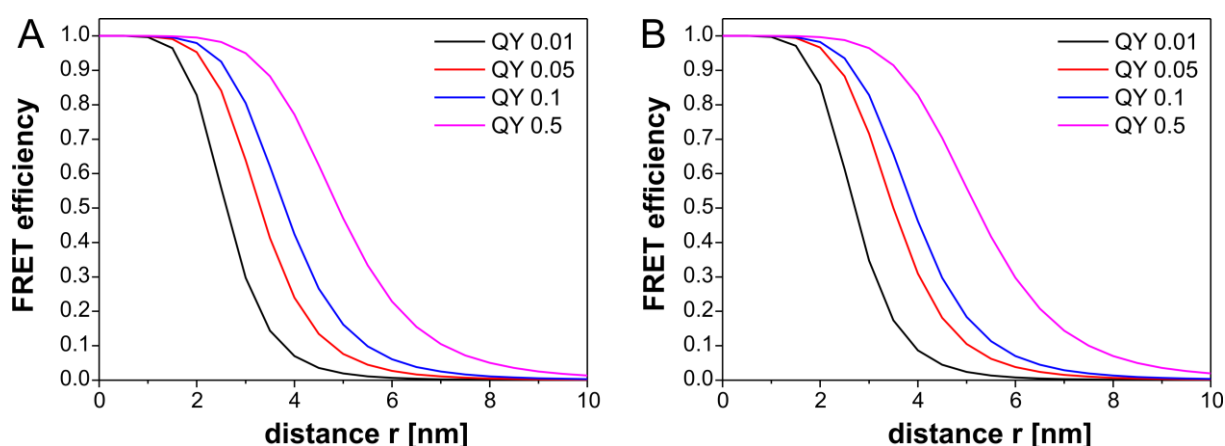


Figure 4.8 | Calculated FRET efficiencies dependent on the distance between donor (Er^{3+}) and acceptor (dye) for (A) rose bengal and (B) sulforhodamine B. Typical Förster distances (FRET efficiency = 0.5) for these systems are in the range of 3 -5 nm. The Förster distance (R_0) and consequently the FRET efficiencies are strongly influenced by the quantum yield (QY) of the donor particles. A higher QY leads to a longer R_0 .

A possible influence of the additional Gd^{3+} -content in these small UCNPs was also investigated. The FRET efficiency of particles of the same size with and without Gd^{3+} was compared. This comparison revealed that the luminescence decay behavior in the presence of the FRET acceptors was almost identical in both cases, resulting in FRET efficiencies of about 60%, independent of the Gd^{3+} -content (Figure 4.9).⁴³

The three highest FRET efficiencies were obtained for both dyes at particle diameters of 21 nm, 26 nm, and 31 nm, respectively. The optical properties of these three systems were therefore further investigated, with respect to the luminescence properties of the FRET acceptor (Figure 4.10).

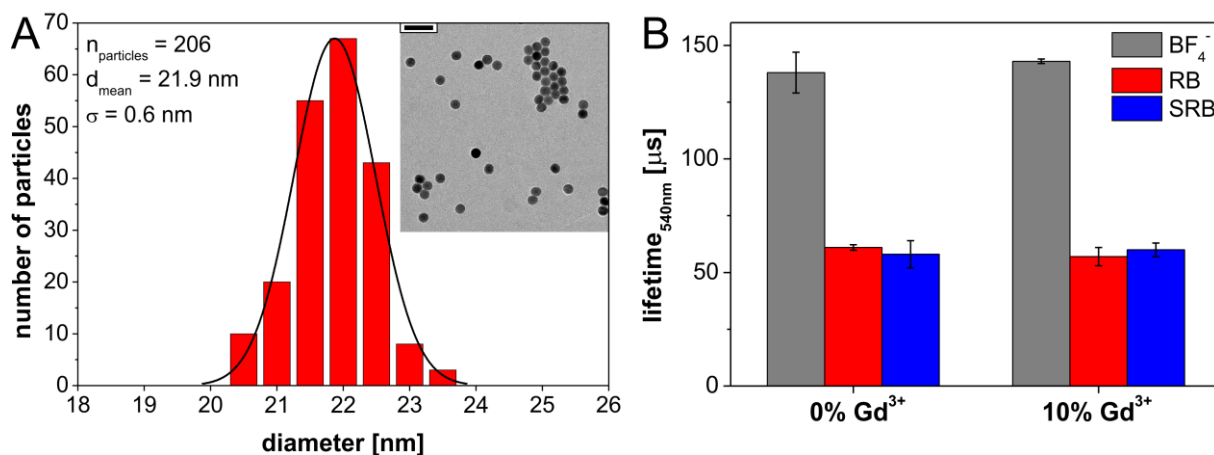


Figure 4.9 | (A) Transmission electron micrograph (scale bar: 60 nm) and corresponding size distribution of oleate-capped NaYF₄ (20% Yb, 2% Er, 10% Gd) UCNPs. (B) Comparison of the lifetime changes of NaYF₄ (20% Yb, 2% Er) and NaYF₄ (20% Yb, 2% Er, 10% Gd) nanocrystals with mean diameters of 21.1 ± 1.0 nm and 21.9 ± 0.6 nm, respectively, before and after ligand exchange with rose bengal (RB) and sulforhodamine B (SRB). In both cases the reduction of the lifetime was very similar, resulting in a FRET efficiency of about 60%. Small concentrations of Gd³⁺ that are used for the control of the crystal size of the UCNPs do not negatively affect the energy transfer. All measurements were performed in DMF.

The lifetimes of SRB and RB were reported as < 2 ns.⁵¹ When bound to the surface of the UCNPs, the fluorescence lifetimes of both dyes increased to the same values as exhibited by the green emission of the UCNPs excited at 980 nm. This extreme extension of the lifetimes to over 100 μs, *i.e.* almost to the lifetime of the corresponding FRET donor, gives further evidence for the occurrence of FRET from the UCNPs to the surface-bound dye molecules.

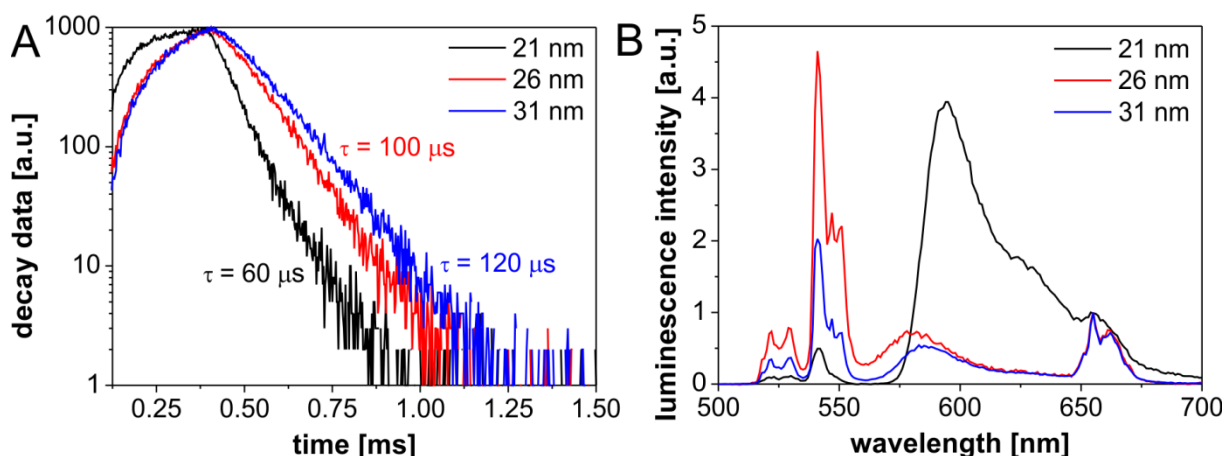


Figure 4.10 | (A) Decay behavior of the fluorescence emission of the FRET acceptor RB at 600 nm and (B) emission spectra normalized on the red upconversion emission around 660 nm of the three NaYF₄ (20% Yb, 2% Er)@RB systems yielding the highest FRET efficiencies (21 nm, 26 nm, and 31 nm) upon CW laser excitation at 980 nm.

Studies were also performed with an intensity-based evaluation of the FRET process in order to compare this more common approach to the results obtained from lifetime studies (Figure 4.10 B and Figure 4.5 B and C). The emission of RB around 580 nm can be excited by ET from UCNPs. Because of the small Stokes shift favoring reabsorption,⁵² the fluorescence maximum of the dye depends on dye loading, which affects also the size of the ET-induced reduction of the green UC emission band. Due to this combination of effects, the decrease of the intensity of the UCNP emission at 540 nm cannot be directly correlated to either ET efficiency or inner-filter effect. Consequently, the ratio I_{DA}/I_D necessary for the calculation of E could not be determined reliably and led to unrealistically high values of E , approximating 100%.

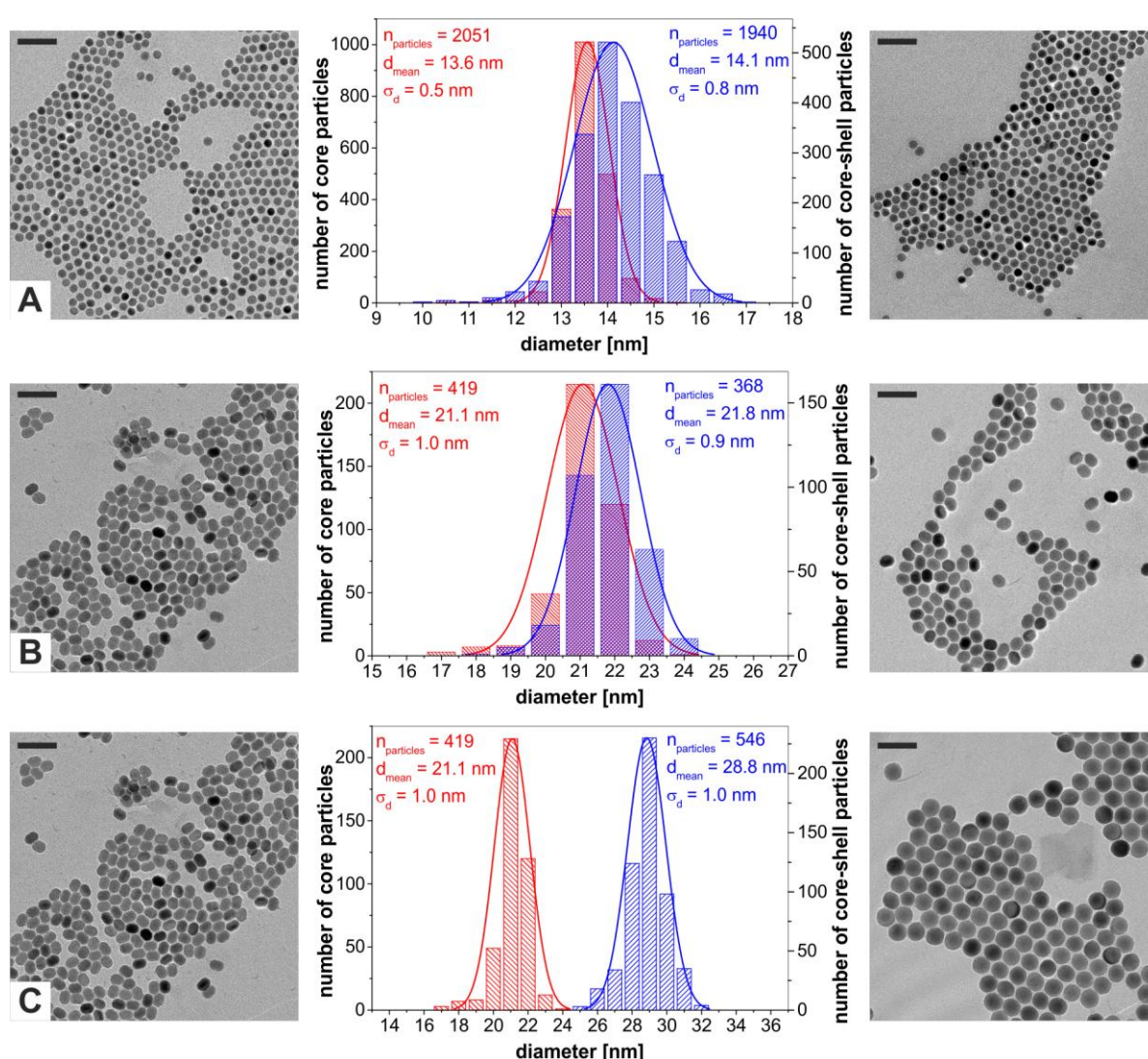


Figure 4.11 | (Row A) Transmission electron micrographs and corresponding size distributions of (left) β - $\text{NaYF}_4(20\% \text{Yb}, 2\% \text{Er}, 20\% \text{Gd})$ core-only and (right) β - $\text{NaYF}_4(20\% \text{Yb}, 2\% \text{Er}, 20\% \text{Gd})@ \text{NaYF}_4$ core-shell UCNPs. (Rows B,C) Transmission electron micrographs and corresponding size distributions of (left) β - $\text{NaYF}_4(20\% \text{Yb}, 2\% \text{Er})$ core-only and (right) β - $\text{NaYF}_4(20\% \text{Yb}, 2\% \text{Er})@ \text{NaYF}_4$ core-shell nanoparticles with two different shell thicknesses. All scale bars are 60 nm. Monodisperse particles were obtained after the shell growth in all cases.

4.3.4 Influence of Luminescence Enhancement on FRET Efficiency

According to Equation 3, the QY of the donor directly affects the FRET efficiency and the Förster distance of a FRET pair (Figure S9). Hence, the FRET efficiency can be improved by increasing the QY of the donor. One popular way to enhance the QY of UCNPs is the growth of a shell, only a few nm thick, consisting of NaYF_4 .^{53,54} This inactive shell reduces non-radiative deactivation of the excitation energy caused by surface quenching by ligand and/or solvent molecules.⁵⁵ Different shell thicknesses around UCNPs of various sizes were prepared (Figure 4.11).

As shown in Figure 4.12, the presence of an inactive shell greatly influenced the resulting FRET efficiencies. For particles < 17 nm, a thin shell with a thickness of less than 1 nm led to an increase of the FRET efficiency up to 40%. This underlines the strong influence of surface deactivation processes on the luminescence of UCNPs with extremely small diameters. For larger UCNPs, e.g., the most efficient ones with a size of 21 nm, such a thin shell did not result in a higher FRET efficiency. A thicker shell of 4 nm led already to a strong decrease of the FRET efficiency to only 20% for both dyes (Figure 4.13). Interestingly, the inactive shell caused an even lower FRET efficiency than that of core-only particles with a similar overall size (around 35% for a diameter of ≈ 31 nm, Figure 4.6). This can be attributed to the reduction of the amount of donor ions within the Förster distance by the shell to roughly 40% compared to about 60% in the absence of the shell.

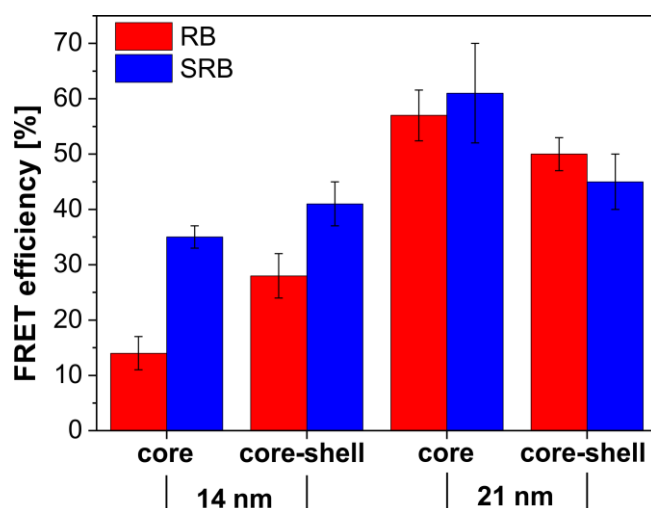


Figure 4.12 | FRET efficiencies of organic dye-capped NaYF_4 (20% Yb, 2% Er) UCNPs dispersed in DMF with and without an additional inactive shell consisting of NaYF_4 with a thickness of below 1 nm. Core particles with diameters of 14 and 21 nm were used for the shell growth, respectively. (n = 3)

The growth of an inactive shell is also a straightforward way of altering the donor-to-acceptor ratio as the increase in particle size by the shell enables the binding of a higher number of acceptor dye molecules relatively to the number of donor ions in the particle core which remained unchanged. For example, by growing a shell of 4 nm thickness on UCNPs with a diameter of 21 nm, the maximum donor/acceptor ratio decreases in case of full surface coverage from 23 to 13. Nevertheless, the FRET efficiency did not increase despite higher amounts of acceptors. These findings demonstrate that the distance between donor and acceptor remains an extremely critical parameter for FRET systems involving UCNPs.

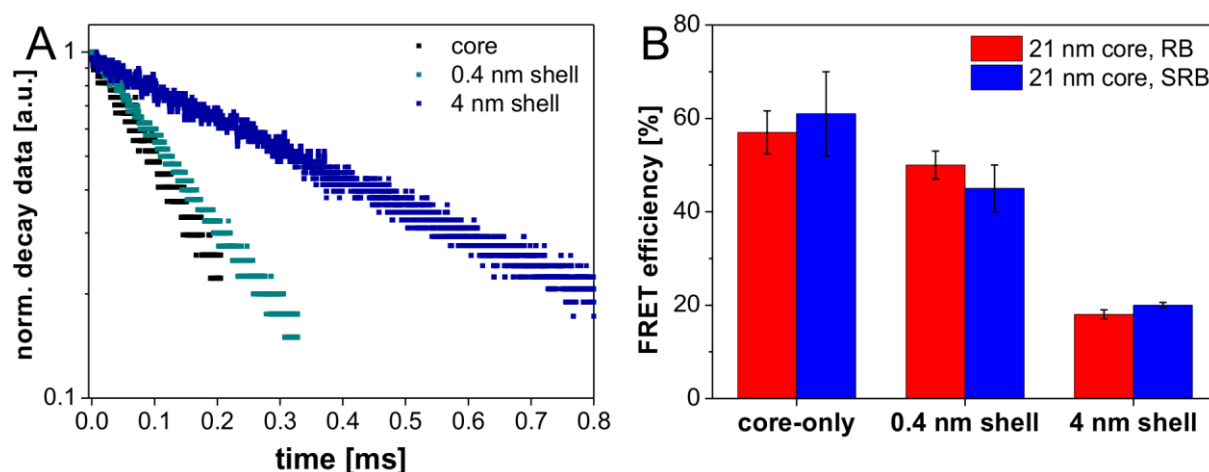


Figure 4.13 | (A) Normalized decay data of BF_4^- -capped NaYF_4 (20% Yb, 2% Er) UCNPs dispersed in DMF with a mean diameter of 21 nm and corresponding NaYF_4 (20% Yb, 2% Er)@ NaYF_4 core-shell particles with shell thicknesses of 0.4 and 4 nm. The inert shell causes an elongation of the upconversion lifetime at 540 nm caused by the reduction of surface deactivation effects. (B) FRET efficiencies of dye-capped NaYF_4 (20% Yb, 2% Er) UCNPs ($d_{\text{core}} = 21$ nm) dispersed in DMF with and without an additional shell consisting of NaYF_4 with thicknesses of 0.4 nm and 4 nm. ($n = 3$)

4.4 Conclusions

In conclusion, systematic studies of the influence of the size of UCNPs on the FRET efficiency to surface-bound acceptor dyes revealed an optimum particle size for efficient FRET. The observed selective shortening of the luminescence lifetime of the green UC luminescence clearly demonstrates the occurrence of FRET. Particles with a mean diameter in the range of 20 - 25 nm showed the highest FRET efficiency of 50 - 60% according to time-resolved fluorescence measurements. Both larger and smaller UCNPs led to lower energy transfer efficiencies. Based on our findings, it is expected that the sensitivity of UCNP-based FRET platforms can be significantly enhanced by adjusting the particle diameter. For classical NaYF_4 (20% Yb^{3+} , 2% Er^{3+}) nanoparticles, a diameter of about 21 nm

increases the dynamic range by a factor of three compared to both smaller (15 nm) and larger (32 nm) particles. This principle can be adapted to improve the performance of UCNP-FRET systems for (bio)sensing and imaging applications as well as theranostics. Moreover, FRET to fluorescent dyes can be utilized to shift the luminescence emission of the UCNPs. This can be used to explore new sensing and imaging applications that require specific emission wavelengths due to interfering substances while still making use of the advantages of NIR excitation. Our findings are also of considerable interest for applications in cancer treatment using FRET from UCNPs to photosensitizers in close vicinity for photodynamic therapy. In the near future, we will extend these studies to FRET systems consisting of UCNPs bearing stimuli-responsive and analyte-sensitive acceptor dyes and their applications in different sensor schemes.

4.5 Materials and Methods

4.5.1 Chemicals

Lanthanide chloride hexahydrates (> 99.9%) were purchased from Sigma Aldrich and Treibacher Industrie AG. Oleic acid and 1-octadecene (both technical grade, 90%) were obtained from Alfa Aesar. Ammonium fluoride, sodium hydroxide, both of analytical grade, nitrosyl tetrafluoroborate (95%), sulforhodamine B (SRB, 75%), and rose bengal (RB, 95%) were purchased from Sigma Aldrich. All other chemicals were of analytical grade and obtained from Sigma Aldrich, Merck or Acros. All chemicals were used as received without further purification.

4.5.2 Characterization Methods.

Transmission electron microscopy was carried out with a 120 kV Philips CM12 microscope. The images were evaluated using the software ImageJ. Dynamic light scattering measurements were performed at 20 °C with a Malvern Zetasizer Nano-ZS. Inductively coupled plasma optical emission spectroscopy for the determination of the real doping ratios of rare-earth ions in the UCNPs was done with a Spectro Flame-EOP. X-ray diffraction patterns were collected on a Huber Guinier G670 diffractometer with a $K\alpha$ -Cu source ($\lambda = 1.54060 \text{ \AA}$). Absorption spectra of the dyes were obtained with a Varian Cary 50 spectrophotometer. Luminescence spectra of UCNPs were recorded with a Perkin-Elmer LS 50 luminescence spectrometer equipped with an external continuous wave (CW) 980 nm laser module (200 mW). All spectra were

recorded at room temperature. The setup for the lifetime measurements consisted of a 980 nm CW laser module (200 mW) from Picotronic and an optical chopper (MC2000 with two slot chopper blade MC1F2) from Thorlabs. The signal was amplified using a photomultiplier tube and analyzed by a digital storage oscilloscope (DSO 8204) from Voltcraft. Optical bandpass filters (FF01-535/150-25 and FF01-665/150-25) from Semrock were used for measuring luminescence decays of the different emission bands. Control measurements were carried out with a commercial Edinburgh Instruments spectrofluorometer FSP-920 equipped with an electrically pulsed 1 W 978 nm laser diode and a red extended PMT (R2658P) from Hamamatsu.

4.5.3 Determination of the Spectral Overlap Integral J

The spectral overlap integrals of the two FRET pairs UCNP-RB and UCNP-SRB were calculated using the software FluorTools [a|e](#). The wavelength range between 500 nm and 600 nm was evaluated. For rose bengal and sulforhodamine B maximum absorption coefficients of $120,000 \text{ L}\cdot\text{mol}^{-1}\cdot\text{cm}^{-1}$ and $100,000 \text{ L}\cdot\text{mol}^{-1}\cdot\text{cm}^{-1}$, respectively, were determined and applied for the calculations.

4.5.4 Synthesis of Hexagonal NaYF₄ (20% Yb, 2% Er, 0-30% Gd)

The synthesis of hexagonal phase, oleate-capped UCNPs with sizes up to 35 nm was carried out starting from rare earth trichlorides in the high boiling solvents 1-octadecene and oleic acid as reported previously.⁴⁵ The rare earth trichlorides with the corresponding molar doping ratios were dissolved in methanol and transferred into a three necked round bottom flask under nitrogen flow. A mixture of 6 mL oleic acid and 15 mL 1-octadecene per 1 mmol of chlorides was added to the solution. The suspension was heated to 160 °C and vacuum was applied for 30 min to form a clear solution. The solution was cooled down to room temperature and 0.148 g (4.0 mmol) NH₄F and 0.1 g (2.5 mmol) NaOH dissolved in methanol were added per 1 mmol of chlorides. The suspension was kept at 120 °C for 30 min and then heated to reflux (approx. 325 °C). The progress of the reaction was monitored with a 980 nm CW laser module. 10 min from the time on, when upconversion luminescence could be observed for the first time, the reaction mixture was cooled down to room temperature. The particles were precipitated by the addition of excess ethanol and collected by centrifugation at 1,000 g for 5 min. The precipitate was washed twice with chloroform/ethanol and 3 times with cyclohexane/acetone by repeated re-dispersion-precipitation-centrifugation cycles.

Finally, the particles were dispersed in cyclohexane, centrifuged at 1,000 g for 3 min to remove aggregates, and the supernatant was collected and stored at 4 °C.

4.5.5 Synthesis of Cubic NaYF₄ (20% Yb, 2% Er) and NaYF₄

The procedure was identical to the synthesis of hexagonal NaYF₄ until the heating step to reflux. Here, the reaction mixture was heated to 240 °C for 40 min without excitation control instead and afterwards cooled down to room temperature. The purification process was the same as described above.

4.5.6 Synthesis of Core-Shell NaYF₄:Yb,Er@NaYF₄:Yb,Er and NaYF₄:Yb,Er@NaYF₄

Core-shell particles were synthesized using an approach based on seed mediated shell growth.⁵⁶ Cubic NaYF₄ nanoparticles (shell material) and hexagonal UCNPs (cores) dispersed in cyclohexane were separately suspended in a mixture of 5 mL oleic acid and 5 mL 1-octadecene per 1 mmol NaYF₄. Vacuum was applied at 100 °C for 30 min to remove the cyclohexane. Afterwards, the cubic particles were kept at 120 °C under N₂ flow. The hexagonal particles were heated to reflux (325 °C) under mild N₂ flow. Small volumes (3 mL at most) of cubic particles were injected into the boiling reaction mixture every 10 min to prevent a temperature drop below 300 °C and the formation of new seeds. The mixture was cooled down to room temperature 10 min after the last injection. The purification process was the same as described above.

4.5.7 Surface Modification with Rose Bengal and Sulforhodamine B.

The oleate on the surface of the UCNPs was replaced by fluorescent dyes in a modified two-step ligand exchange process assisted by nitrosyl tetrafluoroborate.⁵⁷ First, the oleate-capped UCNPs were dispersed in a two-phase system consisting of equal volumes of cyclohexane and N,N-dimethylformamide (DMF). In order to remove the oleate, NOBF₄ (1 mg per 1 mg UCNPs) was added and the dispersion was stirred vigorously for 10 min at 30 °C. The cyclohexane phase containing the oleic acid was discarded and excess chloroform was added to the turbid DMF phase to precipitate the ligand-free, BF₄⁻ stabilized UCNPs. The dispersion was centrifuged at 1,000 g for 5 min. The jellylike precipitate was washed twice with chloroform. Finally, the BF₄⁻ stabilized particles were dispersed in DMF. In a second step, the surface of the ligand-free UCNPs was covered with the fluorescent dyes. For this purpose, a dispersion of

20 mg UCNPs in 1 mL DMF was added to a solution containing excess dye (1 mg) in 1 mL DMF and stirred for 15 min at room temperature. Afterwards, the particles were separated from the solution by centrifugation (21,000 g, 45 min) and washed with DMF until the supernatant was colorless. The colored precipitate was finally dispersed in 2 mL DMF and stored in the dark.

4.5.8 Determination of Dye Loading on UCNPs

The number of dye molecules per particle was obtained from a combination of absorbance and luminescence spectroscopy. First, the UCNP concentration of the dye-capped particle dispersion was determined by comparing the emission intensity of the red upconversion emission around 660 nm before and after the attachment of the dyes. The dye concentration was calculated from absorbance measurements of the dye capped particles using absorption coefficients of $120,000 \text{ L}\cdot\text{mol}^{-1}\cdot\text{cm}^{-1}$ and $100,000 \text{ L}\cdot\text{mol}^{-1}\cdot\text{cm}^{-1}$ for rose bengal and sulforhodamine B, respectively.

Acknowledgements

The authors thank Dr. Christoph Fenzl and Dr. Stefan Wilhelm for the transmission electron micrographs and Prof. Reinhard Rachel for his support with the TEM. Furthermore, Joachim Rewitzer and Vanessa Tomanek are acknowledged for their assistance during the ICP-OES measurements. Dr. Richard Weihrich is acknowledged for his support with the XRD measurements. The authors are grateful to Prof. Yves Mely, Oleksii Dukhno, and Frederic Przybilla from the Laboratory of Biophotonics and Pharmacology, University of Strasbourg, for fruitful discussions.

References

- (1) Ueno, T.; Nagano, T. Fluorescent Probes for Sensing and Imaging. *Nat. Methods* **2011**, *8*, 642–645.
- (2) Kobayashi, H.; Ogawa, M.; Alford, R.; Choyke, P. L.; Urano, Y. New Strategies for Fluorescent Probe Design in Medical Diagnostic Imaging. *Chem. Rev.* **2010**, *110*, 2620–2640.
- (3) Carter, K. P.; Young, A. M.; Palmer, A. E. Fluorescent Sensors for Measuring Metal Ions in Living Systems. *Chem. Rev.* **2014**, *114*, 4564–4601.
- (4) Yuan, L.; Lin, W.; Zheng, K.; Zhu, S. FRET-Based Small-Molecule Fluorescent Probes: Rational Design and Bioimaging Applications. *Acc. Chem. Res.* **2013**, *46*, 1462–1473.

- (5) Fan, J.; Hu, M.; Zhan, P.; Peng, X. Energy Transfer Cassettes Based on Organic Fluorophores: Construction and Applications in Ratiometric Sensing. *Chem. Soc. Rev.* **2013**, *42*, 29–43.
- (6) Ray, P. C.; Fan, Z.; Crouch, R. A.; Sinha, S. S.; Pramanik, A. Nanoscopic Optical Rulers Beyond the FRET Distance Limit: Fundamentals and Applications. *Chem. Soc. Rev.* **2014**, *43*, 6370–6404.
- (7) Stein, I. H.; Steinhauer, C.; Tinnefeld, P. Single-Molecule Four-Color FRET Visualizes Energy-Transfer Paths on DNA Origami. *J. Am. Chem. Soc.* **2011**, *133*, 4193–4195.
- (8) Geißler, D.; Stufler, S.; Löhmannsröben, H.-G.; Hildebrandt, N. Six-Color Time-Resolved Förster Resonance Energy Transfer for Ultrasensitive Multiplexed Biosensing. *J. Am. Chem. Soc.* **2013**, *135*, 1102–1109.
- (9) Rowland, C. E.; Brown, C. W. III; Medintz, I. L.; Delehanty, J. B. Intracellular FRET-based Probes: A Review. *Methods Appl. Fluoresc.* **2015**, *3*, 042006.
- (10) Chinen, A. B.; Guan, C. M.; Ferrer, J. R.; Barnaby, S. N.; Merkel, T. J.; Mirkin, C. A. Nanoparticle Probes for the Detection of Cancer Biomarkers, Cells, and Tissues by Fluorescence. *Chem. Rev.* **2015**, *115*, 10530–10574.
- (11) Yao, J.; Yang, M.; Duan, Y. Chemistry, Biology, and Medicine of Fluorescent Nanomaterials and Related Systems: New Insights into Biosensing, Bioimaging, Genomics, Diagnostics, and Therapy. *Chem. Rev.* **2014**, *114*, 6130–6178.
- (12) Wolfbeis, O. S. An Overview of Nanoparticles Commonly Used in Fluorescent Bioimaging. *Chem. Soc. Rev.* **2015**, *44*, 4743–4768.
- (13) Haase, M.; Schäfer, H. Upconverting Nanoparticles. *Angew. Chem. Int. Ed.* **2011**, *50*, 5808–5829.
- (14) Zheng, W.; Huang, P.; Tu, D.; Ma, E.; Zhu, H.; Chen, X. Lanthanide-doped Upconversion Nano-bioprobes: Electronic Structures, Optical Properties, and Biodetection. *Chem. Soc. Rev.* **2015**, *44*, 1379–1415.
- (15) Auzel, F. Upconversion and Anti-Stokes Processes with f and d Ions in Solids. *Chem. Rev.* **2004**, *104*, 139–174.
- (16) Park, Y. I.; Lee, K. T.; Suh, Y. D.; Hyeon, T. Upconverting Nanoparticles: A Versatile Platform for Wide-field Two-photon Microscopy and Multi-modal *in vivo* Imaging. *Chem. Soc. Rev.* **2015**, *44*, 1302–1317.
- (17) Wu, S.; Han, G.; Milliron, D. J.; Aloni, S.; Altoe, V.; Talapin, D. V.; Cohen, B. E.; Schuck, P. J. Non-blinking and Photostable Upconverted Luminescence from Single Lanthanide-doped Nanocrystals. *Proc. Natl. Acad. Sci.* **2009**, *106*, 10917–10921.
- (18) Li, Z.; Zhang, Y.; Jiang, S. Multicolor Core/Shell-Structured Upconversion Fluorescent Nanoparticles. *Adv. Mater.* **2008**, *20*, 4765–4769.
- (19) Naccache, R.; Yu, Q.; Capobianco, J. A. The Fluoride Host: Nucleation, Growth, and Upconversion of Lanthanide-Doped Nanoparticles. *Adv. Opt. Mater.* **2015**, *3*, 482–509.
- (20) Rojas-Gutierrez, P. A.; DeWolf, C.; Capobianco, J. A. Formation of a Supported Lipid Bilayer on Faceted LiYF₄:Tm³⁺/Yb³⁺ Upconversion Nanoparticles. *Part. Part. Syst. Charact.* **2016**, *33*, 865–870.

- (21) Rinkel, T.; Raj, A. N.; Dühnen, S.; Haase, M. Synthesis of 10 nm β -NaYF₄:Yb,Er/NaYF₄ Core/Shell Upconversion Nanocrystals with 5 nm Particle Cores. *Angew. Chem. Int. Ed.* **2016**, *55*, 1164–1167.
- (22) Alonso-Cristobal, P.; Vilela, P.; El-Sagheer, A.; Lopez-Cabarcos, E.; Brown, T.; Muskens, O. L.; Rubio-Retama, J.; Kanaras, A. G. Highly Sensitive DNA Sensor Based on Upconversion Nanoparticles and Graphene Oxide. *ACS Appl. Mater. Interfaces* **2015**, *7*, 12422–12429.
- (23) Zhou, F.; Noor, M.; Krull, U. A Paper-Based Sandwich Format Hybridization Assay for Unlabeled Nucleic Acid Detection Using Upconversion Nanoparticles as Energy Donors in Luminescence Resonance Energy Transfer. *Nanomaterials* **2015**, *5*, 1556–1570.
- (24) Mattsson, L.; Wegner, K. David; Hildebrandt, N.; Soukka, T. Upconverting Nanoparticle to Quantum Dot FRET for Homogeneous Double Nano Biosensors. *RSC Adv.* **2015**, *5*, 13270–13277.
- (25) Hemmer, E.; Quintanilla, M.; Légaré, F.; Vetrone, F. Temperature-Induced Energy Transfer in Dye-Conjugated Upconverting Nanoparticles: A New Candidate for Nanothermometry. *Chem. Mater.* **2015**, *27*, 235–244.
- (26) Peng, J.; Xu, W.; Teoh, C. L.; Han, S.; Kim, B.; Samanta, A.; Er, J. C.; Wang, L.; Yuan, L.; Liu, X.; Chang, Y.-T. High-Efficiency in Vitro and in Vivo Detection of Zn²⁺ by Dye-Assembled Upconversion Nanoparticles. *J. Am. Chem. Soc.* **2015**, *137*, 2336–2342.
- (27) Wang, D.; Xue, B.; Kong, X.; Tu, L.; Liu, X.; Zhang, Y.; Chang, Y.; Luo, Y.; Zhao, H.; Zhang, H. 808 nm Driven Nd³⁺-sensitized Upconversion Nanostructures for Photodynamic Therapy and Simultaneous Fluorescence Imaging. *Nanoscale* **2015**, *7*, 190–197.
- (28) Cen, Y.; Wu, Y.-M.; Kong, X.-J.; Wu, S.; Yu, R.-Q.; Chu, X. Phospholipid-Modified Upconversion Nanoprobe for Ratiometric Fluorescence Detection and Imaging of Phospholipase D in Cell Lysate and in Living Cells. *Anal. Chem.* **2014**, *86*, 7119–7127.
- (29) Fu, Y.; Chen, X.; Mou, X.; Ren, Z.; Li, X.; Han, G. A Dual-Color Luminescent Localized Drug Delivery System with Ratiometric-Monitored Doxorubicin Release Functionalities. *ACS Biomater. Sci. Eng.* **2016**, *2*, 652–661.
- (30) Lu, Y.; Zhao, J.; Zhang, R.; Liu, Y.; Liu, D.; Goldys, E. M.; Yang, X.; Xi, P.; Sunna, A.; Lu, J.; Shi, Y.; Leif, R. C.; Huo, Y.; Shen, J.; Piper, J. A.; Robinson, J. Paul; Jin, D. Tunable Lifetime Multiplexing Using Luminescent Nanocrystals. *Nat. Photon.* **2014**, *8*, 32–36.
- (31) Arppe, R.; Nareoja, T.; Nylund, S.; Mattsson, L.; Koho, S.; Rosenholm, J. M.; Soukka, T.; Schaferling, M. Photon Upconversion Sensitized Nanoprobes for Sensing and Imaging of pH. *Nanoscale* **2014**, *6*, 6837–6843.
- (32) Wu, X.; Zhang, Y.; Takle, K.; Bilsel, O.; Li, Z.; Lee, H.; Zhang, Z.; Li, D.; Fan, W.; Duan, C.; Chan, E. M.; Lois, C.; Xiang, Y.; Han, G. *ACS Nano* **2016**, *10*, 1060–1066.
- (33) Riuttamäki, T.; Hyppänen, I.; Kankare, J.; Soukka, T. Dye-Sensitized Core/Active Shell Upconversion Nanoparticles for Optogenetics and Bioimaging Applications. *J. Phys. Chem. C* **2011**, *115*, 17736–17742.

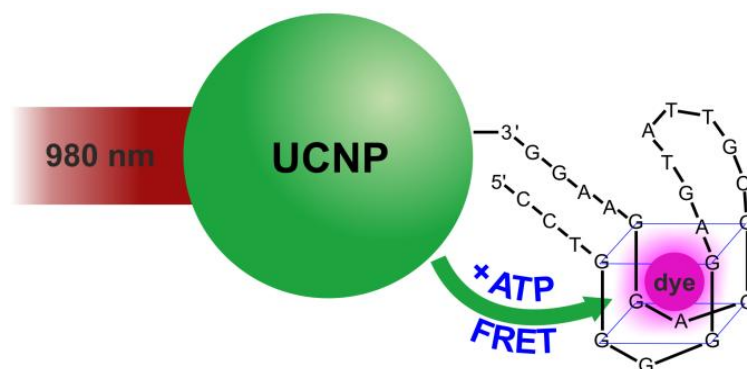
- (34) Xu, C. T.; Zhan, Q.; Liu, H.; Somesfalean, G.; Qian, J.; He, S.; Andersson-Engels, S. Upconverting Nanoparticles for Pre-clinical Diffuse Optical Imaging, Microscopy and Sensing: Current Trends and Future Challenges. *Laser Photon. Rev.* **2013**, *7*, 663–697.
- (35) Wang, Y.; Liu, K.; Liu, X.; Dohnalová, K.; Gregorkiewicz, T.; Kong, X.; Aalders, Maurice C. G.; Buma, W. J.; Zhang, H. J. Critical Shell Thickness of Core/Shell Upconversion Luminescence Nanoplatform for FRET Application. *Phys. Chem. Lett.* **2011**, *2*, 2083–2088.
- (36) Liu, K.; Liu, X.; Zeng, Q.; Zhang, Y.; Tu, L.; Liu, T.; Kong, X.; Wang, Y.; Cao, F.; Lambrechts, Saskia A. G.; Aalders, Maurice C. G.; Zhang, H. Covalently Assembled NIR Nanoplatform for Simultaneous Fluorescence Imaging and Photodynamic Therapy of Cancer Cells. *ACS Nano* **2012**, *6*, 4054–4062.
- (37) Chen, G.; Shao, W.; Valiev, R. R.; Ohulchanskyy, T. Y.; He, G. S.; Ågren, H.; Prasad, P. N. Efficient Broadband Upconversion of Near-Infrared Light in Dye-Sensitized Core/Shell Nanocrystals. *Adv. Opt. Mater.* **2016**, *4*, 1760–1766.
- (38) Sapsford, K. E.; Berti, L.; Medintz, I. L. Materials for Fluorescence Resonance Energy Transfer Analysis: Beyond Traditional Donor-Acceptor Combinations. *Angew. Chem. Int. Ed.* **2006**, *45*, 4562–4589.
- (39) Hildebrandt, N.; Spillmann, C. M.; Algar, W. R.; Pons, T.; Stewart, M. H.; Oh, E.; Susumu, K.; Díaz, S. A.; Delehanty, J. B.; Medintz, I. L. Energy Transfer with Semiconductor Quantum Dot Bioconjugates: A Versatile Platform for Biosensing, Energy Harvesting, and Other Developing Applications. *Chem. Rev.* **2016**, *117*, 536–711.
- (40) Jenkins, R.; Burdette, M. K.; Foulger, S. H. Mini-Review: Fluorescence Imaging in Cancer Cells Using Dye-doped Nanoparticles. *RSC Adv.* **2016**, *6*, 65459–65474.
- (41) Lahtinen, S.; Wang, Q.; Soukka, T. Long-Lifetime Luminescent Europium(III) Complex as an Acceptor in an Upconversion Resonance Energy Transfer Based Homogeneous Assay. *Anal. Chem.* **2016**, *88*, 653–658.
- (42) Frances-Soriano, L.; Liras, M.; Kowalczyk, A.; Bednarkiewicz, A.; Gonzalez-Bejar, M.; Perez-Prieto, J. Energy Transfer in diiodoBodipy-grafted Upconversion Nanohybrids. *Nanoscale* **2016**, *8*, 204–208.
- (43) Wang, F.; Han, Y.; Lim, C. S.; Lu, Y.; Wang, J.; Xu, J.; Chen, H.; Zhang, C.; Hong, M.; Liu, X. Simultaneous Phase and Size Control of Upconversion Nanocrystals through Lanthanide Doping. *Nature* **2010**, *463*, 1061–1065.
- (44) Muhr, V.; Wilhelm, S.; Hirsch, T.; Wolfbeis, O. S. Upconversion Nanoparticles: From Hydrophobic to Hydrophilic Surfaces. *Acc. Chem. Res.* **2014**, *47*, 3481–3493.
- (45) Wilhelm, S.; Kaiser, M.; Würth, C.; Heiland, J.; Carrillo-Carrion, C.; Muhr, V.; Wolfbeis, O. S.; Parak, W. J.; Resch-Genger, U.; Hirsch, T. Water Dispersible Upconverting Nanoparticles: Effects of Surface Modification on Their Luminescence and Colloidal Stability. *Nanoscale* **2015**, *7*, 1403–1410.
- (46) Pauli, J.; Grabolle, M.; Brehm, R.; Spieles, M.; Hamann, F. M.; Wenzel, M.; Hilger, I.; Resch-Genger, U. Suitable Labels for Molecular Imaging – Influence of Dye Structure

- and Hydrophilicity on the Spectroscopic Properties of IgG Conjugates. *Bioconjug. Chem.* **2011**, *22*, 1298–1308.
- (47) Nguyen, T.-L.; Spizzirri, P.; Wilson, G.; Mulvaney, P. Tunable Light Emission Using Quantum Dot-coated Upconverters. *Chem. Commun.* **2008**, *2*, 174-176.
- (48) Shan, G.; Weissleder, R.; Hilderbrand, S. A. Upconverting Organic Dye Doped Core-Shell Nano-Composites for Dual-Modality NIR Imaging and Photo-Thermal Therapy. *Theranostics* **2013**, *3*, 267–274.
- (49) Boyer, J.-C.; Manseau, M.-P.; Murray, J. I.; van Veggel, F. C. J. M. Surface Modification of Upconverting NaYF₄ Nanoparticles with PEG-Phosphate Ligands for NIR (800 nm) Biolabeling within the Biological Window. *Langmuir* **2010**, *26*, 1157–1164.
- (50) Boyer, J.-C.; van Veggel, F. C. J. M. Absolute Quantum Yield Measurements of Colloidal NaYF₄: Er³⁺, Yb³⁺ Upconverting Nanoparticles. *Nanoscale* **2010**, *2*, 1417–1419.
- (51) Lakowicz, J. R. Principles of Fluorescence Spectroscopy; Springer US: Boston, MA, 2006.
- (52) Würth, C.; Lochmann, C.; Spieles, M.; Pauli, J.; Hoffmann, K.; Schüttrigkeit, T.; Franzl, T.; Resch-Genger, U. Evaluation of a Commercial Integrating Sphere Setup for the Determination of Absolute Photoluminescence Quantum Yields of Dilute Dye Solutions. *Appl. Spectrosc.* **2010**, *64*, 733–741.
- (53) Chen, G.; Agren, H.; Ohulchanskyy, T. Y.; Prasad, P. N. Light Upconverting Core-Shell Nanostructures: Nanophotonic Control for Emerging Applications. *Chem. Soc. Rev.* **2015**, *44*, 1680–1713.
- (54) Chen, X.; Peng, D.; Ju, Q.; Wang, F. *Chem. Photon Upconversion in Core-Shell Nanoparticles. Soc. Rev.* **2015**, *44*, 1318–1330.
- (55) Wang, Y.; Tu, L.; Zhao, J.; Sun, Y.; Kong, X.; Zhang, H. Upconversion Luminescence of β -NaYF₄: Yb³⁺, Er³⁺@ β -NaYF₄ Core/Shell Nanoparticles: Excitation Power Density and Surface Dependence. *J. Phys. Chem. C* **2009**, *113*, 7164–7169.
- (56) Johnson, N. J. J.; Korinek, A.; Dong, C.; F. C. J. M. van Veggel. Self-Focusing by Ostwald Ripening: A Strategy for Layer-by-Layer Epitaxial Growth on Upconverting Nanocrystals. *J. Am. Chem. Soc.* **2012**, *134*, 11068–11071.
- (57) Dong, A.; Ye, X.; Chen, J.; Kang, Y.; Gordon, T.; Kikkawa, J. M.; Murray, C. B. A Generalized Ligand-Exchange Strategy Enabling Sequential Surface Functionalization of Colloidal Nanocrystals. *J. Am. Chem. Soc.* **2011**, *133*, 998–1006.

5 SURFACE ENGINEERING OF UPCONVERSION NANOPARTICLES FOR TIME-RESOLVED ANALYSIS OF ATP-RESPONSIVE ENERGY TRANSFER

5.1 Abstract

Upconversion nanoparticles (UCNPs) display exceptional material and luminescence properties for biological applications. They function as donors for energy transfer processes creating prolonged anti-Stokes shifted visible luminescence upon near-infrared excitation. We designed an UCNP probe for lifetime-based Förster resonance energy transfer (FRET) in order to address challenges observed with the common intensity-based approaches which suffer from strong light scattering in biological tissue and depend on the stability of the excitation source. Core-shell UCNPs of 25 nm diameter were synthesized, enabling enhanced upconversion emission intensity in an aqueous environment. Detailed investigations of different surface modifications for colloidal stability in physiological buffered media and efficient FRET capability revealed poly(acrylic acid) as best intermediate layer for further functionalization with receptor molecules. An adenosine triphosphate (ATP)-responsive aptamer was coupled to the particles. An analyte-induced structural change of the aptamer to a G-quadruplex enabled the intercalation of the dye propidium iodide (PI). In contrast to unbound PI, the close proximity of the dye to the particle surface induced FRET, which was monitored by lifetime measurements of the upconversion luminescence. A maximum FRET efficiency of 22% was achieved for physiologically relevant concentrations of ATP between 100 μM and 1.0 mM. Furthermore, the aptamer-modified particles are taken up by normal rat kidney cells (NRK) and do not show any cytotoxic effects even at high particle concentrations up to 300 $\mu\text{g}\cdot\text{mL}^{-1}$. The principle of lifetime-based upconversion detection represents a powerful alternative or add-on to common ratiometric approaches and can be readily adapted to other analytes that can be recognized by structure switching receptors.



Scheme 5.1 | Schematic representation of the detection principle of ATP. The presence of ATP causes a structure change of the ATP-responsive aptamer attached to poly(acrylic acid)-capped UCNPs. Intercalation of the dye propidium iodide induces FRET between the UCNPs and the dye.

This chapter has been submitted.

Verena Muhr, Markus Buchner, Lisa Sauer, Barbara Gorcnik, Joachim Wegener, Antje J. Baeumner, and Thomas Hirsch. *Submitted to ACS Applied Materials & Interfaces.*

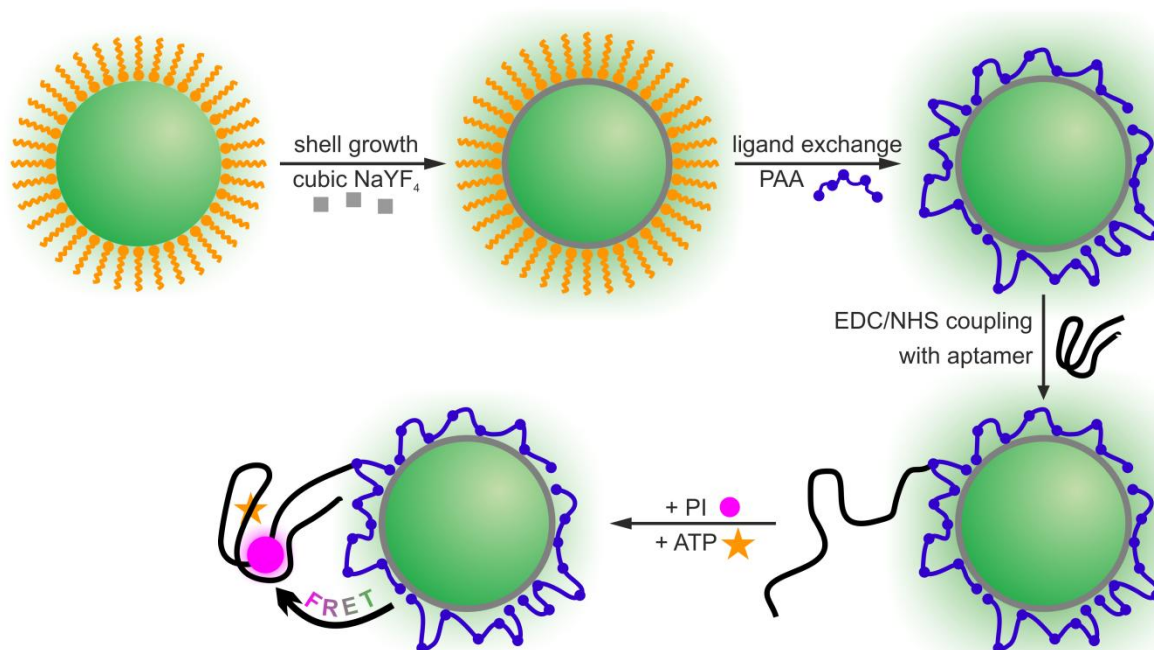
Author contributions

Most of the experimental work was carried out by VM. MB synthesized the amphiphilic polymer and discussed surface modification and characterization. LS performed cellular imaging. BG performed cell viability assays. All authors discussed the results. VM wrote the manuscript. The article was revised by all authors. TH is corresponding author.

5.2 Introduction

Förster resonance energy transfer (FRET) is a powerful luminescent tool in life sciences, as it enables the opportunity to study and monitor molecular interactions, e.g. DNA hybridization, receptor signaling, and changes of the molecular environment with high spatial resolution.¹⁻⁵ Due to its strong dependence on the distance between donor and acceptor, which has to be below 10 nm, FRET is often referred to as a “molecular ruler”.⁶ It is based on energy transfer by non-radiative dipole-dipole interactions between an energy donor and acceptor molecule, both of which are usually fluorescent dyes that exhibit a spectral overlap of donor emission and acceptor absorption.⁷ However, fluorescent proteins and dyes applied in such assays often suffer from photobleaching, light scattering of both excitation and luminescence emission, and strong background fluorescence. These factors profoundly influence ratiometric FRET approaches, but can be circumvented by taking advantage of the luminescence lifetime. The donor lifetime is significantly shortened if FRET occurs. In contrast to the intensity, the luminescence lifetime is not influenced by light scattering, fluctuations of the excitation source, or deviations of the fluorophore concentration. It is either used directly as a measure for FRET efficiency or applied for time-gated detection.⁸ The lifetime of organic dyes is usually very short (< 10 ns), which requires ultra-short pulsed excitation sources and high precision optical components for its acquisition. Much longer decay times (> 100 μ s) allowing for simpler instrumentation are found in upconversion nanoparticles (UCNPs).⁹ These particles display several exceptional properties for biological applications.^{10,11} UCNPs convert near infrared light (NIR, 980 or 808 nm) into visible (and even ultraviolet) luminescence by the sequential absorption of at least two photons.^{12,13} The NIR excitation reduces excitation scattering and photo-damage in biological tissue and eliminates any background fluorescence, resulting in increased signal-to-noise ratios.¹⁴ Applications in drug delivery,¹⁵ photodynamic and photothermal therapy,^{16,17} and most importantly upconversion luminescence energy transfer based imaging of and sensing in biological samples have been explored.¹⁸⁻²⁰ Despite its potential, the application of UCNPs is obstructed by the still not fully investigated cascades of energy transfer processes of UCNPs and limited colloidal stabilization of the UCNPs in physiological media. In our previous work we systematically studied the effect of particle size²¹ and surface loading²² with the acceptor molecules on FRET efficiencies using UCNPs as energy donors. Based on these results we now put focus on surface modification techniques and designed an aptamer-functionalized upconversion probe, which is essentially non-toxic after uptake by mammalian cells and can be used for lifetime-based detection of the central metabolite adenosine triphosphate (ATP). Nucleotides are present at relatively constant levels inside viable cells in order to be able to accomplish various tasks.²³ Based on its vital role for

energy production and storage in living cells, it can be used as an indicator for cell viability or cell damage. Thus, the sensing of ATP levels is extremely useful for metabolic studies in cell biology as well as clinical diagnostics,²⁴ which is why ATP has been the target of choice for UCNP-based sensors previously.²⁵⁻²⁸ Those sensing schemes rely on the upconversion emission intensity and suffer from low reliability as well as from difficult calibration methods. Here we describe a detection scheme based on a structure switching ATP-selective aptamer. The nucleotide stabilizes the G-quadruplex structure of the aptamer. Recognizing the formation of this G-quadruplex structure is provided by specific intercalating dyes, e.g. crystal violet and propidium iodide (PI).²⁹ In contrast to unbound dye molecules, the short distance between dye and the particle surface induced FRET, which can be monitored by lifetime measurements of the upconversion luminescence. The general detection principle is depicted in Scheme 5.2.



Scheme 5.2 | Principle of the design of the ATP sensitive UCNP-based FRET probe. Oleate-capped core-shell UCNPs are prepared by a seed-mediated growth of cubic NaYF_4 particles on hexagonal $\text{NaYF}_4:\text{Yb},\text{Er}$ core particles and functionalized with poly(acrylic acid) (PAA) by ligand exchange. The carboxyl moieties enable covalent coupling of the ATP-responsive aptamer to the surface of the UCNPs. In presence of ATP the aptamer switches its structure into a G-quadruplex form, which is recognized by the intercalating dye propidium iodide (PI). If the dye is confined within the secondary aptamer structure, FRET can occur between UCNPs and PI, reducing the luminescence lifetime of the green upconversion emission.

5.3 Results and Discussion

5.3.1 Design, Synthesis and Characterization of UCNPs

Synthesis of the core-only particles provided UCNPs with a diameter of (23.8 ± 1.0) nm (obtained from TEM analysis of 289 particles) with narrow particle-size distribution and pure hexagonal crystal phase (Figure 1). Core-only UCNPs with mean diameters between 20 and 25 nm had been identified as the optimum size range for the application as energy donors in upconversion FRET processes.²¹ However, these previous studies were performed in the organic solvent DMF due to limited colloidal stability of UCNPs with direct dye-modification in aqueous solutions. Besides its impact on colloidal stability, the aqueous environment increases surface quenching caused by O-H vibrations and surface defects.³⁰⁻³³ This can be reduced by protecting the UCNP surface through an inert shell consisting of the non-doped host material.³⁴ By formation of an inert shell the particle diameter increased to (25.2 ± 0.7) nm (determined from TEM analysis of 2486 particles, see Figure 5.1). A comparison of the decay times of the green emission upon 980 nm excitation of BF_4^- -stabilized particles in DMF revealed that a thin shell with an average thickness of about 1.5 nm prolonged the lifetime from (126 ± 2) μs (core-only particles) to (183 ± 3) μs (core-shell particles). Even if the very thin shell may not be completely homogeneous, this is a clear evidence that the inert shell minimizes the deactivation processes caused by surface defects. During shell growth, monodispersity with a coefficient of variation $< 5\%$ and the hexagonal crystal structure of the particles were retained (Figure 5.1). The composition of the core-only and the core-shell particles as well as the particle concentrations were verified by inductively coupled plasma optical emission spectroscopy (Table 5.1). Small polydispersity indices ($\text{Pdl} < 0.20$) obtained from dynamic light scattering (DLS) measurements also indicated colloidal stability of the UCNP dispersions.

Table 5.1 | Overview of real lanthanide contents determined by inductively coupled plasma optical emission spectroscopy and theoretical composition of $\text{NaYF}_4:\text{Yb},\text{Er}$ core-only and core-shell UCNPs. The shell growth causes an increase in the overall Y^{3+} concentration, since the shell material did not contain Yb^{3+} and Er^{3+} .

theoretical composition	real lanthanide content [%]		
	Y^{3+}	Yb^{3+}	Er^{3+}
$\text{NaYF}_4(20\%\text{Yb},2\%\text{Er})$	78.3 ± 0.5	19.92 ± 0.15	1.81 ± 0.06
$\text{NaYF}_4(20\%\text{Yb},2\%\text{Er})@\text{NaYF}_4$	82.5 ± 0.4	15.86 ± 0.11	1.64 ± 0.05

For FRET-based applications it is mandatory to keep the shell thickness low, since non-radiative energy-transfer is strongly distance dependent. Energy transfer in water was studied by luminescence lifetime measurements of Yb,Er-doped core-only and core-shell UCNPs modified with the acceptor dye rose bengal. The FRET efficiency E was calculated from the upconversion lifetime data in presence (τ_{DA}) and absence (τ_D) of the FRET acceptor according to Equation 1.

$$E = 1 - \frac{\tau_{DA}}{\tau_D} \quad (1)$$

In contrast to studies performed in organic solvents,²¹ an increase of the FRET efficiency was observed in case of the core-shell particles dispersed in water, reaching about 37%. For comparison, the highest FRET efficiency in water observed for core-only UCNPs@rose bengal (diameter (26.4 ± 0.7) nm) was approximately 18%. Thus, core-shell particles of the architecture $\text{NaYF}_4:\text{Yb,Er}@NaYF_4$ were selected for the development of a FRET-based probe for the detection of ATP.

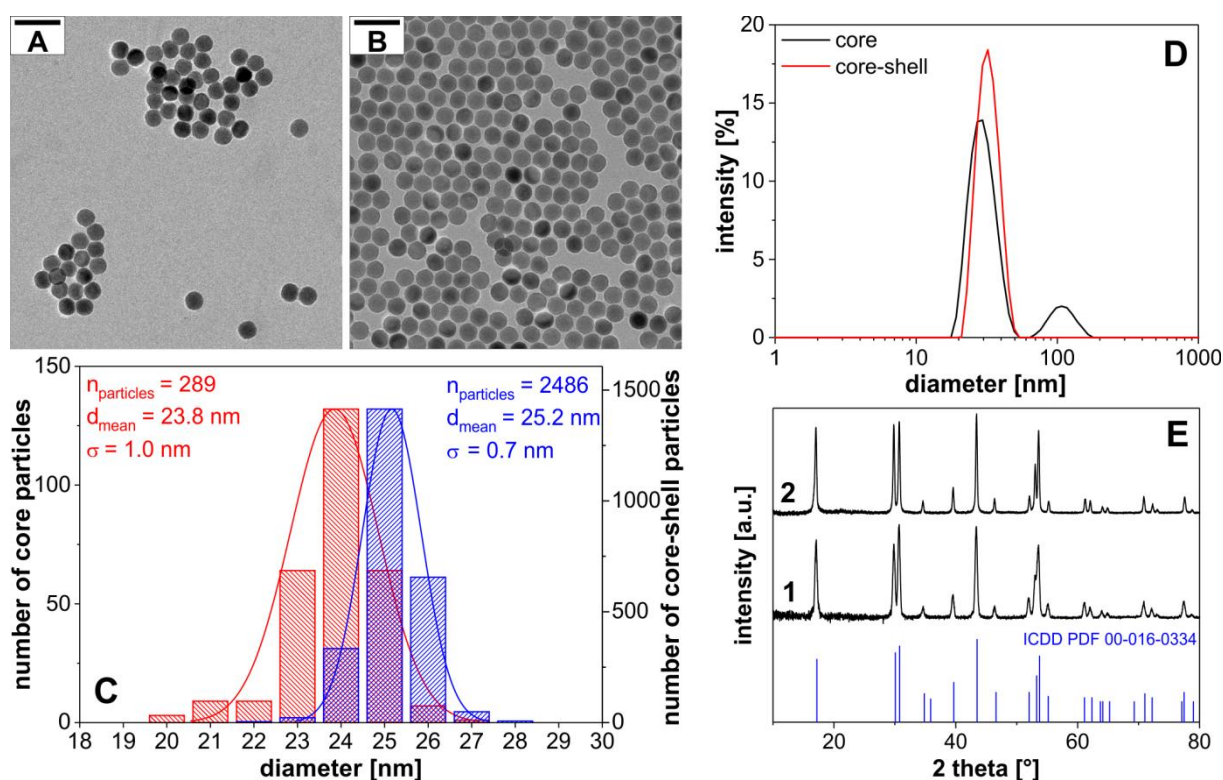


Figure 5.1 | (A,B) Transmission electron micrographs (scale bar: 60 nm) and (C) corresponding size distribution of oleate-capped (A) $\text{NaYF}_4(20\%\text{Yb},2\%\text{Er})$ core-only and (B) $\text{NaYF}_4(20\%\text{Yb},2\%\text{Er})@\text{NaYF}_4$ core-shell UCNPs. The difference between core and shell cannot be visualized by TEM, since the two very similar materials display the same contrast in the images. (D) Intensity-weighted dynamic light scattering measurements of these core and core-shell UCNPs dispersed in cyclohexane at a concentration of about $5 \text{ mg}\cdot\text{mL}^{-1}$. (E) X-ray diffraction patterns of (1) core-only and (2) core-shell UCNPs. The blue lines show the standard reference pattern (ICDD PDF #16-0334) of hexagonal phase NaYF_4 .

5.3.2 Surface Modification and Attachment of the ATP Aptamer

Different surface modifications differ regarding protection of the UCNPs against water quenching, which results in distinct optical characteristics depending on the type of surface modification technique.³⁵ Two main surface modification strategies were tested for the transfer of the hydrophobic UCNPs from organic solvents into water: (a) the oleate is replaced by a new ligand (ligand exchange) and (b) an additional coating is placed on top of the oleate ligand (coating method). It is known that the ligand exchange method is accompanied by better accessibility of water to the particle surface which significantly decreases the efficiency of the upconversion emission for higher energy bands. The intensity of the green-to-red emission intensity gets minimized by a factor of three^{35,36} Ligand exchange with phosphonoglycine (PG) or poly(acrylic acid) (PAA), and coating with the amphiphilic polymer poly(isobutylene-alt-maleic anhydride) (PIBMAD) modified with dodecyl amine side chains were compared regarding colloidal stability. PG is coordinated by phosphonates to the particle surface and therefore known for enhanced stability in media containing phosphate groups.³⁶ The respective lifetimes of the green upconversion luminescence of all particle modifications are summarized in Table 5.2. Amphiphilic coating with PIBMAD resulted in the longest upconversion lifetimes. The hydrophobic bilayer formed around the UCNPs prevents water molecules approaching the particle surface and effectively reduces surface quenching. The two surface modifications obtained by ligand exchange resulted in shorter lifetimes and are quite similar to each other due to their hydrophilicity. In case of PAA and PIBMAD the lifetimes slightly increased by the coupling of the ATP-responsive aptamer.

Table 5.2 | Comparison of the lifetime of the green upconversion luminescence at 540 nm depending on the type of surface ligand used for the functionalization of NaYF₄(20%Yb,2%Er)@NaYF₄ core-shell UCNPs. The lifetimes were measured in HEPES buffer (10 mM, pH = 7.0).

surface ligand	$\tau_{540\text{nm}}$ [μs]	
	ligand	ligand + aptamer
PG	143 ± 5	141 ± 3
PAA	143 ± 3	152 ± 5
PIBMAD	215 ± 1	239 ± 3

All three ligands contain carboxyl groups necessary for electrostatic stabilization of the particles at physiological pH in various buffer systems (MES, HEPES, Tris) and for covalent coupling to the amine modified aptamer. A fast two-step ligand exchange process assisted

by NOBF_4 was chosen for the modification with PG and PAA. In the first step the hydrophobic ligand oleate was removed from the particle surface and the UCNPs were stabilized in hydrophilic organic solvents by weakly coordinating BF_4^- -ions. This electrostatic stabilization reduced aggregation during the ligand exchange process to a minimum. The addition of excess amounts of PG or PAA to the BF_4^- -stabilized particles for the secondary ligand exchange led to the formation of water dispersible particles exhibiting monodispersity and colloidal stability (zeta-potential < -35 mV) in HEPES (10 mM, pH = 7.0). Coating of the oleate surface with the amphiphilic polymer PIBMAD was more time-consuming, but also showed colloidal stability in HEPES buffer (zeta-potential < -30 mV). Ligand exchange by the polymer PAA provided the smallest increase in diameter from all three ligands in favor of efficient energy transfer. Surface modification with PAA and PG resulted in hydrodynamic diameters of (32 ± 5) nm and (34 ± 6) nm, respectively, providing a smaller donor-acceptor distance in FRET systems compared to PIBMAD-coated UCNPs with an average diameter (57 ± 10) nm (Figure 5.2 A). The low Pdl's of < 0.16 for all surface modifications obtained from DLS experiments revealed that there is no agglomeration of particles during the subsequent functionalization with the aptamer *via* EDC/NHS coupling (Figure 5.2 B). For the final particles with aptamer functionalization, the PIBMAD coating revealed the largest hydrodynamic diameter of (142 ± 25) nm, which was twice the diameter of particles with PAA surface modification $((74 \pm 15)$ nm).

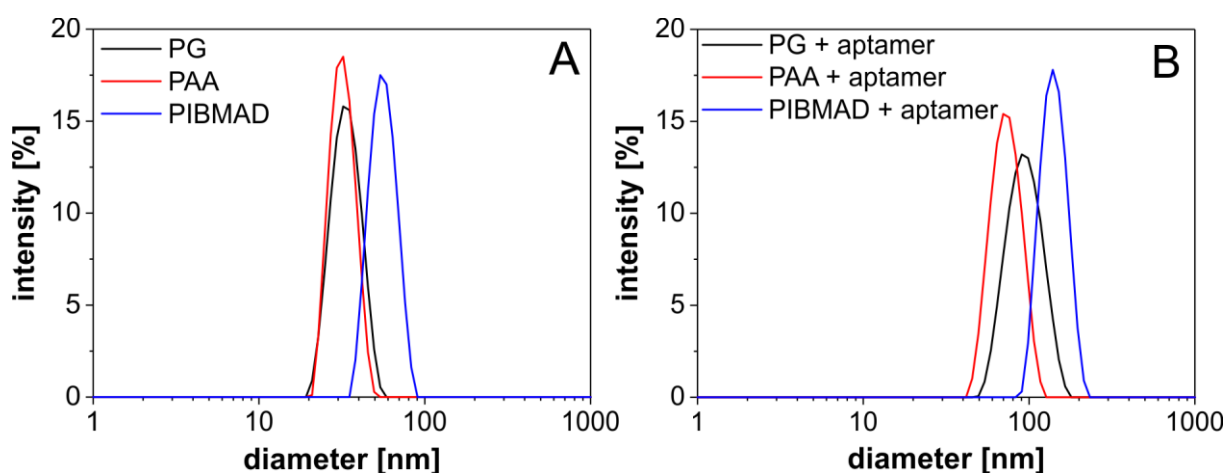


Figure 5.2 | Intensity-weighted dynamic light scattering measurements of $\text{NaYF}_4(20\% \text{Yb}, 2\% \text{Er})@ \text{NaYF}_4$ UCNPs dispersed in HEPES buffer (10 mM, pH = 7.0) at a concentration of $3 \text{ mg} \cdot \text{mL}^{-1}$. The particles were modified with the hydrophilic surface ligands N,N-bis(phosphonomethyl)glycine (PG, black), poly(acrylic acid) (PAA, red) and polymer poly(isobutylene-*alt*-maleic anhydride) modified with dodecyl amine side chains (PIBMAD, blue). The hydrodynamic diameter was determined (A) before and (B) after attachment of the ATP-responsive aptamer to the various surfaces.

Based on these investigations we chose ligand exchange with PAA followed by coupling of the amine modified aptamer for the design of the ATP-responsive UCNPs as the best compromise between reduced surface quenching and increased distance. Despite the weaker suppression of surface quenching by water molecules, only the small hydrodynamic diameter provides small enough donor-acceptor distances that are inevitable for efficient FRET. More than 7% FRET efficiency were not achieved using the amphiphilic coating with PIBMAD.

The EDC/NHS coupling efficiency of the oligonucleotide to the carboxyl groups of the PAA on the UCNP surface was determined as using an additional TAMRA tag on the aptamer. The unbound oligonucleotide was collected during centrifugation steps and the absorbance of the solution was measured (Figure 5.3). From this data, the coupling efficiency was calculated to 55% by considering the dilution of the unbound aptamer during the repeated centrifugation. The colored oligonucleotide allowed for a simple optical tracking of the coupling process, since it led to pink precipitates after the centrifugation steps, which showed the covalent attachment of the aptamer to the nanoparticle surface.

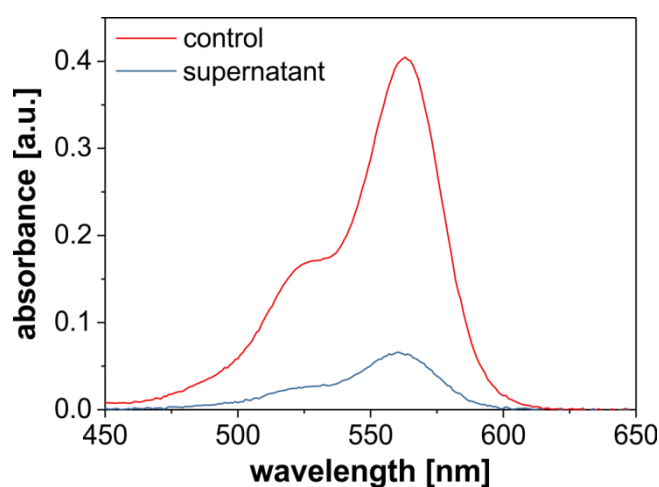


Figure 5.3 | Absorbance spectra of the TAMRA-label coupled to the aptamer. Efficiency of the EDC/NHS coupling between PAA-modified UCNPs and TAMRA-labeled aptamer-NH₃ was determined by measuring the TAMRA absorbance in the supernatant after centrifugation as a measure for unbound TAMRA.

5.3.3 Cytotoxicity Studies and Cellular Uptake

Prerequisite for the application of the upconversion nanoprobe *in vitro* and *in vivo* is a sufficiently low and tolerable cytotoxicity. In contrast to bare UCNPs, coated analogues, especially with negatively charged surface ligands, have been associated with low cytotoxicity.^{37,38} A PrestoBlue[®] assay was performed to study the impact of aptamer-modified UCNPs on cell viability (Figure 5.4 A). Incubation of the cells with aptamer-modified UCNPs

for 4 h had no measurable toxic effect on the cells. No difference in the viability of the treated cells and the untreated cells was found up to a concentration of $300 \mu\text{g}\cdot\text{mL}^{-1}$ modified UCNPs. After a prolonged exposure for 24 h, cell viability slightly decreased at particle concentrations above $50 \mu\text{g}\cdot\text{mL}^{-1}$ but was still at 80% viability for the highest concentration of $300 \mu\text{g}\cdot\text{mL}^{-1}$ under study relative to untreated cells. Concentrations beyond $300 \mu\text{g}\cdot\text{mL}^{-1}$ are typically not required for sensing applications in particular as UCNPs may accumulate inside the cytoplasm with time after sedimentation and binding to the cell surface. The uptake of the modified UCNPs into the cells was investigated by CLSM. Due to the lack of a suitable light source to induce upconversion, the emission of the TAMRA-tagged aptamer bound to the UCNPs was observed by direct excitation with a 543 nm laser. After an incubation time of 24 h, particle aggregates were found to be inside the cells but not inside the nuclei (Figure 5.4 B). Aggregation may be due to entrapment in endocytotic vesicles as a result of membrane-mediated uptake or by particle agglomeration when they are exposed to the very special chemical environment of the cytoplasm.

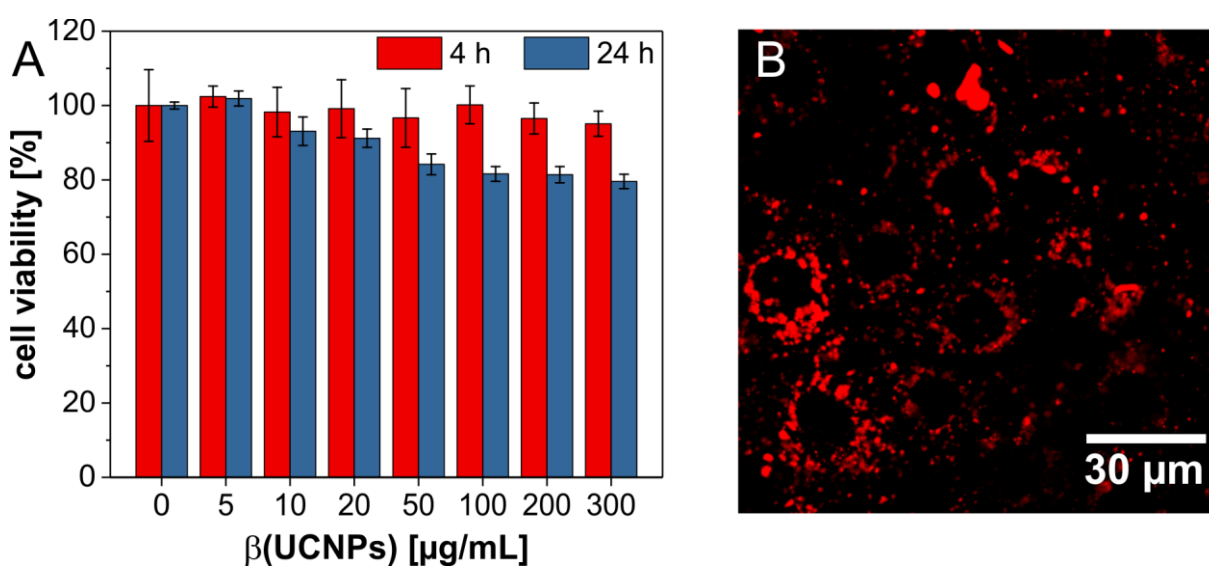


Figure 5.4 | (A) Cytotoxicity assay of NRK cells incubated with varying concentrations ($0 - 300 \mu\text{g}\cdot\text{mL}^{-1}$) of $\text{NaYF}_4(20\%\text{Yb},2\%\text{Er})@\text{NaYF}_4@\text{PAA}$ UCNPs functionalized with the ATP-responsive aptamer. Cell viability was determined by a PrestoBlue[®]-assay after the cells were exposed to the particles for 4 h or 24 h. Results are given as mean \pm standard deviation recorded from five wells of a single assay plate. (B) Confocal laser scanning micrograph of NRK cells after incubation for 24 h with $100 \mu\text{g}\cdot\text{mL}^{-1}$ UCNPs modified with the TAMRA-tagged aptamer. The excitation wavelength was 545 nm. The emission was collected through a 650 nm longpass emission filter.

The brightness of the TAMRA-tag on the ATP aptamer was sufficient to image particle concentrations below $100 \mu\text{g}\cdot\text{mL}^{-1}$. The minimum particle concentration required for microscopic imaging is supposedly significantly lower, when an NIR laser is used as light

source to directly excite the UCNPs instead of the immobilized dye. NIR excitation almost completely suppresses background fluorescence and minimizes scattering of the excitation light within the tissue, which leads to improved sensitivity at lower particle concentrations.

5.3.4 Sensing Properties of Aptamer-modified UCNPs

Propidium iodide (PI) shows a shift of its absorption maximum from 490 nm to 535 nm upon binding to the G-quadruplex form of the aptamer, which matches the green upconversion emission around 540 nm. The maximum absorption coefficient of PI was determined as $5,600 \text{ L}\cdot\text{mol}^{-1}\cdot\text{cm}^{-1}$ from the corresponding spectrum (Figure 5.5).

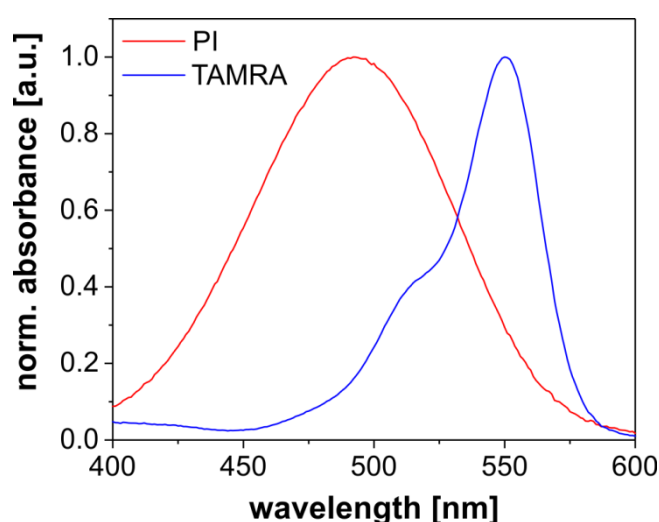


Figure 5.5 | Normalized absorption spectra of aqueous solutions of PI ($c = 50 \mu\text{M}$) and TAMRA ($c = 25 \mu\text{M}$). The maximum extinction coefficients were calculated to $\epsilon_{\text{max}}(\text{PI}) = 5600 \text{ L}\cdot\text{mol}^{-1}\cdot\text{cm}^{-1}$ and $\epsilon_{\text{max}}(\text{TAMRA}) = 31000 \text{ L}\cdot\text{mol}^{-1}\cdot\text{cm}^{-1}$ from the absorption spectra and Lambert-Beer's Law.

In comparison to the free dye, aptamer-intercalated PI more than doubles the overlap integral between the PI absorption and the green upconversion emission (from $2.11\cdot 10^{14} \text{ nm}^4\cdot\text{M}^{-1}$ to $4.51\cdot 10^{14} \text{ nm}^4\cdot\text{M}^{-1}$). In the case of the surface-bound aptamer, a spectral shift of only 20 nm was determined, which results in an integral overlap of $3.74\cdot 10^{14} \text{ nm}^4\cdot\text{M}^{-1}\cdot\text{cm}^{-1}$, which is still 1.5 times the overlap in comparison to the free PI (Figure 5.6 A). Thus, the influence of reabsorption effects of the particle emission and unspecific binding of the dye to the oligonucleotide in absence of the analyte ATP is minimized due to the pronounced spectral shift after binding to the G-quadruplex structure. Furthermore, as the aptamer is oriented on the UCNP surface so that the G-quadruplex is formed in close proximity, efficient FRET sensing is feasible when ATP is present.

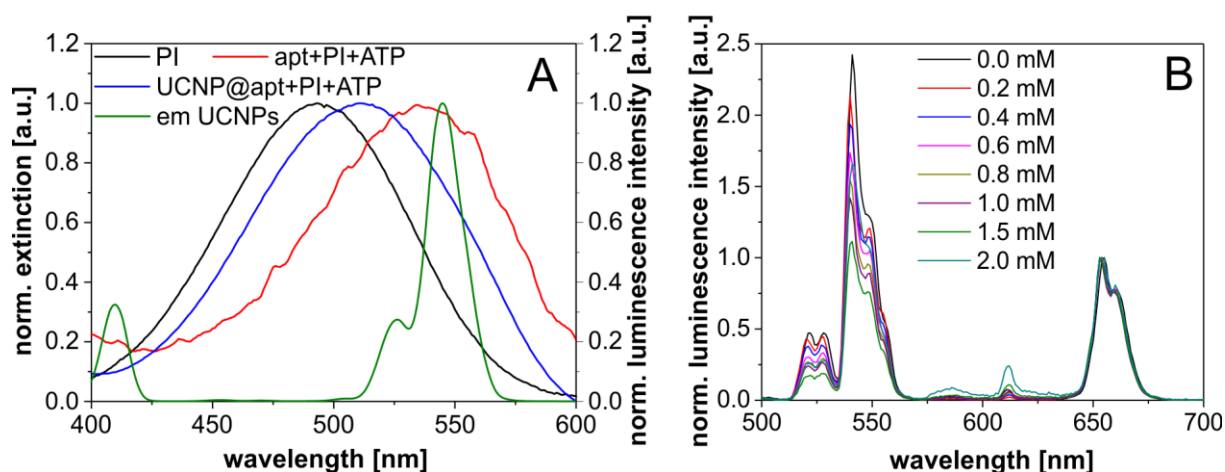


Figure 5.6 | (A) Absorption measurements of the G-quadruplex intercalating dye propidium iodide (PI) in presence and absence of ATP, and the ATP aptamer either bound to the surface of UCNPs or free in solution. All measurements were performed in HEPES buffer (10 mM, pH = 7.0). The addition of ATP causes a shift of the absorbance from 490 nm to 535 nm in case of the free aptamer and to 510 nm in case of the surface bound aptamer. The green line shows the emission spectrum of Yb,Er-doped UCNPs. (B) Luminescence emission spectra of aptamer-modified $\text{NaYF}_4(20\% \text{Yb}, 2\% \text{Er})@ \text{NaYF}_4$ UCNPs in presence of different ATP concentrations (0.2 – 2.0 mM). The particles were dispersed in HEPES buffer (10 mM, pH = 7.0) and excited with a 200 mW laser module at 980 nm. The spectra were normalized on the red upconversion emission at 654 nm.

For the quantitative detection of ATP intensity-based methods were not considered. While increasing concentrations of ATP reduce the peak intensity of the green emission as expected, also scattering effects (best seen at 610 nm) become obvious, which makes detection of ATP in physiological relevant concentrations difficult (Figure 5.6 B). Therefore, lifetime studies were performed. The green emission at 540 nm of the core-shell UCNPs modified with the ATP aptamer possesses a lifetime of about 150 μs . With no ATP present, the lifetime of the UCNPs ($3 \text{ mg} \cdot \text{mL}^{-1}$) did not reveal a change upon the addition of the dye PI ($10 \mu\text{g} \cdot \text{mL}^{-1}$). After the stepwise addition of 3.0 mM ATP, a clear decrease to 120 μs was obtained (Figure 5.7). The exponential fits of the upconversion decay data are depicted in Figure 5.8 A. A saturation effect was observed for ATP concentrations > 0.80 mM, beyond which no further change in luminescence lifetime occurred. The strong decrease of the upconversion decay time by up to 30 μs confirmed the existence of a FRET process between the UCNPs and the PI. The decay data yield a maximum FRET efficiency E of 22% between the UCNPs and PI in the presence of 1.0 mM ATP (Figure 5.8 B). A linear relationship of the experimental lifetime changes and, consequently, the FRET efficiency in dependence on the ATP concentration was observed up to 0.80 mM ATP. The limit of detection (LOD) was calculated to 0.10 mM (3 S/N). The dynamic range covers the lower physiologically relevant concentration range of ATP in mammalian cells (0.4 – 10 mM).

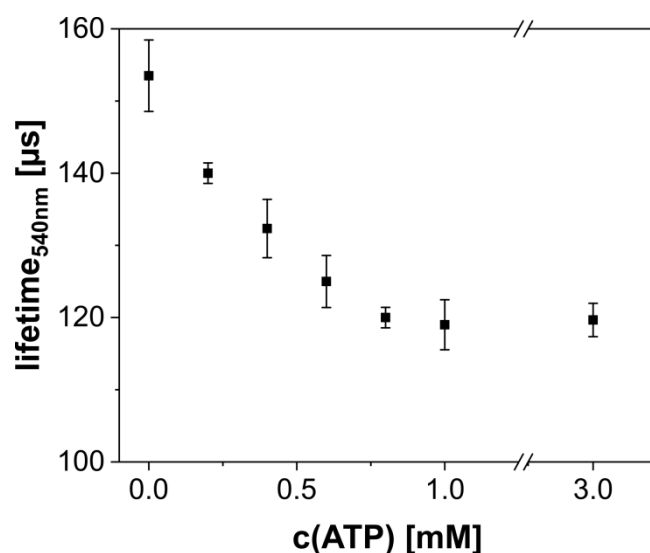


Figure 5.7 | Mean green upconversion lifetime at 540 nm of NaYF₄(20%Yb,2%Er)@NaYF₄@PAA@ATP-aptamer core-shell UCNPs dependent on the concentration of ATP (0.0-3.0 mM) present in the dispersion. The particles were dispersed in HEPES buffer (10 mM, pH = 7.0) at a concentration of 3 mg·mL⁻¹ containing 10 μg·mL⁻¹ PI.

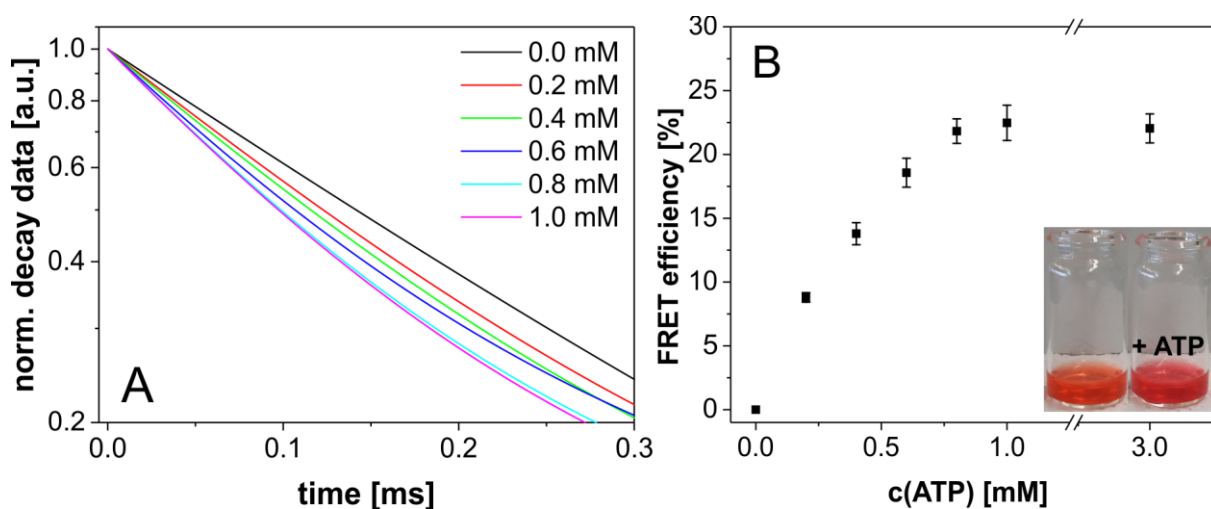


Figure 5.8 | (A) Normalized exponential fits of the decay data (upconversion emission at 540 nm) of NaYF₄(20%Yb,2%Er)@NaYF₄@PAA@ATP-aptamer core-shell UCNPs in presence varying concentrations of the nucleotide ATP. The particles were dispersed in HEPES buffer (10 mM, pH = 7.0) in presence of 5 mg·mL⁻¹ propidium iodide (PI). (B) FRET efficiency of the UCNPs-PI-ATP system calculated from the mean upconversion lifetimes (at 540 nm) before and after the addition of ATP. The inset displays a photograph of a dispersion of aptamer-modified UCNPs in presence of the dye PI (left) before and (right) after addition of ATP. The color changes from orange to pink.

The maximum energy transfer efficiency E of 22% was found to be less than the one obtained from similar UCNPs directly modified with rose bengal (37%). We assume that the difference is due to (a) increased distance between donor and acceptor due to the additional coating with PAA and the size of the aptamer itself, and (b) lower surface loading and a smaller molar absorption coefficient ϵ of PI (5,600 L·mol⁻¹·cm⁻¹, Figure S4) compared to the

dye rose bengal ($120,000 \text{ L}\cdot\text{mol}^{-1}\cdot\text{cm}^{-1}$). In the future, alterations to the detection set-up (CLSM or fluorometers with powerful 980 nm laser sources) will easily improve the LOD, dynamic range and sensitivity of the *in vitro* and *in vivo* assay, but are currently not yet commercially available. Furthermore, increasing the amount of receptor molecules on the surface of the UCNPs and using dyes with higher molar absorption coefficients ($> 100,000 \text{ L}\cdot\text{mol}^{-1}\cdot\text{cm}^{-1}$) and higher selectivity to the aptamer's G-quadruplex structure may lead to improved sensitivity and overall efficiency of the ATP detection.

5.3.5 Selectivity of the ATP Nanoprobe

Despite the innate selectivity of aptamers in general optimized during the SELEX process, potential crossreactivities when working in a complex biological environment have to be considered. The selectivity of the molecular recognition of the ATP nanoprobe was tested against the nucleotide analogs of the analyte ATP. The addition of 1.0 mM ATP yielded a FRET efficiency of approximately 20% and was already in the saturated region. In contrast to ATP itself, the presence of its analogs CTP, GTP and UTP at the same concentration did not significantly change the lifetime of the UCNPs. The normalized raw decay data are summarized in Figure 5.9.

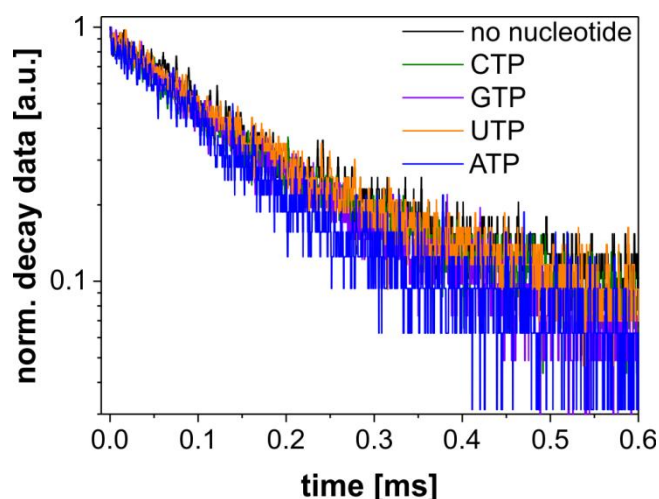


Figure 5.9 | Normalized raw decay data of NaYF_4 (20%Yb, 2%Er)@ NaYF_4 @PAA@ATP-aptamer core-shell UCNPs dispersed in HEPES buffer (10 mM, pH = 7.0) containing PI in presence and absence of 1.0 mM CTP, GTP, UTP or ATP. A noticeable change of the green upconversion luminescence lifetime only occurred in case of the nucleotide ATP.

We conclude that the aptamer was able to recognize and distinguish ATP from its analogues even after immobilization on the surface of the UCNPs. The strong response to ATP in comparison to its analogues is not only indicated by the change of the lifetime itself, but also

by time-gated analysis of decay data (Figure 5.10). The area under the decay curve for a pre-defined time window (here: 0.025 - 0.10 ms) mirrors the decay behavior, since a shorter lifetime equals a smaller area under the fit curve. This method is especially useful for measurements with weak luminescence intensities, which create stronger background noise e.g. due to high photomultiplier voltages, and small expected lifetime changes. The response of the luminescence lifetimes of the nanoprobe in presence of ATP was found to be five times as strong than any of the nucleotide analogues. Additionally, the average concentration in which CTP, GTP and UTP are present in mammalian cells is less than 1/5 (or even 1/8 if only looking at human cells) of the average concentration of ATP itself, *i.e.* much lower than the tested amount.²³ This circumstance further diminishes the influence of ATP analogues on ATP sensing.

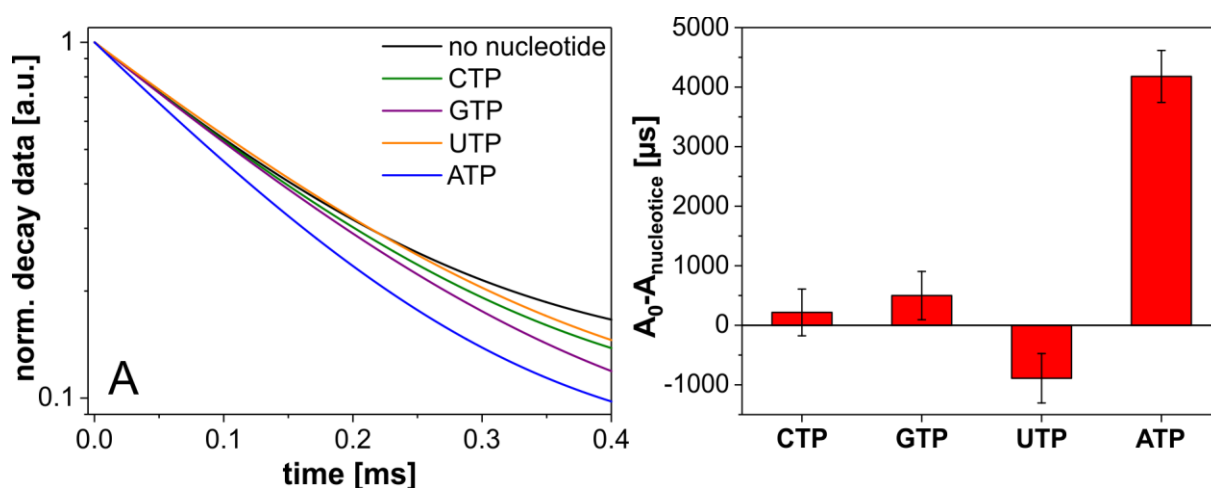


Figure 5.10 | (A) Monoexponential fits of the normalized decay data measured at 540 nm of NaYF_4 (20%Yb, 2%Er)@ NaYF_4 @PAA@ATP-aptamer core-shell UCNPs ($\beta = 3 \text{ mg}\cdot\text{mL}^{-1}$) dispersed in HEPES buffer (10 mM, pH = 7.0) containing $10 \mu\text{g}\cdot\text{mL}^{-1}$ PI in presence and absence of 1.0 mM CTP, GTP, UTP or ATP. A clear change of the green upconversion luminescence lifetime only occurred in case of the nucleotide ATP. (B) Plot of the differential area under the normalized decay curve integrated between 0.025 and 0.10 ms of aptamer-capped UCNPs dispersed in HEPES buffer (10 mM, pH = 7.0) containing PI in absence of any nucleotides and in presence of 1.0 mM CTP, GTP, UTP and ATP.

5.4 Conclusions

In conclusion, we developed and studied the performance of surface-engineered upconversion nanoparticles for efficient lifetime-based resonance energy transfer. Several types of surface modifications for UCNPs were tested regarding colloidal stability in aqueous dispersions, donor-acceptor distance, and influence on surface quenching. Coating with poly(acrylic acid) represented the best compromise between these opposing effects and

provides additional functionalities to couple structure switching bioreceptors to the particles. This concept was applied to the detection of ATP. The selective formation of a G-quadruplex structure of an oligonucleotide bound to the particles was monitored by the change of the green upconversion lifetime due to the intercalation of the acceptor-dye propidium iodide (PI). ATP concentrations between 0.1 mM and 1.0 mM were determined with a maximum FRET efficiency of around 22%. Low cytotoxicity and efficient uptake into cells, combined with advantages of low background and scattering due to NIR excitation in the biological window of the UCNPs showed the potential for applications in cellular imaging and sensing. The concept can be easily transferred to other receptors such as molecular beacons or enzymes. The described method for particle surface modification enables even targeting of the subcellular organelles, by additional functionalization with additional receptors.

5.5 Materials and Methods

5.5.1 Chemicals

Lanthanide chloride hexahydrates (> 99.9%) were obtained from Sigma Aldrich and Treibacher Industrie AG. Oleic acid and 1-octadecene (both technical grade, 90%) were purchased from Alfa Aesar. Ammonium fluoride, sodium hydroxide (both analytical grade), nitrosyl tetrafluoroborate (95%), rose bengal (95%), N,N-bis(phosphonomethyl)glycine (PG, 98%), poly(acrylic acid) sodium salt (PAA, $M_w \approx 2,100$), N-(3-Dimethylaminopropyl)-N-ethylcarbodiimide (EDC, 98%), N-hydroxysuccinimide (NHS, 98%), propidium iodide (PI, 94%) and the nucleotides ATP, CTP, GTP and UTP (99%) were obtained from Sigma Aldrich. Eurofins prepared the two ATP aptamers with the following sequence:
(a) 5'-CCT GGG GGA GTA TTG CGG AGG AAG G-3'-C₃NH₃
(b) TAMRA-5'-CCT GGG GGA GTA TTG CGG AGG AAG G-3'-C₆NH₃.

All other chemicals were of analytical grade and purchased from Sigma Aldrich, Merck or Acros. All chemicals were used as received without further purification. Double distilled water was used for the preparation of all aqueous solutions.

5.5.2 Characterization Methods

Transmission electron microscopy was performed on a Philips CM12 microscope operating at 120 kV. The micrographs were analyzed with the software ImageJ. Dynamic light scattering and zeta-potential measurements were carried out on a Malvern Zetasizer Nano ZS at 20 °C and a particle concentration of 2 - 3 mg·mL⁻¹. The zeta-

potential was measured in 10 mM NaCl with disposable folded capillary zeta cuvettes. Inductively coupled plasma optical emission spectroscopy for the determination of the doping ratios of rare-earth ions in the UCNPs was done with a Spectro Flame-EOP. X-ray diffraction patterns were obtained on a STOE STADI P diffractometer ($K_{\alpha 1}$ -Cu source, $\lambda = 1.54060 \text{ \AA}$). Absorption spectra of the dyes were collected on a Varian Cary 50 spectrophotometer. Luminescence spectra of UCNPs were recorded at room temperature with an Aminco-Bowman Series 2 luminescence spectrometer equipped with an external continuous wave (CW) 980 nm laser module (200 mW) from Picotronic. The setup for the lifetime measurements consisted of a 980 nm CW laser module (200 mW) from Picotronic and an optical chopper (MC2000 with two slot chopper blade MC1F2) from Thorlabs. The signal was amplified using a photomultiplier tube (PreSens) and analyzed by a digital storage oscilloscope (DSO 8204) from Voltcraft. Optical bandpass filters (FF01-535/150-25 and FF01-665/150-25) from Semrock were used for measuring luminescence decays of the green and red upconversion emission bands, respectively.

5.5.3 Synthesis of Hexagonal NaYF₄ (20% Yb, 2% Er) UCNPs

The synthesis of hexagonal phase, oleate-capped UCNPs was carried out starting from rare earth trichlorides in the high boiling solvents 1-octadecene and oleic acid as reported previously.^{35,39} The rare earth trichloride hexahydrates with the corresponding molar doping ratios were dissolved in methanol and transferred into a three necked round bottom flask under nitrogen flow. A mixture of 8 mL oleic acid and 15 mL 1-octadecene per 1 mmol of lanthanide salts was added to the solution. The suspension was heated to 160 °C and vacuum was applied for 30 min to form a clear solution. The solution was cooled down to room temperature and 0.148 g (4.0 mmol) NH₄F and 0.1 g (2.5 mmol) NaOH dissolved in methanol were added per 1 mmol of lanthanide salts. The suspension was kept at 120 °C for 30 min and was then heated to reflux (approx. 325 °C). The progress of the reaction was monitored with a 980 nm CW laser module. 10 min after the first observation of upconversion luminescence, the reaction mixture was cooled down to room temperature. The particles were precipitated by addition of an excess of ethanol and collected by centrifugation at 1,000 g for 5 min. The precipitate was washed twice with chloroform/ethanol and 3 times with cyclohexane/acetone by repeated re-dispersion-precipitation-centrifugation cycles. Finally, the particles were dispersed in cyclohexane, centrifuged at 1,000 g for 3 min to remove aggregates, and the supernatant was collected and stored at 4 °C.

5.5.4 Synthesis of Cubic NaYF₄ nanoparticles

Synthesis of cubic NaYF₄ was identical to the synthesis of hexagonal NaYF₄ until the latter were heated to reflux. Here, the reaction mixture was heated to 240 °C for 40 min without excitation control and afterwards cooled down to room temperature. The purification process was the same as described above.

5.5.5 Synthesis of Core-Shell NaYF₄:Yb,Er@NaYF₄ UCNPs

Core-shell particles were synthesized using an approach based on seed mediated shell growth.⁴⁰ Cubic NaYF₄ nanoparticles (shell material) and hexagonal UCNPs (cores) dispersed in cyclohexane were separately suspended in a mixture of 5 mL oleic acid and 5 mL 1-octadecene per 1 mmol NaYF₄. Vacuum was applied at 100 °C for 30 min to remove the cyclohexane. Afterwards, the cubic particles were kept at 120 °C under N₂ flow. The hexagonal particles were heated to reflux (325 °C) under mild N₂ flow. Small volumes (3 mL at most) of cubic particles were injected into the boiling reaction mixture of hexagonal particles every 10 min to prevent a temperature drop below 300 °C and the formation of new seeds. The mixture was quickly cooled down to room temperature 10 min after the last injection. The purification process was the same as described above.

5.5.6 Surface Modification with Rose Bengal, Poly(acrylic acid) and Phosphonoglycine

The oleate-capped UCNPs were transferred into aqueous dispersions using a two-step ligand exchange process assisted by nitrosyl tetrafluoroborate.⁴¹ In order to remove the oleate, 1 mg NOBF₄ per 1 mg UCNPs was added to a two-phase system consisting of equal volumes of UCNPs dispersed in cyclohexane and N,N-dimethylformamide (DMF). The mixture was stirred vigorously for 10 min at 30 °C. The upper cyclohexane phase containing the oleic acid stripped off from the particles was discarded. The ligand-free, BF₄⁻-stabilized UCNPs were precipitated from the turbid DMF phase by the addition of excess chloroform and centrifuged (1,000 g, 5 min). The transparent, jellylike precipitate was washed with chloroform and finally the BF₄⁻-stabilized particles were dispersed in DMF. For the surface functionalization with rose bengal (RB), poly(acrylic acid) (PAA) or phosphonoglycine (PG), a dispersion of BF₄⁻-stabilized UCNPs (30 mg) in DMF (2 mL) was slowly added to a solution of RB, PAA or PG (30 mg) in water (2 mL) and stirred for 20 min at room temperature. Afterwards, the particles were collected from the solution by centrifugation (21,000 g, 45 min)

and washed three times with water to remove the excess surface ligand. Finally, the precipitate was dispersed in water (6 mL) and stored in the refrigerator.

5.5.7 Surface modification with Amphiphilic Polymer

A solution of poly(isobutylene maleic anhydride) with dodecylamine side chains⁴² (PIBMAD) in CHCl_3 (570 μL , $c_{\text{monomer}} = 0.5 \text{ M}$) was mixed with oleate-capped UCNPs (30 mg) also dispersed in CHCl_3 and stirred for 1.5 h. The solvent was evaporated and the residue was dispersed in NaOH (6 mL, 0.17 M) by sonication for 30 min. For purification, the particles were centrifuged (21,000 g, 60 min) and redispersed in water. This purification step was repeated twice. Finally, the precipitate was dispersed in water (6 mL) and stored in the refrigerator.

5.5.8 Surface Functionalization with ATP Aptamer

The receptor oligonucleotide was bound to hydrophilic PAA-, PG-, or PIBMAD-modified UCNPs via EDC/NHS coupling chemistry. First, hydrophilic UCNPs (5 mg) were dispersed in MES buffer (2 mL, 5 mM, pH = 6.0) and the carboxyl groups on the particle surface were activated by the addition of a freshly prepared solution containing an 80-fold excess of EDC and NHS regarding the amount of oligonucleotide. After slow stirring for 90 min the activated particles were transferred into HEPES buffer (10 mM, pH = 7.4) and a solution (200 μL , also HEPES buffer) containing amine modified oligonucleotide (40 nmol) was added. This mixture was stirred for another 90 min and the carboxyl groups were deactivated by addition of an excess of Tris buffer (5 mM, pH = 7.4). The aptamer-modified particles were collected by centrifugation (12,000 g, 30 min) and washed three times with HEPES buffer (10 mM, pH = 7.0). Approximately 55% of the total amount of aptamer applied in the surface modification reaction were coupled to the UCNPs (Figure S1).

5.5.9 Cytotoxicity Assay

For the viability assay normal rat kidney cells (NRK) were seeded into a 96-well microplate using Dulbecco's Modified Eagle's Medium (DMEM, 4.5 $\text{g}\cdot\text{L}^{-1}$) glucose culture medium (Sigma Aldrich) supplemented with 5% (v/v) fetal calf serum (FCS), 2 mM L-glutamine, and 100 $\mu\text{g}\cdot\text{mL}^{-1}$ penicillin/streptomycin. Cells were allowed to grow to confluence at 37 °C in a 5% CO_2 atmosphere for 7 days prior to the experiment. The culture medium was exchanged once after 6 days and right before the start of the experiment it was replaced by Leibovitz' L-15 culture medium (L-15, Thermo Fisher) containing 5% FCS. The aptamer-modified

UCNPs were added to the wells in 100 μL cell culture medium at concentrations between 5 $\mu\text{g}\cdot\text{mL}^{-1}$ and 300 $\mu\text{g}\cdot\text{mL}^{-1}$ diluted from a stock solution containing 3 $\text{mg}\cdot\text{mL}^{-1}$ particles (determined by ICP-OES) dispersed in water. Control experiments were performed under the same conditions without UCNPs. After incubation for 4 h or 24 h, respectively, at 37 °C the total cell culture medium was replaced by 100 μL PrestoBlue[®] reagent (Thermo Fisher Scientific, 1:10 dilution in PBS⁺⁺ and 1 $\text{g}\cdot\text{L}^{-1}$ glucose). The cells were incubated at 37 °C for 1 h (37 °C, 0% CO₂) and the fluorescence emission of the PrestoBlue[®] reagent was measured with a GENios microplate reader from Tecan at 600 nm upon excitation at 532 nm.

5.5.10 Fluorescence Microscopy

Normal rat kidney cells were grown in DMEM as described above at 37 °C in a 5% CO₂ atmosphere for about 48 h before microscopic studies were conducted. The aptamer-modified UCNPs were added at a concentration of 100 $\mu\text{g}\cdot\text{mL}^{-1}$ in L-15 medium and the cells were incubated with the particles for 24 h at 37 °C in a 0% CO₂ atmosphere. The cells were washed with PBS⁺⁺ and imaged using an upright Nikon Eclipse 90i confocal laser scanning microscope (CLSM) with a C1 scanning unit. Excitation is provided by a 543.5 nm laser (< 5 mW) laser from Melles Griot[®] for the excitation. The emission was collected through a 650 nm longpass filter. CLSM imaging of the particle-loaded cells was performed using a water immersion objective (60x magnification / numerical aperture = 1.0) from Nikon was used with Pinhole L and RGB detector gain of 125. For imaging, the sample was covered with PBS⁺⁺ buffer and the objective was dipped into the solution

5.5.11 Determination of the Spectral Overlap Integral J

The software FluorTools a|e was used to calculate the spectral overlap integrals of the FRET pair UCNP-propidium iodide in presence and absence of ATP. The wavelength range between 450 nm and 600 nm was evaluated. For propidium iodide an absorption coefficient of 5600 $\text{L}\cdot\text{mol}^{-1}\cdot\text{cm}^{-1}$ was used for the calculations.

Acknowledgements

We would like to thank Josef Heiland for the development of the hard- and software of the lifetime measurement system. We are grateful to Dr. Christoph Fenzl and Sandy Franziska Himmelstoß for the transmission electron micrographs. Lisa Marie Wiesholler is acknowledged for her assistance with the XRD and ICP-OES measurements. TH and VM

acknowledge COST Action CM1403 “The European Upconversion Network: From the Design of Photon-Upconverting Nanomaterials to Biomedical Applications”.

References

- (1) Qiu, X.; Guo, J.; Jin, Z.; Petreto, A.; Medintz, I. L.; Hildebrandt, N. Multiplexed Nucleic Acid Hybridization Assays Using Single-FRET-Pair Distance-Tuning. *Small* **2017**, *13*, 1700332.
- (2) Bunt, G.; Wouters, F. S. FRET from Single to Multiplexed Signaling Events. *Biophys. Rev.* **2017**, *9*, 119–129.
- (3) Govor, I. V.; Tatarets; Anatoliy L.; Obukhova; O. M.; Terpetschnig, E. A.; Gellerman, G.; Patsenker, L. D. Tracing the Conformational Changes in BSA Using FRET with Environmentally Sensitive Squaraine Probes. *Methods Appl. Fluoresc.* **2016**, *4*, 24007.
- (4) Poland, S. P.; Krstajić, N.; Monypenny, J.; Coelho, S.; Tyndall, D.; Walker, R. J.; Devauges, V.; Richardson, J.; Dutton, N.; Barber, P. *et al.* A High Speed Multifocal Multiphoton Fluorescence Lifetime Imaging Microscope for Live-cell FRET imaging. *Biomed. Opt. Express* **2015**, *6*, 277–296
- (5) Das, P.; Krull, U. J. Detection of a Cancer Biomarker Protein on Modified Cellulose Paper by Fluorescence Using Aptamer-linked Quantum Dots. *Analyst* **2017**, *142*, 3132–3135.
- (6) Ray, P. C.; Fan, Z.; Crouch, R. A.; Sinha, S. S.; Pramanik, A. Nanoscopic Optical Rulers Beyond the FRET Distance Limit: Fundamentals and Applications. *Chem. Soc. Rev.* **2014**, *43*, 6370–6404.
- (7) Hildebrandt, N.; Spillmann, C. M.; Algar, W. R.; Pons, T.; Stewart, M. H.; Oh, E.; Susumu, K.; Díaz, S. A.; Delehanty, J. B.; Medintz, I. L. Energy Transfer with Semiconductor Quantum Dot Bioconjugates: A Versatile Platform for Biosensing, Energy Harvesting, and Other Developing Applications. *Chem. Rev.* **2017**, *117*, 536–711.
- (8) Rajendran, M.; Miller, L. W. Evaluating the Performance of Time-Gated Live-Cell Microscopy with Lanthanide Probes. *Biophys. J.* **2015**, *109*, 240–248.
- (9) Wang, Y.; Deng, R.; Xie, X.; Huang, L.; Liu, X. Nonlinear Spectral and Lifetime Management in Upconversion Nanoparticles by Controlling Energy Distribution. *Nanoscale* **2016**, *8*, 6666–6673.
- (10) Haase, M.; Schäfer, H. Upconverting Nanoparticles. *Angew. Chem. Int. Ed.* **2011**, *50*, 5808–5829.
- (11) Howes, P. D.; Chandrawati, R.; Stevens, M. M. Colloidal Nanoparticles as Advanced Biological Sensors. *Science* **2014**, *346*, 1247390.
- (12) Chen, G.; Shao, W.; Valiev, R. R.; Ohulchanskyy, T. Y.; He, G. S.; Ågren, H.; Prasad, P. N. Efficient Broadband Upconversion of Near-Infrared Light in Dye-Sensitized Core/Shell Nanocrystals. *Adv. Opt. Mater.* **2016**, *4*, 1760–1766.

- (13) Shao, W.; Chen, G.; Kuzmin, A.; Kutscher, H. L.; Pliss, A.; Ohulchanskyy, T. Y.; Prasad, P. N. Tunable Narrow Band Emissions from Dye-Sensitized Core/Shell/Shell Nanocrystals in the Second Near-Infrared Biological Window. *J. Am. Chem. Soc.* **2016**, *138*, 16192–16195.
- (14) Park, Y. I.; Lee, K. T.; Suh, Y. D.; Hyeon, T. Upconverting nanoparticles: A Versatile Platform for Wide-field Two-photon Microscopy and Multi-modal in vivo Imaging. *Chem. Soc. Rev.* **2015**, *44*, 1302–1317.
- (15) Lai, J.; Shah, B. P.; Zhang, Y.; Yang, L.; Lee, K.-B. Real-Time Monitoring of ATP-Responsive Drug Release Using Mesoporous-Silica-Coated Multicolor Upconversion Nanoparticles. *ACS Nano* **2015**, *9*, 5234–5245.
- (16) Ai, X.; Ho, C. J. H.; Aw, J.; Attia, A. B. E.; Mu, J.; Wang, Y.; Wang, X.; Wang, Y.; Liu, X.; Chen, H. *et al.* In Vivo Covalent Cross-linking of Photon-converted Rare-earth Nanostructures for Tumour Localization and Theranostics. *Nature* **2016**, *7*, 10432.
- (17) Dai, Y.; Yang, D.; Yu, D.; Cao, C.; Wang, Q.; Xie, S.; Shen, L.; Feng, W.; Li, F. Mussel-Inspired Polydopamine-Coated Lanthanide Nanoparticles for NIR-II/CT Dual Imaging and Photothermal Therapy. *ACS Appl. Mater. Interfaces* **2017**, *9*, 26674–26683.
- (18) Han, Y.; Noor, M. O.; Sedighi, A.; Uddayasankar, U.; Doughan, S.; Krull, U. J. Inorganic Nanoparticles as Donors in Resonance Energy Transfer for Solid-Phase Bioassays and Biosensors. *Langmuir* **2017**, DOI: 10.1021/acs.langmuir.7b01483.
- (19) Su, Q.; Feng, W.; Yang, D.; Li, F. Resonance Energy Transfer in Upconversion Nanoplatforms for Selective Biodetection. *Acc. Chem. Res.* **2017**, *50*, 32–40.
- (20) Frances-Soriano, L.; Liras, M.; Kowalczyk, A.; Bednarkiewicz, A.; Gonzalez-Bejar, M.; Perez-Prieto, J. Energy Transfer in DiiodoBodipy-grafted Upconversion Nanohybrids. *Nanoscale* **2016**, *8*, 204–208.
- (21) Muhr, V.; Würth, C.; Kraft, M.; Buchner, M.; Baeumner, A. J.; Resch-Genger, U.; Hirsch, T. Particle-Size-Dependent Förster Resonance Energy Transfer from Upconversion Nanoparticles to Organic Dyes. *Anal. Chem.* **2017**, *89*, 4868–4874.
- (22) Dukhno, O.; Przybilla, F.; Collot, M.; Klymchenko, A.; Pivovarenko, V.; Buchner, M.; Muhr, V.; Hirsch, T.; Mely, Y.; Przybilla, F. *et al.* Quantitative Assessment of Energy Transfer in Upconverting Nanoparticles Grafted with Organic Dyes. *Nanoscale* **2017**, *9*, 11994–12004.
- (23) Traut, T. W. Physiological concentrations of purines and pyrimidines. *Mol. Cell. Biochem.* **1994**, *140*, 1–22.
- (24) Hardie, D. G. Energy Sensing by the AMP-activated Protein Kinase and its Effects on Muscle Metabolism. *Proc. Nutr. Soc.* **2011**, *70*, 92–99..
- (25) He, X.; Li, Z.; Jia, X.; Wang, K.; Yin, J. A Highly Selective Sandwich-type FRET Assay for ATP Detection Based on Silica Coated Photon Upconverting Nanoparticles and Split Aptamer. *Talanta* **2013**, *111*, 105–110.
- (26) Liu, C.; Chang, L.; Wang, H.; Bai, J.; Ren, W.; Li, Z. Upconversion Nanophosphor: An Efficient Phosphopeptides-Recognizing Matrix and Luminescence Resonance Energy Transfer Donor for Robust Detection of Protein Kinase Activity. *Anal. Chem.* **2014**, *86*, 6095–6102.

- (27) Liu, C.; Wang, Z.; Jia, H.; Li, Z. Efficient Fluorescence Resonance Energy Transfer Between Upconversion Nanophosphors and Graphene Oxide: a Highly Sensitive Biosensing Platform. *Chem. Commun.* **2011**, *47*, 4661–4663.
- (28) Song, K.; Kong, X.; Liu, X.; Zhang, Y.; Zeng, Q.; Tu, L.; Shi, Z.; Zhang, H. Aptamer Optical Biosensor without Bio-breakage Using Upconversion Nanoparticles as Donors. *Chem. Commun.* **2012**, *48*, 1156–1158.
- (29) Vummidi, B. R.; Alzeer, J.; Luedtke, N. W. Fluorescent Probes for G-Quadruplex Structures. *ChemBioChem* **2013**, *14*, 540–558.
- (30) Arppe, R.; Hyppanen, I.; Perala, N.; Peltomaa, R.; Kaiser, M.; Würth, C.; Christ, S.; Resch-Genger, U.; Schaferling, M.; Soukka, T. Quenching of the Upconversion Luminescence of NaYF₄:Yb³⁺,Er³⁺ and NaYF₄:Yb³⁺,Tm³⁺ Nanophosphors by Water: the Role of the Sensitizer Yb³⁺ in Non-radiative Relaxation. *Nanoscale* **2015**, *7*, 11746–11757.
- (31) Guo, S.; Xie, X.; Huang, L.; Huang, W. Sensitive Water Probing through Nonlinear Photon Upconversion of Lanthanide-Doped Nanoparticles. *ACS Appl. Mater. Interfaces* **2016**, *8*, 847–853.
- (32) Würth, C.; Kaiser, M.; Wilhelm, S.; Grauel, B.; Hirsch, T.; Resch-Genger, U. Excitation Power Dependent Population Pathways and Absolute Quantum Yields of Upconversion Nanoparticles in Different Solvents. *Nanoscale* **2017**, *9*, 4283–4294.
- (33) Johnson, Noah J. J.; He, S.; Diao, S.; Chan, E. M.; Dai, H.; Almutairi, A. Direct Evidence for Coupled Surface and Concentration Quenching Dynamics in Lanthanide-Doped Nanocrystals. *J. Am. Chem. Soc.* **2017**, *139*, 3275–3282.
- (34) Chen, X.; Peng, D.; Ju, Q.; Wang, F. Photon Upconversion in Core-shell Nanoparticles. *Chem. Soc. Rev.* **2015**, *44*, 1318–1330.
- (35) Wilhelm, S.; Kaiser, M.; Würth, C.; Heiland, J.; Carrillo-Carrion, C.; Muhr, V.; Wolfbeis, O. S.; Parak, W. J.; Resch-Genger, U.; Hirsch, T. Water Dispersible Upconverting Nanoparticles: Effects of Surface Modification on their Luminescence and Colloidal Stability. *Nanoscale* **2015**, *7*, 1403–1410.
- (36) Muhr, V.; Wilhelm, S.; Hirsch, T.; Wolfbeis, O. S. Upconversion Nanoparticles: From Hydrophobic to Hydrophilic Surfaces. *Acc. Chem. Res.* **2014**, *47*, 3481–3493.
- (37) Guller, A. E.; Generalova, A. N.; Petersen, E. V.; Nechaev, A. V.; Trusova, I. A.; Landyshev, N. N.; Nadort, A.; Grebenik, E. A.; Deyev, S. M.; Shekhter, A. B. *et al.* Cytotoxicity and Non-specific Cellular Uptake of Bare and surface-modified Upconversion Nanoparticles in Human Skin Cells. *Nano Res.* **2015**, *8*, 1546–1562.
- (38) Tian, J.; Zeng, X.; Xie, X.; Han, S.; Liew, O.-W.; Chen, Y.-T.; Wang, L.; Liu, X. Intracellular Adenosine Triphosphate Deprivation through Lanthanide-Doped Nanoparticles. *J. Am. Chem. Soc.* **2015**, *137*, 6550–6558.
- (39) Wang, F.; Han, Y.; Lim, C. S.; Lu, Y.; Wang, J.; Xu, J.; Chen, H.; Zhang, C.; Hong, M.; Liu, X. Simultaneous Phase and Size Control of Upconversion Nanocrystals through Lanthanide Doping. *Nature* **2010**, *463*, 1061–1065.

-
- (40) Johnson, Noah J. J.; Korinek, A.; Dong, C.; van Veggel, F. C. J. M. Self-Focusing by Ostwald Ripening: A Strategy for Layer-by-Layer Epitaxial Growth on Upconverting Nanocrystals. *J. Am. Chem. Soc.* **2012**, *134*, 11068–11071.
- (41) Dong, A.; Ye, X.; Chen, J.; Kang, Y.; Gordon, T.; Kikkawa, J. M.; Murray, C. B. A Generalized Ligand-Exchange Strategy Enabling Sequential Surface Functionalization of Colloidal Nanocrystals. *J. Am. Chem. Soc.* **2011**, *133*, 998–1006.
- (42) Lin, C.-A. J.; Sperling, R. A.; Li, J. K.; Yang, T.-Y.; Li, P.-Y.; Zanella, M.; Chang, W. H.; Parak, W. J. Design of an Amphiphilic Polymer for Nanoparticle Coating and Functionalization. *Small* **2008**, *4*, 334–341.

6 CONCLUSIONS AND FUTURE PERSPECTIVES

Comprehensive understanding of efficient probe design for FRET-based detection is a prerequisite for expanding the possibilities of UCNPs in future theranostic applications. Most publications demonstrating the great potential of upconversion nanoparticles in bioanalytical applications are based on proof of concept studies. The first papers on chemical sensing were already published in 2001¹ and upconversion energy transfer has been investigated since 2005,² but up to now no sensing application based on upconversion is at the market. Besides limited instrumentation for the characterization of the material one of the main reasons is that the particle architecture has not yet been sufficiently taken into account. The required knowledge on reproducible synthesis methods, yielding monodisperse UCNPs with pure hexagonal crystal structure, controlled crystal size, and defined core-shell architectures, and on the methods necessary for the complete characterization of composition and optical properties of the particles has been gained only during the last years. These techniques now enable a much more detailed understanding of UCNP systems and facilitate the development of refined UCNP-based luminescent probes. The insights gained from this thesis clearly demonstrate that size, composition and surface modification all profoundly influence the efficiency of FRET-based sensor systems. Full comprehension of the complex interplay between particle size, surface functionalization, colloidal stability and cytotoxicity is necessary for advanced sensor development. Neglecting these aspects can weaken the sensor performance and may increase its dependence on external factors. In contrast to intensity-based methods the FRET efficiencies determined by the investigation of the upconversion lifetime were independent on excitation power density of the laser, UCNP concentration and overall concentration of the dye not bound to the UCNPs. Additionally, the lifetime of the upconversion luminescence is longer than 100 μ s. Such long decay times can be detected with much less expensive equipment than the nanosecond lifetimes of organic dyes. A simple optical chopper is sufficient to intermit the CW laser excitation.³ This feature makes UCNPs even more suited for lifetime-based FRET applications, and the particles represent an important alternative to conventional organic fluorescent dyes used for the study of energy transfer processes.

6.1 Particle Architectures for FRET-based Applications

A paradigm in upconversion science is to design particles as small as possible, which is especially important for *in vivo* applications where the clearance of particles from the body plays a crucial role. However, smaller particles also lead to a lower upconversion quantum

yield (QY), i.e. lower luminescence intensity and shorter lifetime. In this thesis, a similar effect was observed for UCNPs acting as FRET donors modified with organic acceptor dyes, with the difference, that the FRET efficiency is not proportional to the particle size and that there is an optimum particle diameter for highest FRET efficiency. Particles smaller than 20 nm possess such a large surface-to-volume ratio that surface deactivation and quenching, which also mostly occur at the surface of the UCNPs, strongly compete with the energy transfer process. But in this case bigger does not mean better. The size of the UCNPs should not exceed 25 nm if they are intended to be used as FRET donors. In particles 20 - 25 nm in diameter, which represented the optimum, most donor ions within the particle can interact with the FRET acceptor on the particle surface and the most efficient energy transfer can be established. All these relations were only observed evaluating the luminescence decay time of the UCNPs and were not visible in the corresponding emission spectra.

The study of core-shell UCNPs gave an even more detailed picture of FRET processes on the particle surface. The passivation of the UCNP surface with an inert shell effectively reduced surface quenching and increased the upconversion emission. Higher luminescence intensity enabled faster determination of the decay times with lower uncertainty, but the presence of the inert shell also caused an increased distance between donor ions inside the UCNPs and surface bound acceptor dyes. The use of very thin shells represented the best compromise between those two opposing effects. For small UCNPs the suppression of surface quenching outweighed the negative effect of the increased donor-acceptor distance and significantly higher FRET efficiencies were observed compared to the respective core-only UCNPs. This effect was even more pronounced in the solvent water, which strongly quenches the UCNP luminescence. It was demonstrated that not only the presence of an inert shell, but also the type of surface modification used for the preparation of water dispersible UCNPs profoundly influences their optical properties. Additional coatings with amphiphilic molecules enabled better protection against water quenching compared to ligand exchange with hydrophilic ligands due to the presence of a hydrophobic layer around the particle. Despite the enhanced luminescence of the hydrophilic UCNPs coated with the amphiphilic polymer, the increased donor-acceptor distance turned out to be the parameter which influenced the FRET efficiency the most. Ligand exchange with polymers, such as poly(acrylic acid), was identified as the best compromise between strong upconversion emission, minimized donor-acceptor distance, colloidal stability and biocompatibility. However, a detailed study is necessary to determine the optimum shell thickness and surface modification for differently sized UCNPs in aqueous dispersions. One may even have to go one further step back and rethink the doping ratios of sensitizer and activator ions.

Since the doping concentrations were optimized for the corresponding bulk material, they may not represent the most efficient system for Yb/Er and Yb/Tm upconversion on the nanometer scale. We are currently investigating the effect of varying activator contents in Yb/Er-doped core-only and core-shell UCNPs of the same size in hydrophobic and hydrophilic solvents in cooperation with the Federal Institute for Materials Research and Testing in Berlin.

In this thesis, it was also demonstrated that different acceptor dyes lead to different FRET efficiencies. This was ascribed to individual overlap integrals and surface loading density depending on the structure of the dye. The effect of variations in dye loading of the UCNPs on luminescence intensity and lifetime were investigated in cooperation with Yves Mély's group from the University of Strasbourg.⁴ The study revealed higher FRET efficiencies with increasing amounts of immobilized organic dye molecules. It was also shown that the two upconversion emissions in Yb/Er-doped UCNPs (green and red) are not independent from each other, i.e. the complementary emission may not be suitable as reference signal in ratiometric measurements. If all these factors are kept in mind for the design of upconversion nanoprobe intended for the use in biosensing and -imaging the performance of FRET-based applications can be enhanced.

6.2 Future Directions

Efficient energy transfer may also be beneficial for upconversion mediated photodynamic therapy (PDT). The immobilization of photosensitizers that are able to be triggered by the emission of the UCNPs and the generation of singlet oxygen have been investigated by several groups.⁵⁻⁸ In contrast to UV light the NIR excitation reduces photo-damage of healthy tissue and allows for specific treatment of the targeted cells by the local production of reactive oxygen species. Usually, the excitation of the photosensitizers relies mainly on the absorption of the upconversion emission rather than FRET. However, the proficiency of the PDT depends on the energy transfer efficiency from the particle to the photosensitizer dyes. Instead of just making use of dye absorption to trigger the singlet oxygen production an additional efficient non-radiative FRET for excitation of the photosensitizers should be useful for effective PDT. The rational design of UCNP donors with diameters in the range of 20 - 25 nm and thin inert shells in combination with a careful choice of the surface modification strategy for the close attachment of suitable photosensitizers offers the possibility to develop more powerful FRET based PDT systems.

The comprehensive understanding of the energy transfer behavior is not only of importance for systems where the UCNPs act as the energy donor, but also the other way around. Dye sensitization by antenna ligands and the intended enhancement of material absorption and upconversion emission have also been investigated in recent years.^{9,10} Such systems are of particular interest for the use of UCNPs in photovoltaic energy conversion and bio-applications with reduced excitation power or different excitation wavelengths. An increased material absorption in the NIR region can promote the efficiency of solar collectors, which currently show only weak absorption properties in the infrared light range.^{11,12} However, the energy absorbed by antenna ligands needs to be effectively transformed into visible emission by energy transfer to the UCNPs to be able to significantly enhance the overall efficiency of solar cells. Particle size, type of dye, surface modification, and amount of dye loading are likely to influence the energy transfer in this direction as well and must be studied carefully and considered for the development of UCNPs-based absorption materials designed for energy conversion in solar collectors. Similar statements can be made for the application of dye sensitized UCNPs in biosensors. The absorption of the antenna dye and the subsequent energy transfer need to be efficient enough to create bright upconversion luminescence upon lower excitation power and/or alternative wavelengths. The latter is especially important if the heating effect induced by the NIR laser excitation needs to be avoided.^{13,14} The optimization of the energy transfer from the antenna dye to the UCNPs facilitates the design of dye sensitized upconversion probes for biosensing and -imaging. One concern in all these systems, however, is the photostability of the dye itself. Though the stability is higher if the dye is indirectly excited via energy transfer from the nanoparticles compared to dye sensitization, it is always less than that of the UCNPs. Any bleaching effects need to be reduced to a minimum by selecting dyes that show comparably high photostability. For bioanalytical applications, this issue is most significant in case of continuous online measurements, which run for several hours and thus exceed the stability limits of many organic dyes, even upon excitation with low energy NIR radiation.

During the FRET studies, it was shown that the fluorescence emission of the acceptor dye immobilized on the UCNPs surface was triggered via energy transfer. At particle diameters ≤ 20 nm the dye emission was almost as strong as the original upconversion emission of the emission band affected by the FRET. This occurrence can be utilized to shift the fixed emission bands of the UCNPs to different wavelengths. The respective upconversion emission can be almost completely suppressed and a new luminescence at a longer wavelength depending on the fluorescent dye chosen as FRET acceptor can be created. This may help the application of UCNPs as fluorescent labels and receptors for bioimaging. The shift of the emission wavelength enables the detection and distribution mapping of

multiple analytes with NIR excitation since an overlap of the various luminescent signals in one imaging channel can be prevented.

The luminescence intensity of UCNPs is not the only exceptional tool for imaging purposes, but also the upconversion decay data. Fluorescence lifetime imaging microscopy (FLIM) is an established method in biological imaging especially for tissue that induces strong light scattering, which impedes ratiometric intensity measurements.^{15,16} The excitation wavelength of UCNPs in the NIR region enables even further reduction of scattering effects and background luminescence, similar to two-photon excitation techniques used for microscopy.¹⁷ However, unlike these two-photon absorption processes the excitation of UCNPs does not require ultrashort pulsed femtosecond lasers. FRET also plays an important role for FLIM. The change of the donor lifetime depending on the environment of the luminescent probe, e.g. due to protein or membrane interactions, can be visualized by the so called FLIM-FRET.^{18,19} Combining the advantages of the optical and chemical properties of UCNPs with a lifetime-based readout may promote the application of UCNPs as long-lived FRET donors for FLIM-FRET.²⁰ With the optimized particle architecture and surface chemistry the lifetime changes of the upconversion emission and the resulting sensitivity to variations of the particle environment can be maximized. The modification of the UCNP surface with selective receptors and suitable acceptor dyes enables specific targeting of the region and analyte of interest.

The development of the adenosine triphosphate (ATP) responsive upconversion nanoprobe described in this work showed the potential of such a detection method. The surface modification of the UCNPs with structure switching bioreceptors was optimized to obtain biocompatible particles capable of selectively recognizing ATP concentrations between 0.1 -1.0 mM. Such a principle can be extended to multianalyte detection by making use of various receptor molecules and the different luminescence wavelengths characteristic for each activator ion in combination with organic dyes that individually overlap with each of the single upconversion emission bands in the blue, green, red, and NIR region. Receptors, such as oligonucleotides, have to be immobilized on the particle surface to ensure the close proximity of the luminescent probe (the UCNPs) and the targeted analyte molecule. The covalent attachment may negatively influence colloidal stability, cytotoxicity and the recognition ability and selectivity of the receptor, which is often not considered for new sensor designs. During the investigation of the UCNP based ATP detection shown in this work a simple optical method was used to verify the functionality of the aptamer after coupling to the particle surface. Upon binding to the aptamer in presence of the analyte ATP the FRET acceptor dye exhibited a spectral shift in its absorption maximum towards a longer

wavelength. This shift was smaller in case of the UCNP bound aptamer compared to the free aptamer, but still clearly visible. It seems that the recognition capability and binding strength towards ATP of the bound aptamer was reduced but still strong enough to differentiate between ATP and its analogues. The loss of binding efficiency compared to the free aptamers is a common occurrence in immobilized aptamers and restricts tapping the full potential of sensing mechanisms based on surface-bound receptors.²¹ These negative effects are usually suppressed by the use of long linker molecules, which is not an option for FRET applications. Alternatively, careful choice of the surface chemistry and particle dimensions may minimize the influence of the immobilization. Steric hindrance and electrostatic attraction/repulsion have to be controlled in order to reduce unwanted interactions between UCNP surface (or any other nanomaterial) and the receptor molecule as much as possible. This way an environment closest to that of the free receptor can be created and increased recognition capabilities and structural flexibility of the nanoprobe can be obtained. These considerations are necessary for the design of efficient and reliable upconversion FRET probes.

6.3 Remaining Challenges

Public attention is often directed towards environmental and health issues that may arise by an excessive use of nanoparticles rather than beneficial future perspectives and potential applications of the materials. One general concern regarding all kinds of nanomaterials is the still relatively poor understanding of short- and long-term cytotoxic effects. The presence of heavy metal ions, e.g. within quantum dots, or the production of reactive oxygen species limit the application of many nanomaterials *in vitro* and *in vivo*.^{22,23} Several studies ascribe generally low toxicity to UCNPs.²⁴ The results obtained from the cytotoxicity studies performed during this thesis support these claims. Incubation of normal rat kidney cells with various concentrations of UCNPs (up to 300 $\mu\text{g}\cdot\text{mL}^{-1}$) for 24 h did not lead to significant toxic effects and the cell viability was almost identical to the untreated control group. The uptake of the UCNPs into the cells was verified by confocal laser scanning microscopy. One has to keep in mind that both uptake and cytotoxicity are dependent of the type of surface coating of the nanoparticles, which has to be considered for the choice of surface chemistry.²⁵ However, long-term toxic effects caused by leaching or accumulation within certain parts of the cell/body still need to be studied in more detail.²⁶

A few other issues stand in the way of UCNPs and their widespread application in bioanalysis despite the obvious potential for sensing and imaging. One is the local absorption maximum of water at the excitation wavelength of 980 nm with an absorption coefficient of

0.48 cm^{-1} .²⁷ The absorption reduces the effective laser power that reaches the UCNPs dispersed in an aqueous environment and simultaneously heats up the water during excitation, which can cause local heat damage to the surrounding tissue. While the diminished excitation power does not influence the upconversion luminescence lifetime, in addition to strong water quenching effects it does lead to much lower upconversion luminescence intensities compared to UCNPs dispersed in organic solvents. This is particularly problematic in cases where the particle concentration is very low, *i.e.* for basically all intracellular sensing and imaging methods. The suppression of non-radiative surface deactivation by passivation with inert shells consisting of the non-doped host material is often not enough to generate strong upconversion luminescence in very small UCNPs dispersed in an aqueous system. By the incorporation of an alternative sensitization pathway the excitation wavelength of the UCNPs can be shifted to a different wavelength where water shows weaker absorption. This can be achieved by additional doping with Nd^{3+} ions, which absorb light at a wavelength around 808 nm.²⁸ The energy can then be transferred to Yb^{3+} ions that act as the energy bridge for the subsequent energy transfer to the activator ions. The upconversion efficiency of such tandem sensitized systems can even reach levels equal to the traditional Yb/Er and Yb/Tm doping. This can be achieved if Nd^{3+} is separated from the activator ions by core-shell architectures in order to prevent non-radiative energy back transfer between the two, which would otherwise reduce the desired radiative deactivation of the excited activator ions.²⁹ At 800 nm water absorption is much weaker (molar absorption coefficient of 0.02 cm^{-1}) than at 980 nm, *i.e.* the shift of the excitation wavelength avoids loss of excitation power and problematic sample heating upon extended laser excitation.³⁰ A similar effect can be created by the use of antenna dyes on the particle surface that absorb light at a shorter wavelength, usually also around 808 nm, and transfer the energy to the UCNPs.³¹ In contrast to the Nd^{3+} sensitized system the generally weak photostability of the antenna dyes and limited surface functionality of the dye sensitized UCNPs remain concerns to be solved for future applications as luminescent probes.

One problem that comes with working on UCNPs is the lack of commercially available instruments that meet the requirements for upconversion processes. Light sources available for standard fluorimeters do not cover the NIR regime or do not provide enough excitation power to induce sufficient upconversion emission in case of expensive broadband tunable lasers. These instruments need to be modified with external laser diodes (808 nm or 980 nm) or even entirely custom-built devices have to be used, although customizability of the devices from many major companies has improved over the last years. Custom-built instruments create another problem. Information about the instrument specifications is rarely reported, which is particularly critical with respect to the applied laser power density. Since

upconversion is a non-linear optical process the quantum yield and the emission intensity ratios of the upconversion emission bands heavily depend on the excitation power density.³² This fact is a significant drawback in case of intensity-based (ratiometric) applications. The excitation power has to be known and kept stable to prevent a false interpretation of possibly changing emission ratios. It also prevents reliable comparability of results obtained by different research groups and/or on different devices. The use of the upconversion lifetime instead of the emission intensity circumvents some of these issues. The decay time is not dependent on the excitation power density (at least for power densities below $500 \text{ W}\cdot\text{cm}^{-2}$), *i.e.* small fluctuations of the excitation source do not affect the measured lifetime.³³

Nevertheless, no characterization standards for UCNPs exist to date, which would allow for a quantitative comparison between results obtained by different research groups. Such a standardized characterization protocol of UCNPs needs to be established in the near future in order to be able to define “upconversion efficiency” and compare and evaluate results of different researchers based on established definitions. But despite these persisting challenges the outstanding versatile potential of UCNPs easily encourages researchers around the world to make great strides paving the way for the exploration of new possibilities. UCNPs have a bright future ahead.

References

- (1) Niedbala, R.S.; Feindt, H.; Kardos, K.; Vail, T.; Burton, J.; Bielska, B.; Li, S.; Milunic, D.; Bourdelle, P.; Vallejo, R. Detection of Analytes by Immunoassay Using Up-Converting Phosphor Technology. *Anal. Biochem.* **2001**, *293*, 22–30.
- (2) Wang, L.; Yan, R.; Huo, Z.; Wang, L.; Zeng, J.; Bao, J.; Wang, X.; Peng, Q.; Li, Y. Fluorescence Resonant Energy Transfer Biosensor Based on Upconversion-Luminescent Nanoparticles. *Angew. Chem. Int. Ed.* **2005**, *44*, 6054–6057.
- (3) Wilhelm, S.; del Barrio, M.; Heiland, J.; Himmelstoß, S. F.; Galbán, J.; Wolfbeis, O. S.; Hirsch, T. Spectrally Matched Upconverting Luminescent Nanoparticles for Monitoring Enzymatic Reactions. *ACS Appl. Mater. Interfaces* **2014**, *6*, 15427–15433.
- (4) Dukhno, O.; Przybilla, F.; Collot, M.; Klymchenko, A.; Pivovarenko, V.; Buchner, M.; Muhr, V.; Hirsch, T.; Mely, Y. Quantitative Assessment of Energy Transfer in Upconverting Nanoparticles Grafted with Organic Dyes. *Nanoscale* **2017**, *9*, 11994–12004.
- (5) Li, S.; Cui, S.; Yin, D.; Zhu, Q.; Ma, Y.; Qian, Z.; Gu, Y. Dual Antibacterial Activities of a Chitosan-modified Upconversion Photodynamic Therapy System Against Drug-resistant Bacteria in Deep Tissue. *Nanoscale* **2017**, *9*, 3912–3924.
- (6) Lucky, S. S.; Idris, N. M.; Huang, K.; Kim, J.; Li, Z.; Thong, P. S. P.; Xu, R.; Soo, K. C.; Zhang, Y. In vivo Biocompatibility, Biodistribution and Therapeutic Efficiency of Titania

- Coated Upconversion Nanoparticles for Photodynamic Therapy of Solid Oral Cancers. *Theranostics* **2016**, *6*, 1844–1865.
- (7) Wang, P.; Li, X.; Yao, C.; Wang, W.; Zhao, M.; El-Toni, A. M.; Zhang, F. Orthogonal Near-infrared Upconversion Co-regulated Site-specific O₂ Delivery and Photodynamic Therapy for Hypoxia Tumor by Using Red Blood Cell Microcarriers. *Biomaterials* **2017**, *125*, 90–100.
- (8) Xu, J.; Yang, P.; Sun, M.; Bi, H.; Liu, B.; Yang, D.; Gai, S.; He, F.; Lin, J. Highly Emissive Dye-Sensitized Upconversion Nanostructure for Dual-Photosensitizer Photodynamic Therapy and Bioimaging. *ACS Nano* **2017**, *11*, 4133–4144.
- (9) Wang, X.; Valiev, R. R.; Ohulchanskyy, T. Y.; Agren, H.; Yang, C.; Chen, G. Dye-sensitized Lanthanide-doped Upconversion Nanoparticles. *Chem. Soc. Rev.* **2017**, *46*, 4150–4167.
- (10) Wei, W.; Chen, G.; Baev, A.; He, G. S.; Shao, W.; Damasco, J.; Prasad, P. N. Alleviating Luminescence Concentration Quenching in Upconversion Nanoparticles through Organic Dye Sensitization. *J. Am. Chem. Soc.* **2016**, *138*, 15130–15133.
- (11) Hao, S.; Shang, Y.; Li, D.; Agren, H.; Yang, C.; Chen, G. Enhancing Dye-sensitized Solar Cell Efficiency through Broadband Near-infrared Upconverting Nanoparticles. *Nanoscale* **2017**, *9*, 6711–6715.
- (12) Yu, J.; Yang, Y.; Fan, R.; Wang, P.; Dong, Y. Enhanced Photovoltaic Performance of Dye-sensitized Solar Cells Using a New Photoelectrode Material: Upconversion YbF₃-Ho/TiO₂ Nanoheterostructures. *Nanoscale* **2016**, *8*, 4173–4180.
- (13) Wu, X.; Zhang, Y.; Takle, K.; Bilsel, O.; Li, Z.; Lee, H.; Zhang, Z.; Li, D.; Fan, W.; Duan, C. *et al.* Dye-Sensitized Core/Active Shell Upconversion Nanoparticles for Optogenetics and Bioimaging Applications. *ACS Nano* **2016**, *10*, 1060–1066.
- (14) Zou, X.; Xu, M.; Yuan, W.; Wang, Q.; Shi, Y.; Feng, W.; Li, F. A Water-dispersible Dye-sensitized Upconversion Nanocomposite Modified with Phosphatidylcholine for Lymphatic Imaging. *Chem. Commun.* **2016**, *52*, 13389–13392.
- (15) Shivalingam, A.; Izquierdo, M. A.; Le Marois, A.; Vyšniauskas, A.; Suhling, K.; Kuimova, M. K.; Vilar, R. The Interactions Between a Small Molecule and G-quadruplexes are Visualized by Fluorescence Lifetime Imaging Microscopy. *Nat. Commun.* **2015**, *6*, 8178.
- (16) Niehorster, T.; Loschberger, A.; Gregor, I.; Kramer, B.; Rahn, H.-J.; Patting, M.; Koberling, F.; Enderlein, J.; Sauer, M. Multi-target Spectrally Resolved Fluorescence Lifetime Imaging Microscopy. *Nat. Methods* **2016**, *13*, 257–262.
- (17) Zong, W.; Wu, R.; Li, M.; Hu, Y.; Li, Y.; Li, J.; Rong, H.; Wu, H.; Xu, Y.; Lu, Y. *et al.* Fast High-resolution Miniature Two-photon Microscopy for Brain Imaging in Freely Behaving Mice. *Nat. Methods* **2017**, *14*, 713–719.
- (18) Long, Y.; Stahl, Y.; Weidtkamp-Peters, S.; Postma, M.; Zhou, W.; Goedhart, J.; Sánchez-Pérez, M.-I.; Gadella, T. W. J.; Simon, R.; Scheres, B. *et al.* In Vivo FRET-FLIM Reveals Cell-type-specific Protein Interactions in Arabidopsis Roots. *Nature* **2017**, *548*, 97–102.

- (19) Dalton, G.; An, S.-W.; Al-Juboori, S. I.; Nischan, N.; Yoon, J.; Dobrinskikh, E.; Hilgemann, D. W.; Xie, J.; Luby-Phelps, K.; Kohler, J. J. *et al.* Soluble klotho binds monosialoganglioside to regulate membrane microdomains and growth factor signaling. *Proc. Natl. Acad. Sci.* **2017**, *114*, 752–757.
- (20) Baggaley, E.; Botchway, S. W.; Haycock, J. W.; Morris, H.; Sazanovich, I. V.; Williams, J. A. G.; Weinstein, J. A. Long-lived Metal Complexes Open Up Microsecond Lifetime Imaging Microscopy Under Multiphoton Excitation: From FLIM to PLIM and beyond. *Chem. Sci.* **2014**, *5*, 879–886.
- (21) Balamurugan, S.; Obubuafo, A.; Soper, S. A.; Spivak, D. A. Surface Immobilization Methods for Aptamer Diagnostic Applications. *Anal. Bioanal. Chem.* **2008**, *390*, 1009–1021.
- (22) Oh, E.; Liu, R.; Nel, A.; Gemill, K. B.; Bilal, M.; Cohen, Y.; Medintz, I. L. Meta-analysis of Cellular Toxicity for Cadmium-containing Quantum Dots. *Nat. Nanotechnol.* **2016**, *11*, 479–486.
- (23) Courtney, C. M.; Goodman, S. M.; McDaniel, J. A.; Madinger, N. E.; Chatterjee, A.; Nagpal, P. Photoexcited Quantum Dots for Killing Multidrug-resistant Bacteria. *Nat. Mater.* **2016**, *15*, 529–534.
- (24) Gnach, A.; Lipinski, T.; Bednarkiewicz, A.; Rybka, J.; Capobianco, J. A. Upconverting Nanoparticles: Assessing the Toxicity. *Chem. Soc. Rev.* **2015**, *44*, 1561–1584.
- (25) Guller, A. E.; Generalova, A. N.; Petersen, E. V.; Nechaev, A. V.; Trusova, I. A.; Landyshev, N. N.; Nadort, A.; Grebenik, E. A.; Deyev, S. M.; Shekhter, A. B. *et al.* Cytotoxicity and Non-specific Cellular Uptake of Bare and Surface-modified Upconversion Nanoparticles in Human Skin Cells. *Nano Res.* **2015**, *8*, 1546–1562.
- (26) Yu, J.; Yin, W.; Peng, T.; Chang, Y.-n.; Zu, Y.; Li, J.; He, X.; Ma, X.; Gu, Z.; Zhao, Y. Biodistribution, Excretion, and Toxicity of Polyethyleneimine Modified NaYF₄:Yb,Er Upconversion Nanoparticles in Mice via Different Administration Routes. *Nanoscale* **2017**, *9*, 4497–4507.
- (27) McNichols, R. J.; Gowda, A.; Kangasniemi, M.; Bankson, J. A.; Price, R. E.; Hazle, J. D. MR Thermometry-based Feedback Control of Laser Interstitial Thermal Therapy at 980 nm. *Lasers Surg. Med.* **2004**, *34*, 48–55.
- (28) Hou, Z.; Deng, K.; Li, C.; Deng, X.; Lian, H.; Cheng, Z.; Jin, D.; Lin, J. 808 nm Light-triggered and Hyaluronic Acid-targeted Dual-photosensitizers Nanoplatform by Fully Utilizing Nd³⁺-sensitized Upconversion Emission With Enhanced Anti-tumor Efficacy. *Biomaterials* **2016**, *101*, 32–46.
- (29) Zhong, Y.; Tian, G.; Gu, Z.; Yang, Y.; Gu, L.; Zhao, Y.; Ma, Y.; Yao, J. Elimination of Photon Quenching by a Transition Layer to Fabricate a Quenching-Shield Sandwich Structure for 800 nm Excited Upconversion Luminescence of Nd³⁺-Sensitized Nanoparticles. *Adv. Mater.* **2014**, *26*, 2831–2837.
- (30) Wang, Y.-F.; Liu, G.-Y.; Sun, L.-D.; Xiao, J.-W.; Zhou, J.-C.; Yan, C.-H. Nd³⁺-Sensitized Upconversion Nanophosphors: Efficient In Vivo Bioimaging Probes with Minimized Heating Effect. *ACS Nano* **2013**, *7*, 7200–7206.
- (31) Lee, J.; Yoo, B.; Lee, H.; Cha, G. D.; Lee, H.-S.; Cho, Y.; Kim, S. Y.; Seo, H.; Lee, W.; Son, D. *et al.* Ultra-Wideband Multi-Dye-Sensitized Upconverting Nanoparticles for

Information Security Application. *Adv. Mater.* **2017**, *29*, DOI: 10.1002/adma.201603169.

- (32) Kaiser, M.; Würth, C.; Kraft, M.; Hyppanen, I.; Soukka, T.; Resch-Genger, U. Power-dependent Upconversion Quantum Yield of NaYF₄:Yb³⁺,Er³⁺ Nano- and Micrometer-sized Particles - Measurements and Simulations. *Nanoscale* **2017**, *9*, 10051–10058.
- (33) Zhao, J.; Lu, Z.; Yin, Y.; McRae, C.; Piper, J. A.; Dawes, J. M.; Jin, D.; Goldys, E. M. Upconversion Luminescence with Tunable Lifetime in NaYF₄Yb,Er nanocrystals: Role of Nanocrystal Size. *Nanoscale* **2013**, *5*, 944–952.

7 SUMMARY

This thesis describes the preparation, surface modification, and application of lanthanide doped upconversion luminescent nanoparticles (UCNPs) in bioanalytical sensing and imaging based on time-resolved Förster resonance energy transfer processes (FRET). **Chapter 1** provides an overview of optical properties of lanthanides and highlights outstanding aspects of luminescence phenomena occurring in trivalent lanthanide ions with respect to chemical sensing. Down- and upconversion luminescence are defined and UCNPs are introduced and characterized as a unique class of nanomaterials that show exceptional potential for bioanalytical applications. FRET processes using UCNPs as energy donors are introduced and current issues that limit the more widespread implementation of ratiometric measurements with UCNPs in bioanalytical applications are addressed. In **Chapter 2** the aim of the work is presented as the investigation of FRET between UCNP donors and organic dye acceptors based on lifetime changes of the upconversion luminescence, with respect to a detailed characterization of the effect of interplay between particle architecture and surface modification on the FRET efficiency. The comprehensive understanding of energy transfer processes is needed to design an efficient FRET nanoprobe applicable in biosensing and – imaging.

Challenges regarding the choice of the type of surface modification to transfer hydrophobic nanoparticles into hydrophilic ones are described in **Chapter 3**. Amphiphilic coatings, encapsulation with inorganic materials, and ligand replacement are introduced as commonly used techniques to fabricate UCNPs that display colloidal stability in buffers and biological media. Advantages and disadvantages of the different methods are critically discussed and suggestions and examples for the application of each single technique depending on and tailored towards the desired individual applications are given.

Chapter 4 presents a study of the effect of nanocrystal size on the time-resolved FRET efficiency from UCNPs acting as energy donors to organic dyes as acceptors. Ligand exchange was selected for the attachment of the two acceptor dyes rose bengal and sulforhodamine B to the UCNP surface, which enables the shortest possible donor-acceptor distance and high, reproducible dye loading. UCNPs with diameters in the range of 20 - 25 nm were identified as the ones that yield the highest FRET efficiencies based on lifetime measurements of the upconversion luminescence. Lower FRET efficiencies at both smaller and larger UCNP sizes were ascribed to an increasing competition of surface quenching and lower amounts of FRET donors within Förster distance to the acceptor dye on

the particle surface, respectively. Comparison with conventional ratiometric intensity measurements illustrates the independence of the lifetime based approach on inner-filter-effects, particle concentration and excitation power.

The information gained from these FRET studies was the basis for the design of the upconversion FRET nanoprobe for the metabolite adenosine triphosphate (ATP), which is described in **Chapter 5**. Different surface modification strategies of core-shell UCNPs were investigated for the subsequent attachment of a structure switching ATP-responsive aptamer. Ligand exchange with poly(acrylic acid) represented the best compromise between colloidal stability, reduced surface quenching and increased distance to the FRET acceptor propidium iodide (PI). In presence of ATP the aptamer formed a G-quadruplex, which was recognized by the dye PI. The spectral shift of the absorption spectrum of PI bound to the G-quadruplex led to minimized background absorption and influence of unspecific binding. Successful FRET to the bound PI in close proximity to the UCNPs was shown by the reduction of the lifetime of the UCNP emission for ATP concentrations between 0.2 and 1.0 mM. The nanoprobe was selective for ATP and showed no cytotoxic effects.

Eventually, **Chapter 6** provides a concise discussion of the main results and insights gained within this thesis with respect to ideal particle design and surface functionalization for upconversion luminescent energy transfer processes in bioanalytical applications. Future perspectives as well as remaining challenges in the field are critically addressed.

8 ZUSAMMENFASSUNG

Die vorliegende Dissertation beschreibt die Synthese, Oberflächenmodifizierung und Anwendung von Nanopartikeln mit der Fähigkeit zur Generierung aufwärtskonvertierender Lumineszenz (englisch: upconversion luminescent nanoparticles, UCNPs) im Bereich der Bioanalytik und des Imaging. Schwerpunkt ist dabei die Untersuchung geeigneter Techniken zur Oberflächenmodifizierung für die Entwicklung einer Nanosonde basierend auf dem Prinzip des Förster-Resonanzenergietransfers (FRET). **Kapitel 1** gibt einen generellen Überblick über die optischen Eigenschaften von Lanthanoiden. Einzigartige Aspekte der in dreiwertigen Lanthanoidionen auftretenden Lumineszenz werden besonders im Hinblick auf (bio-)chemische Sensorik herausgestellt. Das herausragende Potential der UCNPs für den Einsatz als Labels und Rezeptoren in der Bioanalytik und für bildgebende Verfahren wird erläutert. UCNPs werden als Energie-Donoren in FRET-Prozessen vorgestellt und aktuelle Probleme und Herausforderungen, die bei intensitätsbasierten Messmethoden in der Bioanalytik auftreten können, beschrieben. In **Kapitel 2** werden die detaillierte Untersuchung von FRET-Prozessen zwischen UCNPs und organischen Farbstoffen sowie die Entwicklung eines auf FRET basierenden Biosensors werden als Ziele dieser Arbeit vorgestellt. Der Schwerpunkt wird dabei auf Lebensdauermessungen der Donorlumineszenz (= Lumineszenz der UCNPs) als verlässliche Alternative oder Ergänzung zu herkömmlichen ratiometrischen Methoden gelegt. Das Verständnis der Energietransfer-Prozesse insbesondere an der Partikeloberfläche stellt die Voraussetzung für das Design leistungsstarker UCNP-Sonden in der Bioanalytik dar.

Kapitel 3 beschreibt die Vielfalt an Möglichkeiten, aber auch die Herausforderungen, denen man gegenübersteht, wenn es um die Oberflächenmodifizierung und -funktionalisierung der UCNPs für bioanalytische Anwendungen geht. Verschiedene Techniken zur Oberflächenmodifizierung, z.B. Umhüllung mit amphiphilen Molekülen und Ligandenaustausch, werden erläutert, die die Herstellung kolloidal stabiler Dispersionen der ursprünglich hydrophoben UCNPs in wässrigen, gepufferten und biologischen Systemen ermöglichen. Vor- und Nachteile der einzelnen Methoden werden kritisch diskutiert, sowie Vorschläge und Beispiele für deren Anwendung bezogen auf individuelle Anforderungen je nach Einsatzgebiet vorgestellt.

Der Einfluss der Partikelgröße von UCNPs auf die Effizienz des Energietransfers zu organischen Akzeptor-Farbstoffen wird in **Kapitel 4** untersucht. Die beiden Farbstoffe Rose Bengal und Sulforhodamin B wurden dazu per Ligandenaustausch auf der Partikeloberfläche

immobilisiert, um den Donor-Akzeptor Abstand möglichst gering zu halten und eine hohe und reproduzierbare Farbstoffbeladung zu gewährleisten. Die daraus resultierenden FRET-Effizienzen wurden auf Grundlage der Lebensdaueränderungen der UCNP-Donoren bestimmt. Partikel mit Durchmessern zwischen 20 - 25 nm wiesen die stärksten Änderungen ihrer Abklingzeit auf und lieferten die höchste FRET-Effizienz von allen untersuchten UCNPs. Sowohl größere, als auch kleinere Partikeldurchmesser ergaben eine geringere FRET-Effizienz. Als Gründe dafür wurden bei großen UCNPs der kleinere Anteil von Donor-Ionen innerhalb des Förster-Radius und bei kleinen UCNPs der verhältnismäßig stärkere Einfluss von Quenching an der Partikeloberfläche genannt. Im Gegensatz zu intensitätsbasierten Methoden blieben die Lebenszeitmessungen unabhängig von reinen Absorptionsprozessen, der verwendeten Partikelkonzentration und der Anregungsleistung.

In **Kapitel 5** wurde auf Grundlage der in den vorherigen Kapiteln gewonnenen Erkenntnisse eine UCNP-basierte Detektionsmethode für Adenosintriphosphat (ATP) entwickelt. Verschiedene Techniken zur Oberflächenmodifizierung von Kern-Schale UCNPs wurden untersucht, um die Anbindung eines Aptamers zu gewährleisten, das selektiv ATP binden kann. Ligandenaustausch mit Polyacrylsäure stellte sich hierbei als bester Kompromiss zwischen verminderter Oberflächendeaktivierung, vergrößertem Abstand zum Akzeptorfarbstoff, und kolloidaler Stabilität heraus. In Gegenwart von ATP nimmt das Aptamer eine G-Quadruplex Struktur an, die vom Akzeptor Propidiumiodid (PI) spezifisch erkannt wurde. Damit ging eine deutliche Verschiebung des Absorptionsmaximums von PI in Richtung einer besseren Überlappung mit der UCNP Emission einher. Diese Verschiebung wurde dazu genutzt, den Einfluss von Hintergrundabsorption und unspezifischer Bindung zu minimieren und die Funktionalität des Aptamers nach der Immobilisierung an den UCNPs zu überprüfen. Eine deutliche Verkürzung der Lebensdauer der UCNP-Emission und damit das Auftreten von FRET konnte in Anwesenheit verschiedener ATP-Konzentrationen beobachtet werden. Als wichtige Voraussetzung für zukünftige Anwendungen in der Bioanalytik zeigte die UCNP-Nanosonde nur sehr geringe Zytotoxizität.

Kapitel 6 erörtert in einer abschließenden Diskussion die wichtigsten Ergebnisse und Einblicke, die in der Arbeit hinsichtlich der Funktion von UCNPs als FRET-Donoren gewonnen wurden. Es wird ein Ausblick gegeben, der Perspektiven und potentielle Anwendungen der UCNPs, aber auch bleibende Herausforderungen kritisch beleuchtet.

CURRICULUM VITAE

Persönliche Daten

Name Verena Muhr
Adresse Gertrud-von-le-Fort-Straße 18, 93051 Regensburg
Geburtsdatum 23. Februar 1989
Geburtsort Roding
Staatsangehörigkeit Deutsch

Ausbildung

- 11/2013 – 12/2017 **Promotionsstudium Chemie**, Universität Regensburg
"Design, Synthesis and Surface Modification of Lanthanide-Doped Nanoparticles for FRET-Based Biosensing Applications"
Institut für Analytische Chemie, Chemo- und Biosensorik (Dr. Thomas Hirsch, Prof. Antje J. Baeumner)
- 10/2011 - 09/2013 **Masterstudium Chemie**, Universität Regensburg
Hauptfach: Analytische Chemie
1. Nebenfach: Anorganische Chemie; 2. Nebenfach: Physikalische Chemie
Thema der Masterarbeit: *"Surface Modification of Lanthanide-doped Sodium Yttrium Fluoride Upconverting Nanoparticles"*
Institut für Analytische Chemie, Chemo- und Biosensorik (Dr. Thomas Hirsch, Prof. Otto S. Wolfbeis)
- 10/2008 - 10/2011 **Bachelorstudium Chemie**, Universität Regensburg
Thema der Bachelorarbeit: *"Referenzfarbstoffe für Farbkameramessungen"*
Institut für Analytische Chemie, Chemo- und Biosensorik (Prof. Otto S. Wolfbeis)
- 06/2008 **Allgemeine Hochschulreife**, Joseph-von-Fraunhofer-Gymnasium, Cham

Auszeichnungen

- 2017 **Nano Convergence Best Paper Award**
für den besten Vortrag des Symposiums „Luminescent Materials for Photon Upconversion“ beim MRS Spring Meeting, Phoenix (AZ), USA

2015 **Posterpreis**
11th Workshop on Biosensor & Bioanalytical Microtechniques in
Environmental, Food & Chemical Analysis, Regensburg, Germany

2015 **Vortragspreis**
9. Interdisziplinäres Doktorandenseminar, Berlin, Germany

Sonstiges

2015 Teilnahme am **9th Advanced Study Course on Optical Chemical
Sensors - Nanotechnology for (Bio)chemical Sensors**, Porto,
Portugal

2015 **Mitglied des Organisationsausschusses** für den 11th Workshop on
Biosensor & Bioanalytical Microtechniques in Environmental, Food &
Chemical Analysis (BBMEC 11), Regensburg, Germany

PUBLICATIONS

11. M. Kraft, C. Würth, **V. Muhr**, T. Hirsch and U. Resch-Genger. Size-, Power Density and Surface-Controlled Color Tuning and (De)Population Pathways of Upconversion Nanoparticles. *In preparation*.
10. M. Buchner, P. G. Calavia, **V. Muhr**, A. J. Baeumner, T. Hirsch, D. A. Russell and M. J. Marín. Surface Engineering of Upconversion Nanoparticles for Efficient Theranostics in Living Cells. *To be submitted to Journal of Materials Chemistry B*.
9. **V. Muhr**, M. Buchner, L. Sauer, B. Goricnik, J. Wegener, A. J. Baeumner, and T. Hirsch. Surface Engineering of Upconversion Nanoparticles for Time-Resolved Analysis of ATP-Responsive Energy Transfer. *Submitted to ACS Applied Materials & Interfaces*.
8. O. Dukhno, F. Przybilla, M. Collot, A. Klymchenko, V. Pivovarenko, M. Buchner, **V. Muhr**, T. Hirsch, and Y. Mély. Quantitative Assessment of Energy Transfer in Upconverting Nanoparticles Grafted with Organic Dyes. *Nanoscale* **2017**, 9, 11994-12004.
7. **V. Muhr**, C. Würth, M. Kraft, M. Buchner, A. J. Baeumner, U. Resch-Genger, and T. Hirsch. Particle Size-dependent Förster Resonance Energy Transfer from Upconversion Nanoparticles to Organic Dyes. *Analytical Chemistry* **2017**, 89, 4868–4874.
6. S. F. Himmelstoß, L. M. Wiesholler, M. Buchner, **V. Muhr**, S. Märkl, A. J. Baeumner, and T. Hirsch. 980 nm and 808 nm Excitable Upconversion Nanoparticles for the Detection of Enzyme-related Reactions. *Proceedings of SPIE* **2017**, 100770L.
5. **V. Muhr***, M. Buchner*, T. Hirsch, D. J. Jovanović, S. D. Dolić, M. D. Dramićaninb, and O. S. Wolfbeis. Europium-doped GdVO₄ Nanocrystals as a Luminescent Probe for Hydrogen Peroxide and for Enzymatic Sensing of Glucose. *Sensors and Actuators B: Chemical* **2017**, 241, 349-356.
4. M. Buchner*, **V. Muhr***, S. F. Himmelstoß, and T. Hirsch. Upconverting Nanomaterials – Perspectives, Synthesis and Application; Chapter 4: Functionalization Aspects of Water Dispersible Upconversion Nanoparticles. *CRC Press* **2017**, 69-100.

* contributed equally

3. A. Sedlmeier, A. Hlaváček, L. Birner, M. J. Mickert, **V. Muhr**, T. Hirsch, P. L. A. M. Corstjens, H. J. Tanke, T. Soukka, and H. H. Gorris. Highly Sensitive Laser Scanning of Photon-Upconverting Nanoparticles on a Macroscopic Scale. *Analytical Chemistry* **2016**, 88, 1835–1841.
2. S. Wilhelm, M. Kaiser, C. Würth, J. Heiland, C. C. Carrion, **V. Muhr**, O. S. Wolfbeis, W. J. Parak, U. Resch-Genger, and T. Hirsch. Water Dispersible Upconverting Nanoparticles: Effects of Surface Modification on Luminescence and Colloidal Stability. *Nanoscale* **2015**, 7, 1403–1410.
1. **V. Muhr**, S. Wilhelm, T. Hirsch, and O. S. Wolfbeis. Upconversion Nanoparticles: From Hydrophobic to Hydrophilic Surfaces. *Accounts of Chemical Research* **2014**, 47, 3481–3493.

PRESENTATIONS

Oral Presentations

2017 MRS Spring Meeting, Phoenix (AZ), USA

Effect of Nanoparticle Size on Time-resolved Upconversion Resonance Energy Transfer.

2016 Europt(r)ode XIII, Graz, Austria

Efficient Upconversion Luminescent Resonance Energy Transfer for Sensing Applications.

2015 9. Interdisziplinäres Doktorandenseminar, Berlin, Germany

Surface Modification of Upconverting Nanoparticles Suitable for Förster Resonance Energy Transfer.

Poster Presentations

2015 Deutsches BioSensor Symposium, Munich, Germany

Effects of Surface Modification on Luminescence and Colloidal Stability of Water Dispersible Upconverting Nanoparticles.

2015 ANAKON, Graz, Austria

Surface Modification of Upconverting Nanoparticles Suitable for Foerster Resonance Energy Transfer.

2015 Conference on Methods and Applications in Fluorescence 14, Würzburg, Germany

Upconverting Nanoparticles with High Förster Resonance Energy Transfer Efficiency.

2015 11th Workshop on Biosensor & Bioanalytical Microtechniques in Environmental, Food & Chemical Analysis, Regensburg, Germany

Lifetime-based FRET Sensing Using Upconverting Nanoparticles.

EIDESSTÄTTLICHE ERKLÄRUNG

Ich erkläre hiermit an Eides statt, dass ich die vorliegende Arbeit ohne unzulässige Hilfe Dritter und ohne Benutzung anderer als der angegebenen Hilfsmittel angefertigt habe; die aus anderen Quellen direkt oder indirekt übernommenen Daten und Konzepte sind unter Angabe des Literaturzitats gekennzeichnet.

Weitere Personen waren an der inhaltlich-materiellen Herstellung der vorliegenden Arbeit nicht beteiligt. Insbesondere habe ich hierfür nicht die entgeltliche Hilfe eines Promotionsberaters oder anderer Personen in Anspruch genommen. Niemand hat von mir weder unmittelbar noch mittelbar geldwerte Leistungen für Arbeiten erhalten, die im Zusammenhang mit dem Inhalt der vorgelegten Dissertation stehen.

Die Arbeit wurde bisher weder im In- noch im Ausland in gleicher oder ähnlicher Form einer anderen Prüfungsbehörde vorgelegt.

Ort, Datum

Unterschrift